MULTIRESOLUTION-MULTIVARIATE ANALYSIS OF VIBRATION SIGNALS; APPLICATION IN FAULT DIAGNOSIS OF INTERNAL COMBUSTION ENGINES

Multiresolution-multivariate analysis of vibration signals; application in fault diagnosis of internal combustion engines

By

SEYYED REZA HAQSHENAS, B.Sc., M.Sc.

A Thesis
Submitted to the School of Graduate Studies
in Partial Fulfillment of the Requirements
for the Degree
Master's of Applied Science

McMaster University

MASTER'S OF APPLIED SCIENCE (2012) MCMASTER UNIVERSITY
(Mechanical Engineering) Hamilton, Ontario

TITLE: Multiresolution-multivariate analysis of vibration signals; application in fault diagnosis of internal combustion engines

AUTHOR: SEYYED REZA HAQSHENAS
B.Sc., M.Sc.

SUPERVISOR: Professor Saeid Habibi, Professor Samir Ziada

MULTIRESOLUTION-MULTIVARIATE ANALYSIS OF VIBRATION SIGNALS; APPLICATION IN FAULT DIAGNOSIS OF INTERNAL COMBUSTION ENGINES

ABSTRACT

Condition monitoring and fault diagnosis of mechanical systems are two important issues that have received considerable attention from both academia and industry. Several techniques have been developed to date to address these issues. One category of these techniques which has been successfully applied in many industrial plants is based on the multiresolution multivariate analysis algorithms and more specifically the multi-scale principal component analysis (MSPCA). The present research aims to develop a multi-resolution multivariate analysis technique which can be effectively used for fault diagnosis of an internal combustion engine. Crank Angle Domain (CAD) Analysis is the most intuitive strategy for monitoring internal combustion engines. Therefore, MSPCA and CAD analysis were combined and a new technique, named CAD-MSPCA, was developed. In addition to this contribution, two indices were defined based on estimation of covariance matrices of scores and fault matrices. These indices were then employed for both fault localization and isolation purposes. In addition to this development, an interesting discovery made through this research was to use the statistical indices , calculated by MSPCA, for fault identification. It is mathematically shown that in case these indices detect a fault in the system, one can determine the spectral characteristics of the fault by performing the spectrum analysis of these indices. This analysis demonstrated the MSPCA as an attractive and reliable alternative for bearing fault diagnosis. These new contributions were validated through simulation examples as well as real measurement data.

Author: Seyyed Reza Haqshenas

Advisors: Professor Saeid Habibi, Professor Samir Ziada

Date: 11, 22, 2012

Department: Mechanical Engineering

Degree: Master's of Applied Science - Mechanical Engineering

This work is dedicated to my mom and dad, Farzaneh and Mojtaba, for their endless love, constant support and encouragement.

Acknowledgments

This research was a rewarding two-year journey which ended up successfully with help of many individuals who stood by me through this journey. This journey took place in the Ford Powertrain Engineering Research and Development Center (PERDC) located at the Ford Motors' Essex Engine Plant in Windsor, and the the Center of Mechatronics and Hybrid Technology (CMHT) located at McMaster University, Hamilton. I would like to offer my gratitude to my supervisors, Professor Saeid Habibi and Professor Samir Ziada, who have continuously supported me throughout this research. I appreciate their thoughtful advices and the consultation time they could set aside for me in their intense schedule. Furthermore, the invaluable opportunity of researching at PERDC afforded by their supports is greatly appreciated. This incredible experience provided me with a significant insight about this research theme and objectives.

The experimental part of this work would not have been possible without kind supports of engineers at PERDC. Special thanks go to Christopher Kelly, Ahmed Sobh, Kirk Taylor, Haran Arasaratnam and Tony Fountaine. I would also like to express my appreciation to my fellows at CMHT, specially Wanlin Zhang and Ryan Ahmed. Their help with experimentations and constructive points are appreciated.

Last but not the least, I would like to extend my sincerest gratitude and acknowledgments to my family for their limitless love, endless support and persistent encouragements. I certainly owe my achievements to them. Love you all.

List of Acronyms

CAD	Crank Angle Domain
CAD-MSPCA	Crank Angle Domain Multiscale Principal Components Analysis
CID	Cylinder Identification Sensor
CWT	Continues Wavelet Transform
DWT	Discrete Wavelet Transform
Mod-MSPCA	Modified Multiscale Principal Components Analysis
MSPCA	Multiscale Principal Components Analysis
MRA	Multi-Resolution Analysis
MVA	Multi-Variate Analysis
NVH	Noise Vibration Harshness
PCA	Principal Components Analysis
PCs	Principal Components
RBC	Reconstruction Based Contributions
SPE	Squared Predicted Error
SPWVD	Smoothed Pseudo Wigner-Ville Distribution
STFT	Short Fourier Transform
SVD	Singular Value Decomposition
SVM	Support Vector Machines
VRS	Variable Reluctance Sensor
WVD	Wigner-Ville Distribution

List of Symbols

$\mathbf{x}$	Vector $\mathbf{x}$
$\mathbf{X}$	Matrix $\mathbf{X}$
$\mathbf{X}^T$	Transpose of matrix $\mathbf{X}$
$\mathbf{X}^*$	Complex conjugate transpose of matrix $\mathbf{X}$
$\mathbf{X} \circ \mathbf{Y}$	The Hadamard product of matrices $\mathbf{X}$ and $\mathbf{Y}$
$\|\cdot\|$	Euclidian norm of a vector
$sgn(\cdot)$	Sign function
$\star$	Convolution product
$\mathcal{H}(\cdot)$	Hilbert transform of a vector
$E(\cdot)$	Expectation operator

Table of Contents

List of Tables

List of Figures

Chapter 1

Introduction

It is widely accepted that the monitoring of the working condition of a mechanical system is an important task. This can impact safety as well as functionality, reliability and cost. System malfunction is usually an evolutionary phenomena and therefore detecting faults at early stages could prevent catastrophic events. A fault detection and diagnosis strategy should serve the following objectives:

- detect malfunctions and abnormalities in the system;
- isolate and localize the fault; and
- identify and quantify the fault condition.

Fault diagnosis is hard particularly in complex systems. There is no universal approach for fault diagnosis. Venkatasubramanian et. al. have classified fault diagnosis approaches into two main categories, [1]. They are: (i) model-based techniques; and (ii) signal-based techniques. Model based approaches try to derive a mathematical model (linear or nonlinear) for the system and use the model in an observer. This category is a good choice when deriving an accurate model for the system is attainable and practical. When one is dealing with complex systems with many dynamic components, the signal-based approaches are usually chosen, [1]. In the case of combustion engines, the system is complicated and includes many rotary and reciprocating components. In this research, fault detection and diagnosis is applied to an internal combustion engine and therefore a signal based strategy was chosen.

Signal-based approaches are classified into subcategories depicted in figure 1.1, [2]. Venkatasubramanian et. al in their third work reviewed these approaches, [2].

This review revealed that each of them has strengths and weaknesses. No single technique has all of the desired characteristics. Depending on the application, a combination of these methods may provide better performance. A major subcategory is the quantitative approaches which explain the fault diagnosis as a pattern recognition problem. Hence, a baseline data from the system working under normal condition is required. An important consideration in signal based fault detection and diagnosis is the type; number and location of sensors. For example, hundreds of transducers may be used for monitoring the working conditions of a chemical plant. Multivariate statistical methods have shown promising performance under such circumstances, specifically in process monitoring and control applications in chemical engineering. One of the most prevailing multivariate analysis techniques is the Principal Component Analysis (PCA) method. PCA is a simple, non-parametric technique which enables extraction of significant dynamics that underlie a complex data set. Although PCA has been successfully applied for condition monitoring and fault diagnosis of chemical processes, its application to mechanical systems is less developed, particularly in the automotive industry. Some of the example applications for monitoring and diagnosis of mechanical systems are reviewed here.

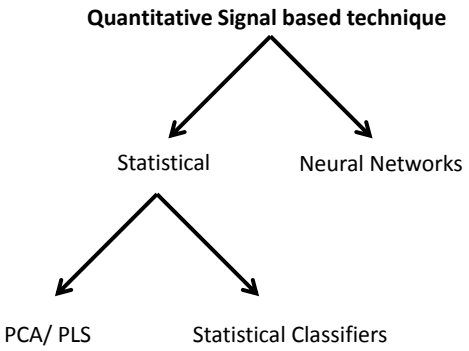

Figure 1.1: Classification of signal-based techniques.

Zanoli et. al. developed a fault diagnosis approach for a multi-shaft centrifugal compressor based on the PCA. Bearing vibrations, temperature, mass flow rates and power were measured as statistical variables, [3]. Bearing faults in the compressor were reported to be successfully diagnosed. Borguet and Leonard combined the PCA with the Kalman filter in order to develop a real time condition monitoring technique for a turbofan engine, [4]. In another application, Chang et. al. coupled PCA with support vector machines (SVM) technique for fault diagnosis in mine hoist, [5] . The incipient faults in the gearbox, the hydraulic system and the wire rope were diagnosed by the PCA-SVM technique. In another research the use of PCA was explored to detect localized faults in a two-stage industrial helical gearbox, [6]. Vibration signals obtained from several accelerometers are used for multivariate analysis. This work showed that PCA can detect incipient local faults at an early stage in a gearbox. In order to detect and identify damages of ball bearings, a technique is developed by [7] using vibration signal. This method uses PCA as a dimension reduction mean. Halligan and Jagannathan explored use of PCA for fault prognosis with application to a centrifugal water pump, [8].

Although PCA is a strong multivariate analysis technique, it has shortcomings in dealing with complex systems and fault conditions. A new technique was formulated by Bakshi to remedy weaknesses of the PCA, [9]. This technique combines discrete wavelet transform (as the multi-resolution analysis tool) with PCA (as the multivariate analysis technique) and named MSPCA for short. MSPCA is a powerful technique for fault detection and diagnosis of complicated signals and faulty conditions, e.g. autocorrelated signals which PCA often fails in dealing with them. Wenying combined the MSPCA technique with support vector machines (SVM), [10]. This MSPCA-SVM technique was then applied on vibration signals acquired from accelerometers attached to an AC motor to diagnose faults in the motor. Lachouri et.

al. applied the MSPCA technique on vibration data with its application to fault diagnosis of roller bearing, [11]. They built a model based on baseline data and used it for condition monitoring of a bearing with the aid of statistical indices.

The present research aims to develop a multi-resolution multivariate analysis technique which can be effectively used for fault diagnosis of an internal combustion engine. Although the primary focus was the internal combustion engine, particularly V type, the contributions of this research can be more broadly applied. Thus, in addition to an engine, a DC motor with a faulty roller bearing was used for validating the new technique.

1.1 Research Objective

Internal combustion engines are complicated mechanical systems with many rotational and reciprocal components. The engine's performance and efficiency are susceptible to manufacturing quality and the conditions of its components. This research is concerned with the development of a fault diagnosis approach that utilizes vibration signature to detect and localize mechanical faults in engines. It is expected that any abnormality in moving components inside the engine (like valves, pistons, cam shaft and crank shaft, etc.) would cause deviations from the normal vibration signatures and should be identifiable by proper processing of vibration signals. Jayaswal et. al. presented a brief review of fault diagnosis of machines through vibration analysis, [12]. Leboid et. al. considered the application of vibration analysis for fault diagnosis of gearbox, [13]. Jones and Hua investigated a broad range of fault diagnosis techniques applied and used for diagnosis of diesel engines, [14]. Several review papers considered the application of different fault diagnosis approaches based on vibration analysis to engine and other mechanical machines, [15, 16]. The element that is almost consis-

tent in all of them is the analysis of accelerometers' readings separately one at a time. Multivariate analysis has seldom been applied on a matrix of vibration data picked up from different location of a system in order to monitor the system state and perform diagnosis. Wang et. al. work is amongst the few works that used multivariate analysis for fault diagnosis of a diesel engine, [17]. It considers a simulated fault, that is air leakage in an inlet manifold plenum. The measured variables were fuel flow, air flow, air temperature and pressure at the inlet manifold and turbocharger. Hu applied the PCA on engine speed time series for detecting misfire in an in-line engine, [18]. King et. al applied PCA as a dimension reduction technique for detecting the misfire fault in an engine, [19]. They measured eight engine parameters including engine speed, coolant temperature, and air intake flow and generated two PCA models for both baseline and faulty data sets. These models were then compared in order to detect the change in the engine and to correlate the change to the misfire fault condition.

In terms of performing signal processing on data collected from engines, the most intuitive and helpful domain for processing is the crank angle domain (CAD). Many researchers have transformed the vibration signals, cylinder pressure readings, crankshaft torsional vibration data and other recordings of sensors into CAD for analysis of engine performance. A literature review of fault diagnosis methods applied to engine in CAD is presented in chapter 2.

Given the many advantages of processing data in the crank angle domain for fault diagnosis in engines in addition to the capabilities of MSPCA technique for monitoring complex systems, the main objective of this research was to combine these two approaches for developing a new fault detection and diagnosis technique suitable for internal combustion engines. Experimental tests were carried out in test cells provided by the industrial partner of this project, namely the Ford Powertrain Engineering Research and Development Center (PERDC) located at the Ford Motors'

Essex Engine Plant in Windsor.

1.2 Research Contributions and Novelty

Several contributions have been made through this research. The main contribution was to develop a new technique for fault detection and diagnosis of an internal combustion engine. The multi-scale PCA (MSPCA) technique was combined with the crank angle domain analysis. The new technique was named CAD-MSPCA. The CAD-MSPCA was then applied on vibration signals acquired from accelerometers installed on a V-type Ford engine.

In addition to this application, an interesting discovery made through this research was the use of statistical indices for fault identification. It is mathematically proven that when these indices detect a fault in the system, one can determine the spectral characteristics of the fault by performing a spectrum analysis of these indices. Furthermore, it is demonstrated that in case of periodic modulating faults, spectra of these indices contain the information of the spectrum of the envelope of the faulty variable. This result is practically very useful as one can identify the nature of the fault by inspecting these spectra. These findings make MSPCA an attractive and reliable alternative approach for bearing fault diagnosis.

The MSPCA and the CAD-MSPCA use the wavelet analysis to decompose signals in different scales. The final contribution of this research was to define two indices based on the estimated covariance matrices of the scores and the fault. These proposed indices were then used for fault localization in the scale domain and fault isolation. In addition to these major contributions, the reconstruction-based contribution analysis (RBC) were introduced to the MSPCA algorithm. The RBC guarantees that the faulty variable has the largest contribution and consequently leads to more

accurate results than the traditional contribution analysis.Thus, this facilitates fault detection and improves the fault isolation accuracy of the MSPCA algorithm. Overall, the contributions of this research are as follows:

- combining CAD analysis and the MSPCA algorithm to create the CAD-MSPCA technique for fault detection and diagnosis of engines;
- performing spectrum analysis of statistical indices and extracting the relationship between them and spectrum of faulty variable; and
- proposing two indices for localizing fault in the scale domain and isolating faulty variable.

At the end, all of these new improvements and findings were validated by applying them on real faults situations in a DC motor and a V8 engine.

1.3 Thesis Structure

The structure of this thesis is organized as follows. The CAD transformation and time-frequency analysis using the discrete wavelet transform are described in chapter 2. Chapter 3 is devoted to review of the multivariate analysis using Principal Components Analysis (PCA) and statistical process monitoring. The combination of PCA with multi-scale analysis is the subject explored in chapter 4. This chapter also presents the new contributions made through this research. The CAD-MSPCA and all other contributions are verified and validated using illustrative examples as well as real experimental data in chapter 5. A summary of accomplishments and recommendations for future works are provided in the chapter 6. The test rigs, instrumentation and test configurations are described in the Appendix B.

Chapter 2

Data Processing Techniques

This chapter describes the data processing techniques used for signal-based fault diagnosis with an especial attention to those techniques used for investigating the engine data. Since measurements are done in the time domain, time series analysis is an intuitive approach for data processing. There are several techniques already developed for time series analysis which mainly look at the statistical indices of the signal in order to extract the information buried in the signal or identify the signal's trend. The most commonly used ones are mean, peak to peak intervals, variance or standard deviation, Kurtosis, skewness, Crest factor, root mean square value (RMS). Generally, fault diagnosis strategies in the time domain include the following steps:

- statistical parameters for the machine running in normal condition are determined;
- the same parameters are calculated from a similar machine but with unknown condition; and
- the statistical parameters of the two machines are compared. Deviations between these determine the severity of fault condition.

Many researchers have applied time series analysis on vibration signals and they have achieved promising results on simple mechanical systems. For example, Sohn and Farrar have presented a procedure for damage detection and localization within a mechanical system solely based on the analysis of time history of vibration data, [20]. Leboid et. al. reviewed methods for gearbox diagnostics and prognostics which

employ time domain analysis of vibration signals, [13]. They reported that these statistical measures were used in successfully detecting bearing faults.

Advanced time domain techniques have been developed in order to extract features from signals more effectively. Some examples include: Cepstrum (inverse Fourier transform of logarithmic spectrum), envelope method (Hilbert transform) and fitting parametric models like Autoregressive (AR) or Autoregressive Moving Average (ARMA) to data. Nevertheless, time domain techniques have shortcomings that make them inappropriate for monitoring complex machines; for instance they assume stationary signals, which is not true in many applications, or they are excessively computationally expensive. Furthermore, time domain techniques are barely able to identify the fault beyond detecting its presence. Therefore, in fault diagnosis of engines, vibration and noise signals are not usually analyzed in the time domain. That is mainly because it is hard to extract the information and events happening in the engine from only time domain data. Therefore it is necessary to perform the post processing of the signal in order to extract more information and at the same time overcome the weaknesses of time domain approaches. A common alternative in signal processing is to transform signals into the frequency domain and analyze their spectrum. This transformation provides valuable information on the signal's frequency content though missing the link to the time domain events. As such, it is unable to estimate the instance at when the fault happens or the machine's performance degrades. Time-Frequency techniques have dealt with this issue and can effectively break up the signal into maps that contain information in both time and frequency domains simultaneously. The wavelet transform is a powerful technique that belongs to this category of signal processing methods. These post processing techniques are elaborated in this chapter.

In addition to the above mentioned approaches, there is a specific processing technique that is especially developed for analysis of cyclic signals pertinent to rotating machinery, i.e. Angle Domain Analysis. Considering an internal combustion engine as a cyclic system in which events at each cycle is correlated to a particular position of the crankshaft, this leads to analyzing the engine performance in angle domain (i.e. Crank Angle domain for engines) as a very logical and intuitive strategy. The following section describes the Crank Angle Domain analysis.

2.1 Crank Angle Domain Analysis

Pontoppidan applied the mean field independent component analysis technique on acoustic emission signals mapped into Crank Angle Domain (CAD) for condition monitoring and fault diagnosis of large diesel engines, [21]. Tjong and Relf have developed a new fault diagnosis technique based on an analysis of an engine's vibrations in CAD, [22]. Transforming the vibration signals, cylinder pressure readings, crankshaft torsional vibration data and all other recordings of sensors attached to engine into CAD for detailed and thorough analysis of engine performance have been reported in some research works. It was shown by Chin that all engine dynamics, except fuel dynamics, are less varying in the crank-angle domain than in the time domain, [23]. As a result, they are best described in CAD rather than the time domain. With respect to engine control, Yurkovicht and Simpsonf developed an engine model in the crank angle domain and demonstrated that a simple and effective controller can be designed utilizing this CAD-based model, [24]. Jones and Hua remarks that crankshaft position measurement is an essential measurement for condition monitoring of internal combustion engines, [14]. In addition, given the correlation of fault signature to the crankshaft position, modern engine control units (ECU) need the

crankshaft position data as feedback for performing control. Therefore fault diagnosis strategies that rely on CAD can be readily implemented. The essence of CAD analysis is to correlate measured signals (vibration, cylinder pressure, torque, etc) with mechanical events happening in the engine such as:

- valve train (intake and exhaust) operation;
- fuel injection and ignition;
- combustion and knock due to incomplete combustion; and
- piston stroke position.

Consequently signal abnormalities caused by defective components can be mapped to the crank angle position.

There are several ways available for mapping data from time domain to CAD. One of the intuitive approaches is to configure the data acquisition system to sample all sensors simultaneously according to the angle of the crankshaft. So pulses sent from the camshaft position sensor trigger the data acquisition unit to read and save data. Another approach is to record all data including the crankshaft or camshaft position sensor and perform mapping after the measurement. This was the technique used in this research and will be discussed as follows.

The test setup described in Appendix B existed at a Ford engine test cell and used for running their daily NVH tests, therefore the same measurement configuration was used for this research work. As it is described in the Appendix B the crankshaft position was estimated by looking at the camshaft position sensor called Cylinder IDentification (CID) sensor. The operation of an Otto-cycle engine includes the following four strokes; intake, compression, combustion and exhaust which is equivalent to one complete revolution of the camshaft or two complete revolutions

of the crankshaft. In modern engines, ECU uses The CID signal as a reference to adjust the sequential fuel injection, spark events and valve train operation. There is one CID sensor for each camshaft, the one attached to the intake valve positioning camshaft is a Hall effect sensor and the one attached to the exhaust valve camshaft is a Variable Reluctance Sensor (VRS). Both sensors use the same working principle based on change in the magnetic field resulting from the camshaft tabs passing by a magnetic pickup. The Hall effect sensor generates a digital square wave pulse but the VRS generates a sinusoidal wave. The camshaft position signal was taken from the VRS sensor harness and used to transfer data from time domain to CAD. A CID signal and time history of vibration signal picked up from an accelerometer mounted on at the head location on cylinder one is depicted in figure 2.1. According

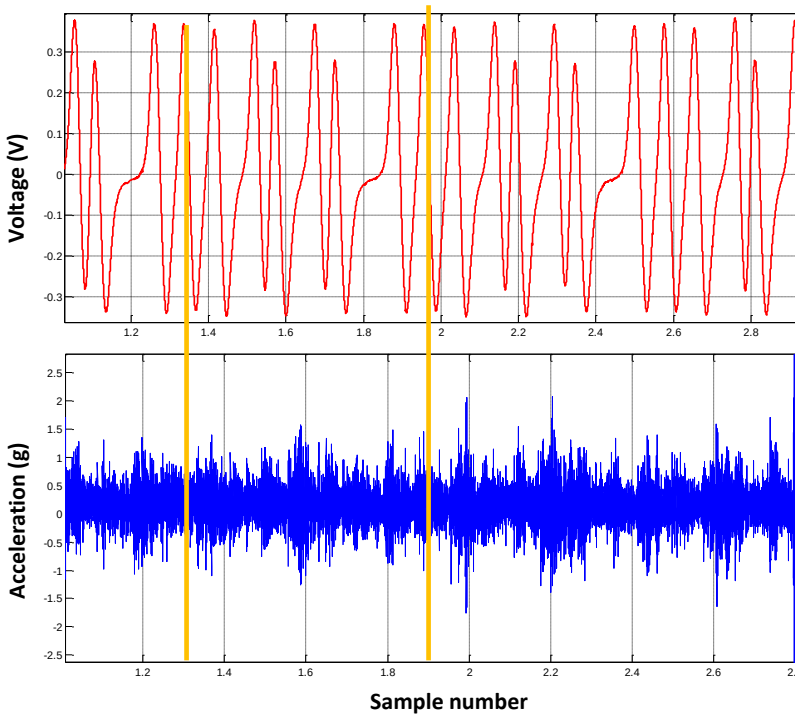

Figure 2.1: CID and vibration signals in time domain, the region between orange lines refer to one engine cycle

to figure 2.1, for this particular engine, the CID generates a unique signal which includes seven sinusoidal like pulses for each engine cycle. Each of these peaks (pulses) are apart from each other 90 °,120 °,60 °,120 °,60 °,180 °,90 ° respectively. It should be noted that one engine cycle is 720 ° of crank angle. The location of the zero angle of the crank wheel coincides with the top-dead-center of the first cylinder which is placed some degrees away from the zero crossing of the first pulse of the CID signal crankshaft position. Thus, given the location of the zero degree in the CID signal and knowing the angular distance between subsequent zeros, the signal mapping to CAD problem turns into chopping the acquired signal at different engine cycles and resampling each period (cycle). The resampling task is basically interpolation between captured samples in accordance with the distribution of angles. There are several interpolation techniques available for this purpose, one of the easiest, computationally fastest and at the same time accurate one is linear interpolation which is employed in this research work. Arasaratnam et. al. developed a sinc interpolation method for resampling which gave more precise signal reconstruction in CAD than using linear and cubic spline interpolation but it is quite slow and consumes more computational power, [25]. Figure 2.2 shows the flowchart of CAD transformation.

2.2 Time-Frequency Analysis

Time-Frequency analysis is an important subject in signal processing specially for analyzing non-stationary signals whose frequency content and magnitudes change over time. Various methods have been developed in order to serve practical needs like sonar, ultrasonic application for non-destructive testing, fault diagnosis, remote sensing and many others. Short Time Fourier Transform (STFT), Bilinear (or quadratic) time-frequency distributions [1] and Wavelet transform are tools developed for in-

[1] also called Cohen's Class distribution functions

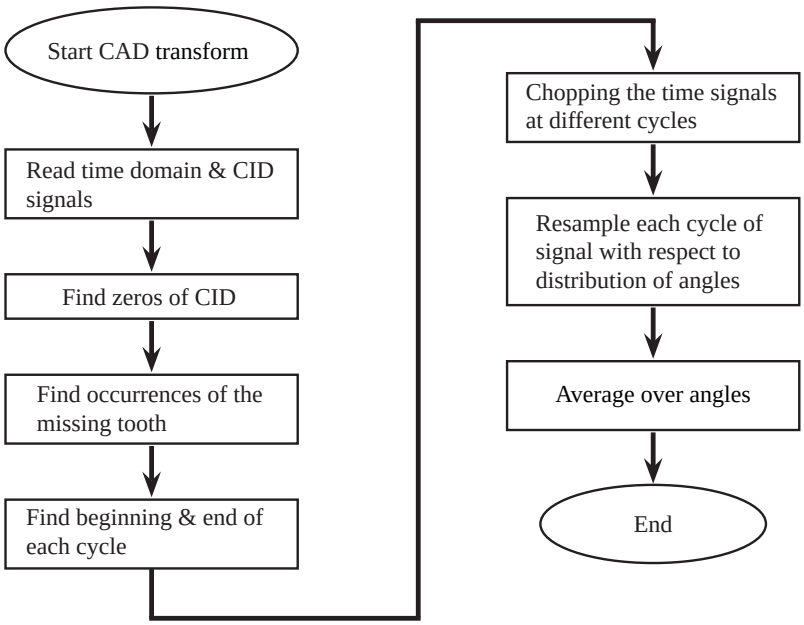

Figure 2.2: CAD transform procedure

vestigating the temporal and spectral information of signal. Wigner-Ville Distribution (WVD) and its variations like smoothed pseudo-Wigner-Ville distributions (SPWVD), Choi-Williams distribution functions and some others are techniques that fit in the category of Bilinear time-frequency distributions. These distribution-based methods have not shown better clarity or overall performance over STFT while suffer from shortcomings like cross-term contamination. All of the time-frequency analysis techniques have been extensively reported for successful fault diagnosis applications in the countless number of articles [26, 27, 28, 29, 30, 31, 32, 33, 34] . However, there are limitations and downfalls associated with each of them that should be taken into account. The STFT is one of the most practically applied time-frequency techniques and Wavelet transform is the newest member of this family. These are discussed in the present and the following sections respectively.

In contrast to a separate time and frequency representations of a signal, the

aim of the time-frequency analysis is to distribute the energy of a signal over time and the frequency bins simultaneously. The STFT of a signal is a quadratic map that transforms a signal to jointed time and frequency domains. It is defined as:

$$S_x(t,f) = \int_{-\infty}^{\infty} x(t)\ w(t)\ e^{(-j2\pi ft)}\ dt \tag{2.1}$$

where $w(t)$ is a window function and $x(t)w(t)$ is a windowed signal. Several window functions are available and have been proposed for different signal processing applications. The choice of the window function depends on the signal characteristics and its ability to suppress side lobs and spectral leakage. $S_x(t,f)$ is called the short time Fourier transform (STFT) of signal $x(t)$. What the STFT does is to divide up the signal into different time intervals and take the Fourier transform of each segment. The energy spectrum of STFT is mathematically obtained by the following equation:

$$\hat{S}_x(t,f) = \left| \int_{-\infty}^{\infty} x(t)\ w(t)\ e^{(-j2\pi ft)}\ dt \right|^2 \tag{2.2}$$

$$= \left| S_x(t,f) \right|^2 \tag{2.3}$$

Equation 2.2 can be interpreted as a joint time and frequency energy density. Hence point (t,f) in the spectrogram is a measure of energy density of the signal at that particular coordinate which is usually visualized by the aid of colorful spectrum. Therefore the total energy of a signal can be calculated using the following relation:

$$E_x = \int_{-\infty}^{\infty}\int_{-\infty}^{\infty} \hat{S}_x(t,f)\ df\ dt \tag{2.4}$$

One of the main drawbacks of the STFT is its fix resolution. The windowing function length determines the frequency resolution, the wider the time window the

more precise the frequency spectrum. On the other hand, a broad window abates the chance of detecting the time that frequencies change especially in transient signals or in cases which changes happen quickly. This compromise between time resolution and frequency resolution is absolutely important in fault diagnosis applications. The multiresolution analysis and at its heart, the wavelet transform, comes to play a key role in overcoming this shortcoming of the STFT. Multiresolution techniques give good time resolution for high-frequency events and good frequency resolution for low-frequency events. The wavelet transform is discussed in the next section.

2.2.1 Wavelet Transform

Wavelet theory has many benefits that have made it one of the most quickly evolving mathematical and signal processing tools. Wavelet analysis has been successfully applied in machine diagnostics, because of its advantages in multiresolution analysis, low computational complexity and its ability to be easily combined with other signal processing and classification algorithms. It is not the goal of this section to provide a complete description of the wavelet theory. Rather, the fundamentals necessary to understand, interpret and implement wavelet analysis correctly would be reviewed.

The wavelet theory has a fascinating history. The novel concept of wavelet was put forward by Morlet in 1984 for the first time. Morlet was a geophysical engineer at Elf Aquitaine (a French oil company which later joined the Total Inc.). Everything started from the problem he faced at his work which was analyzing signals that are comprised of two components. One was a long-lasting low frequency signal and the other is a high frequency component with a short time span. STFT is able to analyze them separately given a proper window type and segment length but not both at the same time. Morlet's ingenious idea was to use variable size windows for different frequency bands with all of these windows being translated and dilated/compressed

versions of a Gaussian prototype, [35]. He named his basis functions as *wavelets of constant shape*. Morlet realized that he needed to improve the mathematical implementation of his idea. Therefore, he decided to look for help to reinforce the mathematical definition of his idea. In co-operation with Alex Grossman, a physicist of quantum mechanics, Morlet eventually developed the Continuous Wavelet Transform (CWT) and Inverse Wavelet Transform using a rigorous mathematical proof. The word *wavelet* was coined by them for the first time, [35]. After this stage, Yves Meyer, a French mathematician, noticed that Morlet's work is actually a rediscovery of Albert Calderon's work carried out in 1964, twenty years earlier! Moreover, Meyer developed a new orthonormal basis functions (or wavelets) that had absolutely great combined time and frequency localization properties. Later on, it became known that Alfred Haar, a German mathematician, was the first one who invented and developed the first and simplest orthonormal basis function in 1909, [36]. These were developments in continuous time wavelets which is the kernel of wavelet theory. The transition to modern wavelet theory which is in discrete format was conducted by Ingrid Daubechies, a former student of Alex Grossman and Stephane Mallat. Daubechie constructed the wavelet frames for discretization of time and scale parameters in continuous wavelet transform. In his PhD. studies, Mallat developed the multresolution analysis (MRA) technique using the quadrature mirror filters (QMF) and sub-band filtering for Discrete wavelet transform (DWT). The Mallat technique is explained later in this section.

In the continuous wavelet transformation, a signal is represented in terms of a dictionary (family) of time and frequency *atoms*[2].Since atoms are localized in time,

[2]this terminology was used first by physicist Gabor in 1946 where he proposed to decompose signals over dictionary of time-frequency localized atoms, many mathematicians used the term *atom* for similar applications after him. They attempted to find atoms as elementary functions that can construct complex functions using an assembly rule.

they need to be translated in time in order to cover the entire time domain. Likewise, since atoms are localized in frequency, they need to be scaled in time in order to cover several frequency bands. A wavelet function is a function $\psi \in \mathbf{L^2}(\mathbb{R})$ with a zero average, energy of unity and centered in the neighborhood of *t=0*, see [37] :

$$\int_{-\infty}^{\infty} \psi(t)\, dt = 0 \tag{2.5}$$

$$\|\psi\| = 1 \tag{2.6}$$

Translating the wavelet function ψ by u and scaling it by s forms a dictionary of time frequency atoms which are used for continuous wavelet transform, that dictionary is:

$$\mathcal{D} = \left\{ \psi_{u,s}(t) = \frac{1}{\sqrt{s}}\, \psi\left(\frac{t-u}{s}\right) \right\}_{u\in\mathbb{R}, s\in\mathbb{R}^+} \tag{2.7}$$

and all the atoms satisfy the unit energy condition[3]:

$$\|\psi_{u,s}\| = 1 \tag{2.8}$$

Eventually the continuous wavelet transform of $f \in \mathbf{L^2}(\mathbb{R})$ at time u and scale s would be:

$$\mathcal{W}_f(u,s) = \int_{-\infty}^{\infty} f(t)\, \frac{1}{\sqrt{s}}\, \psi^*\left(\frac{t-u}{s}\right) dt \tag{2.9}$$

where $\psi^*(u)$ is the complex conjugate of $\psi(u)$. The continuous wavelet transform can

[3]they remain normalized

be written in the form of convolution product as well, i.e.:

$$\mathcal{W}_f(u,s) \;=\; \int_{-\infty}^{\infty} f(t)\,\frac{1}{\sqrt{s}}\,\psi^*\!\left(\frac{t-u}{s}\right)dt \;=\; f\star\bar{\psi}_s(u) \tag{2.10}$$

where

$$\bar{\psi}_s(u) \;=\; \frac{1}{\sqrt{s}}\,\psi^*\!\left(\frac{-t}{s}\right). \tag{2.11}$$

and $\star$ is the convolution product. Equation 2.10 plays an important role in linking the wavelet transform to the filtering notion. To better understand this point, the Fourier transform of a wavelet function $\bar{\psi}_s(t)$ needs to be determined first, that is:

$$\hat{\bar{\psi}}_S(\omega) \;=\; \sqrt{s}\;\hat{\psi}^*(s\omega) \tag{2.12}$$

Appendix A contains details of the Fourier transform. Considering that $\hat{\bar{\psi}}(0) = 0$, thus $\hat{\psi}$ looks like a transfer function of a bandpass filter. Consequently, one can safely draw the conclusion that equation 2.10 performs the wavelet transform with a bank of dilated bandpass filters. Further to conditions elaborated in equations 2.5 and 2.6 a wavelet function needs to meet the so-called *admissibility condition*. This condition allows the reconstruction of function $f(t)$ from its continuous wavelet transform. In other words, admissibility conditions ensures that the wavelet transform is complete and maintains the conservation of energy. A wavelet function is admissible if its Fourier transform satisfies the following condition:

$$C_\psi \;=\; \int_{-\infty}^{\infty} \frac{|\hat{\psi}(\omega)|^2}{\omega}\,d\omega \;<+\infty \tag{2.13}$$

If $\hat{\psi}(0) = 0$ and $\hat{\psi}(\omega)$ is continuously differentiable, then the above integral is defi-

nitely finite and ψ is an admissible wavelet [37]. To wrap up the continuous wavelet transform review, there is another type of atoms that needs to be accounted for and discussed. This atom is the complement of wavelet function. Assuming the $\mathcal{W}_f(u,s)$ for $s < s_0$ is given, in order to reconstruct f from its wavelet transform, the complementary information of $\mathcal{W}_f(u,s)$ for $s > s_0$ is required. This information is obtained by introducing a new function called *scaling function* which is an accumulation of wavelets at scales larger than 1[4]. The scaling function ϕ is therefore defined as:

$$|\hat{\phi}(\omega)|^2 = \int_1^{+\infty} |\hat{\psi}(s\omega)|^2 \frac{ds}{s} \tag{2.14}$$

the scaling function has the following properties:

$$\|\phi\| = 1 \tag{2.15}$$

$$\phi_s(t) = \frac{1}{\sqrt{s}} \phi\left(\frac{t}{s}\right) \tag{2.16}$$

$$\hat{\phi}_s(t) = \phi_s^*(-t) \tag{2.17}$$

In terms of filtering, the scaling function can be seen as a lowpass filter since ϕ estimates the impulse response of a lowpass filter. Hence, the low frequency approximation of f at a scale s is shown by $\mathcal{L}_f(u,s)$ and obtained by:

$$\mathcal{L}_f(u,s) = f \star \bar{\phi}_s(u) \tag{2.18}$$

This section has so far elaborated on: (i) the mathematical definition of atoms for the wavelet theory; (ii) the continuous wavelet transform; and (iii) the relationship between a dictionary of wavelet and a bank of filters. In the ensuing part of this section

[4]the higher the scale s the more dilated the wavelet function and therefore more concentrated on low frequency contents. For $0 < s < 1$ the wavelet function is being compressed rather than dilated.

the wavelet transform for discrete functions using the discrete wavelets (Discrete Wavelet Transform) would be discussed and the famous MRA or Pyramid algorithm used for its implementation would be reviewed.

The continuous wavelet transform of a discrete signal can reveal a wealth of information buried in the signal. Since in this form of the wavelet transform a continuous wavelet function is used, the scale and translation parameters are $u \in \mathbb{R}$ and $s \in \mathbb{R}^+$ respectively, and theoretically take on infinite values. This leads to redundancy usually as the spectrum does change very little between adjacent scales. This sparked the enthusiasm for discretization of the wavelet transform.

The discrete form of the wavelet and the scaling functions are achieved by dividing up the scale s to octave intervals; i.e. $s = 2^j, j \in \mathbb{Z}$. Thus the discrete scaling $\phi(n)$ and wavelet $\psi(n)$ functions are reformulated as:

$$\psi_j(n) = \frac{1}{\sqrt{2^j}}\,\psi\left(\frac{n}{2^j}\right) \tag{2.19}$$

$$\phi_j(n) = \frac{1}{\sqrt{2^j}}\,\phi\left(\frac{n}{2^j}\right) \tag{2.20}$$

Mallat counts the simplification in computer implementation as the main reason for this dyadic discretization of the scaling parameter, [37]. The discrete dyadic wavelet transform therefore would be:

$$\mathcal{W}_f(u, 2^j) = f \star \bar{\psi}_{2^j}(u) \tag{2.21}$$

Mallat proved in his PhD dissertation that the discrete dyadic wavelet transform can be computed with a fast filter bank algorithm called *algorithm a trous*. Let h and g be a pair of finite impulse response filters calculated from scaling and wavelet functions respectively. The following theorem gives the cascaded convolution formulas

to compute the discrete wavelet transform and its inverse, [37].

Theorem. For any $j \geq 0$

$$a_{j+1}[n] = a_j \star \bar{h}_j[n] \tag{2.22}$$

$$d_{j+1}[n] = a_j \star \bar{g}_j[n] \tag{2.23}$$

and for reconstruction

$$a_j[n] = \frac{1}{2}\left(a_{j+1} \star \tilde{h}_j[n] + d_{j+1} \star \tilde{g}_j[n] \right) \tag{2.24}$$

where a_0 is equal to the original signal $f_[n]$. a_j refers to *approximation* at level j which contains the low frequency contents of the filtered signal and d_j refers to *details* at level j and includes high frequency information of the filtered signal.The schematic of cascading convolution is shown in Fig2.2. As an extension to this theorem, Mallat developed the algorithm named Fast orthogonal wavelet transform which calculates the wavelet decomposition coefficients (a_j and d_j) using the cascades discrete convolutions and subsamplings. The Fast orthogonal wavelet transform is summarized in the following theorem stated by Mallat, [37].

Theorem. Mallat. At the decomposition (or sometimes called Analysis)

$$a_{j+1}[p] = \sum_{n=-\infty}^{+\infty} h[n-2p]a_j[n] = a_j \star \bar{h}[2p] \tag{2.25}$$

$$d_{j+1}[p] = \sum_{n=-\infty}^{+\infty} g[n-2p]a_j[n] = a_j \star \bar{g}[2p] \tag{2.26}$$

[4]this is called Pyramid algorithm or Multi-resolution analysis as well.

and at the reconstruction (or sometimes called Synthesis)

$$a_j[p] = \sum_{n=-\infty}^{+\infty} h[p-2n]\ a_{j+1}[n] + \sum_{n=-\infty}^{+\infty} g[p-2n]\ d_{j+1}[n] \tag{2.27}$$

$$= \check{a}_{j+1} \star h[p] + \check{d}_{j+1} \star g[p] \tag{2.28}$$

Upsampling by two was denoted by $\vee$ accent and defined as:

$$\check{a}[n] = \begin{cases} a[p] & \text{if } n = 2p \\ 0 & \text{if } n = 2p+1 \end{cases} \tag{2.29}$$

further, $\bar{g}[n] = g[-n]$.

Figure 2.3 , recreated from [37], demonstrates the Fast orthogonal wavelet transform schematically. This is a neat algorithm for computation of discrete wavelet transform. This form of performing DWT with the aid of a bank of filters is the cornerstone of developing more complex signal processing techniques which would benefit from multiresolution analysis property of the wavelet transform. DWT of a finite discrete

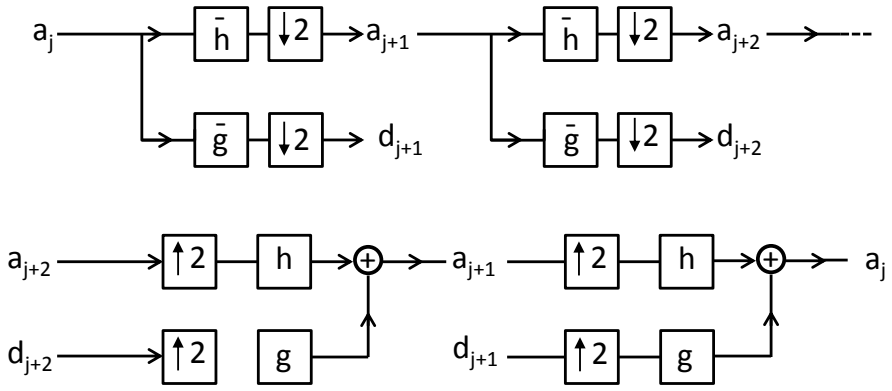

Figure 2.3: Fast orthogonal wavelet transform

signal can be expressed in the matrix form as well. With respect to the Mallat algo-

rithm and definition of the circular convolution, discrete wavelet transform matrix, sometimes called analysis matrix, would be given by:

$$\mathbf{W}_A = \begin{pmatrix} \mathbf{G} \\ \mathbf{G\,H} \\ \mathbf{G\,H\,H} \\ \vdots \\ \mathbf{G\,H\,H} \underbrace{\cdots}_{\text{(J-1)}} \mathbf{H} \\ \mathbf{H\,H\,H} \underbrace{\cdots}_{\text{J}} \mathbf{H} \end{pmatrix} = \begin{pmatrix} \mathbf{G}^{(1)} \\ \mathbf{G}^{(2)} \\ \mathbf{G}^{(3)} \\ \vdots \\ \mathbf{G}^{(J)} \\ \mathbf{H}^{(J)} \end{pmatrix} \tag{2.30}$$

where $\mathbf{G}$ and $\mathbf{H}$ are matrices made using the wavelet and scaling filters. For a wavelet filter with length L, the matrix $\mathbf{G}$ would be constructed as the following:

$$\mathbf{G} = \begin{pmatrix} & \vdots & \vdots & \vdots & \vdots & & \vdots & \vdots & \vdots & \\ \cdots & g(L-1) & g(L-2) & \cdots & g(0) & 0 & 0 & 0 & 0 & \cdots \\ \cdots & 0 & 0 & g(L-1) & g(L-2) & \cdots & g(0) & 0 & 0 & \cdots \\ \cdots & 0 & 0 & 0 & 0 & g(L-1) & g(L-2) & \cdots & g(0) & \cdots \\ & \vdots & \vdots & \vdots & \vdots & & \vdots & \vdots & \vdots & \end{pmatrix} \tag{2.31}$$

Matrix $\mathbf{H}$ is created similarly by using filter h rather than filter g. Therefore, the discrete wavelet transform of a data matrix $\mathbf{X}$ would be equal to $\mathcal{W}_x = \mathbf{W_A X}$. The inverse DWT matrix, usually called the synthesis matrix, would be equal to the transpose of $\mathbf{W}_A$, i.e. $\mathbf{W}_S = \mathbf{W}_A^T$. This is due to the characteristics of the wavelet functions which are orthogonal.

2.2.2 Choosing A Wavelet Function

Various types of wavelet and scaling functions have been created. Each of them was designed to fulfill a particular demand needed by a specific application. It should be however noted that many of them share similar properties and can be used interchangeably. As far as choosing the optimal wavelet and scaling functions are concerned, there is no universal approach available for this purpose. The choice is dependent on the signal type and the objective of performing the wavelet transform; for instance Yan and Gao have proposed a method for an optimal basis function selection based on the the ratio of the signal energy and the Shannon entropy which is specifically suitable for condition monitoring of bearings, [38]. Furthermore, with respect to denoising of ECG [5] signal with the aid of wavelet transform, Ranjeet and Farida have developed a technique for wavelet basis function selection using the retained energy, the percentage root mean square difference and the mean square error parameters, [39]. Although various fields of science and engineering have warmly welcomed the wavelet transform, the selection of the wavelet basis function has been left as an ad-hoc procedure so far. In the fault diagnosis of dynamical systems using vibration data, the focus is on the transient part of the signal which often reveals an anomaly in the process. The rule of thumb for wavelet basis function selection is the more wavelet function resembles the fault signature, the better it would be able to extract the signal features. This is implemented by Singh and Tiwari through determination of the cross correlation coefficient between the desired signal signature and the various wavelet functions, [40]. They employed this approach for optimal wavelet function selection for cleaning the ECG signal up. A heuristic approach was taken in this research. Several types of wavelet base functions were investigated and

[5] ElectroCardioGraphy

used in the fault diagnosis algorithm. Considering that the wavelet transform is used as a tool for multi-scale analysis and is complemented by the multivariate statistical analysis, the final result is not significantly susceptible to wavelet base function as long as it matches the signal signature to some extent. This issue is further discussed in chapter 5.

In this chapter, a review of post-processing techniques in the time domain, angle domain and joint time-frequency domain were presented. More emphasis was put on angle domain analysis and the wavelet transform as powerful tools for fault detection and diagnosis of engines. In the coming chapters, these two methods will be combined and complemented by the multivariate analysis to shape up a rigorous and effective fault detection and diagnosis technique specifically suitable for rotating machineries.

Chapter 3

Multivariate Analysis

As the name suggests, Multivariate Analysis (MVA) comprises a set of statistical techniques for observation and analysis of multiple statistical variables. MVA attempts to produce an overall result considering the relationship between variables and specifies the contribution of each variable at the final outcome. MVA has been widely used for data analysis in all fields of science, from telecommunication and array signal processing to neuroscience and biology. Multivariate analysis techniques are in general divided into two categories: (i) techniques that are inherently a generalization of the univariate analysis; and (ii) techniques that are unique to MVA and usually investigate the inter-relationship between variables. Multivariate Analysis of variance (MANOVA), regression and multivariate T^2test are examples of techniques that fit into the first category. Good examples of the second category approaches would be Principal Component Analysis (PCA), Factor Analysis and Multidimensional Analysis. The latter group of MVA approaches have found popularity in a fascinating area of signal processing named Blind signal separation[1].

Most likely one of the oldest and most prevailing MVA technique is the Principal Component Analysis (PCA) method which is employed to describe the multivariate structure of data in science and engineering. A review of the PCA is presented in the next section. Some statistical measures are then introduced to supplement PCA for its application to condition monitoring of dynamical systems. The missing piece of the puzzle for fault identification with the aid of multivariate analysis will be discussed in the last section of this chapter.

[1]sometimes called Blind source separation

3.1 Principal Components Analysis

The origin of PCA goes back to Pearson in 1901 or even to Cauchy in 1829. Its modern formulation and instantiation was performed by Hotelling in 1933, [41]. The term Principal Component was coined by him as well. Assuming a data set of multiple variables which are probably correlated, then what the PCA does is to map this data to another space that is made up of uncorrelated orthogonal axes and the distribution of data along these new axes. Axes with higher variances enjoy from more data points in their vicinity and therefore contribute more. Thus, the immediate application of PCA would be data compression by filtering out the data points oriented around axes with lower variances. PCA is a simple, non-parametric technique which enables extraction of significant dynamics that underlie a complex data set. In general one can enumerate the following goals for PCA:

- compressing the size of a data set by keeping the most significant information; and
- statistical analysis of the structure of data and variables.

Assuming $\mathbf{X}$ is the data matrix of size $n \times m$ which encompasses n measurements (or observations) of m variables, then PCA transforms $\mathbf{X}$ by combining the variables as a linear weighted sum as:

$$\mathbf{T} = \mathbf{XP} \tag{3.1}$$

where elements of $\mathbf{T}$ are called *the principal component scores* and matrix $\mathbf{P}$ includes the *principal component loadings* (or just the principal components which is usually written in short PCs) [2]. $\mathbf{P}$ is a square matrix of size $m \times m$ where each column of it represents a vector that is a basis vector of the new principal component space. In

[2] matrices $\mathbf{T}$ and $\mathbf{P}$ are usually called the scores and loading matrices respectively.

order to fulfill the above mentioned goals of PCA, the transformation matrix $\mathbf{P}$ should satisfy specific conditions, that are: (i) the basis vectors (PCs) should be orthonormal; and (ii) the *principal* direction is associated with the largest variance. The aim is to reduce redundancy and extract the structure of data, as a result each transformed variable is likely to co-vary as little as possible with others. This requires that the off-diagonal components of the covariance matrix $\mathbf{T}$ be equal to zero. In other words, the covariance matrix of $\mathbf{T}$ should be diagonal. To sum up, given a data matrix $\mathbf{X}$, the goal is to find some orthonormal transform matrix $\mathbf{P}$ which would map $\mathbf{X}$ to a new matrix $\mathbf{T}$ that has a diagonal covariance matrix. In other words, this transformation removes the cross-correlation in the data matrix. To derive the solution for this problem, the covariance for $\mathbf{T}$ is first calculated:

$$\begin{aligned}
\Sigma_T &= \frac{1}{n-1}\,\mathbf{T}^T\mathbf{T} \\
&= \frac{1}{n-1}\,(\mathbf{XP})^T\mathbf{XP} \\
&= \frac{1}{n-1}\,\mathbf{P}^T\mathbf{X}^T\mathbf{XP} \\
&= \frac{1}{n-1}\,\mathbf{P}^T(\mathbf{X}^T\mathbf{X})\mathbf{P} \\
&= \frac{1}{n-1}\,\mathbf{P}^T\mathbf{AP} \qquad (3.2)
\end{aligned}$$

where $\mathbf{A} = \mathbf{X}^T\mathbf{X}$ is a *square* $m \times m$ *symmetric* matrix. According to the Eigendecomposition (or spectral decomposition) of a matrix formulation, matrix $\mathbf{A}$ can be factorized to the following:

$$\mathbf{A} = \mathbf{V}\Lambda\mathbf{V}^{-1} \qquad (3.3)$$

matrix $\mathbf{V}$ is made of eigenvectors of $\mathbf{A}$ as its columns and matrix Λ is a diagonal matrix which its elements are eigenvalues corresponding to eigenvectors in $\mathbf{V}$. Since $\mathbf{A}$ is symmetric one can show its eigenvectors are orthogonal. Furthermore, it's known that transpose of an orthogonal matrix is equal to its inverse, so $\mathbf{V}^T = \mathbf{V}^{-1}$. Therefore equation 3.3 can be re-written as follows:

$$\mathbf{A} = \mathbf{V}\Lambda\mathbf{V}^T \tag{3.4}$$

Plugging the factorized matrix $\mathbf{A}$ in equation 3.2, the covariance of matrix $\mathbf{T}$ would be:

$$\Sigma_T = \frac{1}{n-1}\,\mathbf{P}^T(\mathbf{V}\Lambda\mathbf{V}^T)\mathbf{P} \tag{3.5}$$

Λ is a diagonal matrix and the primary goal of this calculation is to end up with a diagonalized covariance for $\mathbf{T}$, so by choosing $\mathbf{P} = \mathbf{V}$, equation 3.5 is simplified to the desired result;

$$\Sigma_T = \frac{1}{n-1}\,\Lambda \tag{3.6}$$

Additionally, as already pointed out, matrix $\mathbf{V}$ is orthogonal which can be normalized to be orthonormal, so the PCA transformation matrix $\mathbf{P}$ meets all the requirements if it is selected to be equal to the eigenvector matrix of the product $\mathbf{X}^T\mathbf{X}$ for a given data matrix $\mathbf{X}$.

In order to avoid numerical errors especially for some matrices that are ill-conditioned, the PCA transform is implemented with the aid of *Singular Value Decomposition (SVD)* theorem. It is shown in the following that SVD and PCA are intimately related. SVD theorem states that any arbitrary matrix $\mathbf{X}$ with size of

$n \times m$ can be factorized as follows:

$$\mathbf{X} = \mathbf{U}\Sigma\mathbf{V}^T \tag{3.7}$$

where $\mathbf{U}$ is a unitary matrix of $n \times n$ size, $\mathbf{V}$ is also a unitary matrix [3] of $m \times m$ size and Σ is a $n \times m$ rectangular diagonal matrix. $\mathbf{U}$, $\mathbf{V}$ and Σ are called *Left singular matrix*, *Right singular matrix* and *Singular values matrix* respectively.To realize how SVD gives a hand to PCA analysis, consider the following:

$$\begin{aligned} \mathbf{X}^T\mathbf{X} &= \mathbf{V}\Sigma^T\mathbf{U}^T\ \mathbf{U}\Sigma\mathbf{V}^T \\ &= \mathbf{V}\Sigma^T\Sigma\mathbf{V}^T \end{aligned} \tag{3.8}$$

Note that $\mathbf{U}^T\ \mathbf{U} = I$. Comparing equation 3.4 with 3.8, and taking $\mathbf{P} = \mathbf{V}$ into account, one can deduce that the transformation matrix $\mathbf{P}$ is obviously equal to the Right singular matrix $\mathbf{V}$ obtained from SVD of data matrix $\mathbf{X}$. Furthermore, $\Lambda = \Sigma^T\Sigma$. A significant point to be noted is that all eigenvectors (columns of $\mathbf{V}$) and their corresponding singular values (elements of Σ) are sorted in descending order, from the most important principal component to the least important one. This is a key point for data compression or reducing redundancy. In practice, measured variables with small eigenvalues are mainly contaminated by error and suffers from small SNR. Thus the contribution of the error in the data matrix can be reduced by removing those variables that have negligible eigenvalues in comparison to others. The procedure is as follows:

I map the data to PC domain, determine the loadings (columns of $\mathbf{P}$), scores (columns of $\mathbf{T}$) and eigenvalues (elements of Σ^2);

[3] unitary matrix is the matrix which its transpose is equal to its inverse, in other words it is orthogonal matrix

II assign a threshold to the PCs; i.e. specifying the threshold value which eigenvalues below this limit are negligible;

III eliminate the scores and loadings corresponding to these small eigenvalues; and

IV reconstruct the rectified (filtered) matrix by projecting the data from PC space back to the original domain using the inverse PCA transform:

$$\hat{\mathbf{X}} = \hat{\mathbf{T}}\hat{\mathbf{P}}^T \tag{3.9}$$

$\hat{\mathbf{T}}$ and $\hat{\mathbf{P}}$ are selected scores and loadings respectively. Making an appropriate selection for the threshold method is crucial in PCA. It itself is an active field of research and several thresholding techniques have been developed and used in various applications. The two common thresholding rules are the *heuristic rule (or proportion of total variance)* and *Kaiser's rule*. These rules are expressed as:

- the heuristic rule is a simple statistical criterion that keeps the components comprising 95% of the total variance. Therefore the PCs that have associated eigenvalues greater than 0.05 times of the total variance are kept.

- the Kaiser's rule retains the components with eigenvalues greater than the mean of eigenvalues. It means that components that posses information at least above the average are the major ones. This is the default criterion in many statistical softwares.

These thresholding rules were applied in this research and the Kaiser's rule was selected for thresholding since it keeps components that have significantly variances

(eigenvalues). The matrix of eigenvalues is shown in the following:

$$\mathbf{\Lambda} = \begin{pmatrix} \lambda_1 & 0 & \dots \\ 0 & \lambda_2 & \dots \\ \vdots & \dots & \vdots \\ 0 & \dots & \lambda_m \end{pmatrix} \tag{3.10}$$

The Kaiser's rule then states that components that their corresponding eigenvalues are greater than the mean of eigenvalues would be kept; i.e. $\lambda_i > \frac{1}{m}\sum_{j=1}^{m}\lambda_j \implies$ *keep* i^{th} *PC*. A consideration in PCA is the pre-treatment of data according to application demands. In general there are three different approaches for pre-processing of data. These are:

- using raw data with no adjustment or processing, this type of scaling is called *non-centered PCA*;
- compensating for the mean of each variable streams by subtracting the mean value. This is called *centered PCA* or *covariance PCA*; and
- scaling the data such that each variable is adjusted by removing its mean value and dividing it by its standard deviation. Therefore instead of using the raw data, the normalized data in *standard units* with a zero mean and unit standard deviation is used. This is called *correlation PCA*.

These scaling methods have their own advantages and applications. When variables are all in the same units and have similar amount of variability the pre-processing is usually skipped and non-centered PCA is taken. In data sets where variables do have different deviations from their mean values, it is preferable to use the covariance PCA. Many quality control applications use the covariance PCA as it helps with diagnostics.

In other applications that the first two scaling approaches are not rational and viable, the correlation PCA is usually used. The two potential situations that the correlation PCA is a desired choice are:

I the original variables are in different units. For instance one variable is output of an accelerometer in m/s^2 , one is temperature, the other one is displacement in m and another is displacement in cm. In this case studying the covariance matrix is meaningless. The variable with the unit of centimeter compared to the other displacement variable expressed in meter, would have a variance that will be 10000 times larger. Consequently that variable exerts more influence on the formation of the principal components. Hence, normalizing the original variables will circumvent the problem.

II in cases that even all variables are expressed in the same units but their variances differ largely and treating data with variance-stabilizing techniques [4] does not work, scaling data into the standard unit is recommended and employed.

In this research, the correlation PCA approach is adopted. Therefore the data matrix $\mathbf{X}$ is centered and normalized column-wise. The theory of PCA and its implementation procedure have been explained in this section. In order to use PCA for statistical process monitoring, further tools are necessary. The last point to note is a limitation of PCA. Indeed, PCA makes one important assumption; i.e. linearity. This assumption confines PCA to non-parametric modeling of the data as a linear combination of its basis vectors.

[4] for instance taking logs of data and redefining variables with their logs

3.2 Statistical Condition Monitoring

PCA is used to model a multivariate data set and extracts the relationship between variables. Equation 3.9 shows that the data matrix $\mathbf{X}$ can be approximated by its major PCs. This equation can be re-expressed in a more comprehensive form by the following:

$$\begin{aligned} \mathbf{X} &= \hat{\mathbf{X}} + \tilde{\mathbf{X}} \\ &= \hat{\mathbf{T}}\hat{\mathbf{P}}^T + \tilde{\mathbf{T}}\tilde{\mathbf{P}}^T \\ &= [\hat{\mathbf{T}} \;\; \tilde{\mathbf{T}}]\,[\hat{\mathbf{P}}^T \;\; \tilde{\mathbf{P}}^T] \\ &= \mathbf{T}\mathbf{P}^T \end{aligned} \tag{3.11}$$

This equation states that the data matrix $\mathbf{X}$ is projected on to two orthogonal subspaces, one is the PCs subspace (or scores space) spanned by the first l PCs, the $\hat{\mathbf{X}}$ in the above formula, and the other is the residual space formed by the rest of $(m-l)$ PCs, the $\tilde{\mathbf{X}}$ in the above formula. Matrices $\tilde{\mathbf{T}}$ and $\tilde{\mathbf{P}}$ are scores and loading matrices associated with the $(m-l)$ smallest PCs. In order to use PCA for condition monitoring one needs to calculate the loading matrix (basis vectors of PC subspace) for fault-free data. The first l PCs define the directions in PC space that posses the maximum variance of the data. In other words, these basis vectors construct a reduced dimension subspace that accounts for the major portion of the total variance and, features uncorrelated projected variables. Thus, when one builds this subspace for training (healthy) data, any fault-free observations of the same system should fall inside this subspace as well. The PCA model made by training data is sometimes called *in-control* PCA model. In order to examine the condition of the system using the in-control PCA model and new observed data, two indices are usually determined,

one is to detect deviations in the PCs space (scores space) and the other one in the residual space. The multivariate statistic that measures variations in PCs space is the Hotteling's $\mathcal{T}^2$ and is defined as, [42]:

$$\mathcal{T}^2 = \mathbf{x}_{new}\, \hat{\mathbf{P}}\hat{\mathbf{\Lambda}}^{-\mathbf{1}}\hat{\mathbf{P}}^T\, \mathbf{x}_{new}^T \tag{3.12}$$

$$\mathcal{T}^2 = \mathbf{x}_{new}\, \hat{\mathbf{D}}\, \mathbf{x}_{new}^T \tag{3.13}$$

where $\mathbf{x}_{new}$ is a vector of new observation with the size of $1 \times m$ variables put together in columns. $\hat{\mathbf{D}} = \hat{\mathbf{P}}\hat{\mathbf{\Lambda}}^{-\mathbf{1}}\hat{\mathbf{P}}^T$ and is a positive semidefinite matrix. Further, $\hat{\mathbf{\Lambda}} = \frac{1}{n-1}\hat{\mathbf{T}}\hat{\mathbf{T}}^{\mathbf{T}}$ which are principal eigenvalues of the product matrix calculated using the training data. In the literatures, this statistic is usually formulated for real time applications which is defined using every new observation rather than putting them all together in a matrix whereas the matrix form is more favorable in this research since monitoring and diagnosis are performed off-line. The index that measures the variation in the residual space is $\mathcal{Q}$-statistic or Squared Prediction Error (SPE) defined as followings, [42]:

$$\mathcal{Q} = \|\tilde{\mathbf{x}}_{new}\|^2 = \|\mathbf{x}_{new}\tilde{\mathbf{C}}\|^2 \tag{3.14}$$

where $\tilde{\mathbf{C}} = \tilde{\mathbf{P}}\tilde{\mathbf{P}}^T$. In fact the $\tilde{\mathbf{x}}$ can be written as projection of the data vector $\mathbf{x}$ to the residual subspace using the $\tilde{\mathbf{C}}$ matrix, that is: $\tilde{\mathbf{x}} = \mathbf{x}\tilde{\mathbf{P}}\tilde{\mathbf{P}}^T = \mathbf{x}\tilde{\mathbf{C}}$. This procedure is repeated for each observation vector in order to determine these indices at all data points.

The in-control PCA model extracts the structure of the multivariate data and expresses it as a linear combination of principal component basis vectors. Thus what $\mathcal{Q}-$statistic represents is essentially the unstructured residuals that the in-control

PCA model cannot account for. In a case that an irregular or odd event happens that was not observed in the training (healthy or reference data) and this observation leads to variations in the mean or covariance structure of the process data, $\mathcal{Q}-$statistic peaks at that instant. There is upper control limit for both $\mathcal{Q}-$ and $\mathcal{T}^2$ statistics. An abnormality in data can be detected when $\mathcal{Q}-$ and $\mathcal{T}^2$ statistics graphs violate their corresponding upper limits. Assuming variables possess multivariate normal distribution, these upper control limits have been estimated in the literatures. Nomikos and Macgregor approximated the upper control limit [5] for $\mathcal{Q}-$statistic for a given significance level α as a weighted chi-squared distribution which is expressed as, [43]:

$$\delta_{\mathcal{Q},\alpha} = g\chi^2_\alpha(h) \tag{3.15}$$

where g is the weight and h is the degree of freedom. They showed that mean and variance of the $g\chi^2(h)$ distribution, i.e. $\mu = gh, \sigma^2 = 2g^2h$, should be equal to the sample mean (m) and variance (v), therefore the control limit of $\mathcal{Q}-$statistic for a given significance level α is calculated by:

$$\delta_{\mathcal{Q},\alpha} = (\frac{v}{2m})\chi^2_\alpha(\frac{2m^2}{v}) \tag{3.16}$$

Again presuming that variables have multivariate normal distribution, Jackson and in another research Tracy et. al. state that $\mathcal{T}^2$ statistic is directly related to the F-distribution, then the upper control for $\mathcal{T}^2$ charts can be estimated using the following

[5] the terms upper control limit, control limit, detection limit and confidence control limit have been interchangeably used through this thesis while they all refer to the same quantity but from different angle

relationship, respectively [41] and [44]:

$$\tau_\alpha^2 = \frac{l(n-1)}{n-l} F_\alpha(l, n-l) \tag{3.17}$$

where $F_\alpha(l, n-l)$ is the upper $100\alpha\%$ critical point of the F-distribution with l and $n-l$ degrees of freedom. Tracy et. al. developed a modified format of this equation for situations that mean and covariance of the population are estimated from data, that is, [44]:

$$\tau_\alpha^2 = \frac{l(n^2-1)}{n(n-l)} F_\alpha(l, n-l) \tag{3.18}$$

in above formulas, the l is the number of selected principal components after thresholding and n is the number of samples. As long as $\mathcal{Q} \leq \delta_{\mathcal{Q},\alpha}$ and $\mathcal{T}^2 \leq \tau_\alpha^2$ the process is considered normal with confidence $(1-\alpha).100\%$.

Given the fact that basis vectors of residual and scores subspaces are orthogonal, $\mathcal{Q}-$statistic and $\mathcal{T}^2$ statistic would be independent from each other. Nevertheless, they work in a complementary manner. The $\mathcal{Q}-$statistic is defined in residual subspace and measures variability that breaks the normal process correlation structure, which often indicates an abnormal situation or faults that violate the process restrictions indicated by training data, [42]. On the other hand, $\mathcal{T}^2$ statistic measures the distance to the origin in the principal component subspace. The τ_α^2 limit defines a region in the principal component subspace that contains the normal operation scores. Since the principal component is constructed by the components with the largest variances, this normal operating region is typically large. Consequently faults with higher magnitudes should exceed the τ_α^2 limit. On the contrary, considering that $\mathcal{Q}-$statistic is defined in residual subspace which usually contains noise and small variations, it

typically exceeds the upper control limit when a small or moderate fault happens, [42]. There might be situations that a fault or normal change in process output takes place which conserves the correlation structure. In this case the $\mathcal{T}^2$ statistic limit is usually violated but not the $\mathcal{Q}-$statistic one. This particular case should be treated carefully because it may be due to a normal change in throughput. Taking the potential abilities of these statistical indices for condition monitoring, It is practically desirable to define a single index for this purpose. This new index combines these two indices featuring their capabilities for fault detection. Henry and Qin proposed such a global index which incorporates $\mathcal{Q}-$statistic and $\mathcal{T}^2$ statistic in a balanced way, [45]. This new index is called φ statistic and defined as:

$$\varphi = \frac{\mathcal{Q}}{\delta^2} + \frac{\mathcal{T}^2}{\tau^2} \tag{3.19}$$

$$= \mathbf{x}_{new}\, \mathbf{\Phi}\, \mathbf{x}_{new}^T \tag{3.20}$$

Matrix $\mathbf{\Phi}$ is symmetric and positive definite. Following the above mentioned definition, the matrix $\mathbf{\Phi}$ can be obtained from the following relationship:

$$\mathbf{\Phi} = \frac{\tilde{\mathbf{P}}\tilde{\mathbf{P}}^T}{\delta_\alpha^2} + \frac{\hat{\mathbf{P}}\hat{\mathbf{\Lambda}}^{-1}\hat{\mathbf{P}}^T}{\tau_\alpha^2} \tag{3.21}$$

$$= \frac{\tilde{C}}{\delta_\alpha^2} + \frac{\hat{D}}{\tau_\alpha^2} \tag{3.22}$$

Henry and Qin proved that φ has the distribution of the form $g^\varphi \chi^2(h^\varphi)$, assuming that variables have the multivariate normal distribution. Thus the upper control limit for $\varphi-$statistic with confidence level $(1-\alpha).100\%$ can be determined by, [45]:

$$\zeta_\alpha^2 = g^\varphi \chi_\alpha^2(h^\varphi) \tag{3.23}$$

where the weight g^{φ} and degree of freedom h^{φ} are determined from:

$$g^{\varphi} = \left(\frac{l}{\tau_{\alpha}^4} + \frac{\theta_2}{\delta_{\alpha}^4}\right) \Bigg/ \left(\frac{l}{\tau_{\alpha}^2} + \frac{\theta_1}{\delta_{\alpha}^2}\right) \tag{3.24}$$

$$h^{\varphi} = \left(\frac{l}{\tau_{\alpha}^2} + \frac{\theta_1}{\delta_{\alpha}^2}\right)^2 \Bigg/ \left(\frac{l}{\tau_{\alpha}^4} + \frac{\theta_2}{\delta_{\alpha}^4}\right) \tag{3.25}$$

$\theta_1 = trace(\tilde{\mathbf{\Lambda}})$ and $\theta_2 = trace(\tilde{\mathbf{\Lambda}}^2)$ where $\tilde{\mathbf{\Lambda}}$ is the counterpart of $\hat{\mathbf{\Lambda}}$ which was defined earlier, this can be determined from $\tilde{\mathbf{\Lambda}} = \frac{1}{n-1}\tilde{\mathbf{T}}\tilde{\mathbf{T}}^{\mathbf{T}}$. In fact the covariance matrix of scores $\mathbf{T}$ in the feature space, i.e. $\mathbf{\Lambda}$, is divided up into two matrices which include variances associated with PCs and residuals, it would be expressed as:

$$\mathbf{\Lambda} = \begin{pmatrix} \hat{\mathbf{\Lambda}} & \mathbf{0} \\ \mathbf{0} & \tilde{\mathbf{\Lambda}} \end{pmatrix} \tag{3.26}$$

Three statistical indices -namely $\mathcal{Q}$, $\mathcal{T}^2$ and φ - have been described so far to detect anomaly in comparison with healthy system data (which is considered as a fault). Having detected a fault, the next important task would be to isolate and diagnose the fault. The ensuing section is devoted to this subject and describes the approach that is taken for this purpose.

3.3 Fault Isolation Using Multivariate Analysis

The main approach for fault isolation (or localization) with the aid of PCA model is the use of contribution plots. Contribution plots are created by calculating the contribution of each variable to the value of the statistical index. The main concept behind the contribution plots is the variable with the largest contribution to the faulty index is most likely the faulty variable. Alcala and Qin explained the way to perform contribution analysis for each of the three statistical indices which follows,

[46]. Assuming that $\mathbf{x}$ is one new sample vector with size $1 \times m$, m is the number of variables, then the contribution of the i^{th} variable to the $\mathcal{Q}$-statistic can be calculated using the equation 3.14 as it comes in the following:

$$c_{i,Q} \;=\; \left(\mathbf{x}\, \tilde{\mathbf{C}}\, \xi_i \right)^2 \;=\; \tilde{\mathbf{x}}_i^2 \tag{3.27}$$

where ξ_i is a zero vector of size $m \times 1$ with only i^{th} element equals to unity:

$$\xi_i \;=\; \begin{bmatrix} 0 & 0 & 0 & \dots & 0 & 1 & 0 & \dots & 0 & 0 \end{bmatrix}^T \tag{3.28}$$

Likewise, the contribution value for $\mathcal{T}^2$-statistic can be estimated with the aid of equation 3.12, given by:

$$c_{i,T^2} \;=\; \left(\mathbf{x}\, \hat{\mathbf{D}}^{1/2}\, \xi_i \right)^2 \tag{3.29}$$

Eventually, the variable contribution for the φ index is obtained by:

$$c_{i,\varphi} \;=\; \left(\mathbf{x}\, \mathbf{\Phi}^{1/2}\, \xi_i \right)^2 \tag{3.30}$$

An important question to answer is what do the contribution plots look like under normal, no fault condition. Alcala and Qin state that contribution plots are not evenly distributed across variables when healthy data are fed to the in-control model, [46]. This essentially means that if a fault occurs, especially a small magnitude fault, in a variable which has small contribution, the proper fault isolation will be so hard and contribution plots may lead to mis-diagnosis. Dunia and Qin demonstrated that the traditional contribution plots fail to guarantee correct diagnosis even for large magnitude faults, [47]. An alternative approach which remedies this shortcoming is

Reconstruction-Based Contributions (RBC for short) suggested by Dunia and Qin, [47]. They showed that RBC fault diagnosis guarantees that the faulty variable has the largest contribution and consequently leads to higher rate of correct diagnosis. They modeled the fault in an additive form of $x = x^* + f$, where x^* is sample vector for normal operation condition and f is the fault vector and is defined as $f = \mathbf{f}\xi_i$. The vector ξ_i is a direction vector defined in the equation 3.28. The fault was modeled in this fashion to determine the contribution of each variable to the reconstructed vector x^* at a time. The concept behind RBC is to reconstruct x^* from new sample vector x along all possible fault directions. The direction that x^* becomes minimum, which means the fault contribution is maximum, is used to identify the faulty variable if the fault direction is defined such that to coincide along a variable like relationship 3.28. The formulas of RBC of statistical indices were derived and presented in [47] and [46]. They are reproduced here.

$$RBC_{i,\mathcal{Q}} = \frac{\left(\mathbf{x}\, \tilde{\mathbf{C}}\, \xi_i \right)^2}{\tilde{c}_{ii}} \tag{3.31}$$

where $\tilde{c}_{ii} = \xi_i^T\, \tilde{\mathbf{C}}\, \xi_i$ which is the i^{th} diagonal element of the matrix $\tilde{\mathbf{C}}$.

$$RBC_{i,T^2} = \frac{\left(\mathbf{x}\, \hat{\mathbf{D}}\, \xi_i \right)^2}{\hat{d}_{ii}} \tag{3.32}$$

similarly $\hat{d}_{ii} = \xi_i^T\, \hat{\mathbf{D}}\, \xi_i$ which is the i^{th} diagonal element of the matrix $\hat{\mathbf{D}}$.

$$RBC_{i,\varphi} = \frac{\left(\mathbf{x}\, \mathbf{\Phi}\, \xi_i \right)^2}{\phi_{ii}} \tag{3.33}$$

at the end $\phi_{ii} = \xi_i^T\, \mathbf{\Phi}\, \xi_i$ which is likewise the i^{th} diagonal element of the matrix $\mathbf{\Phi}$.

To summarize, the concept of principal components analysis was explained in this chapter and all the required formulas for fault detection with the aid of PCA were

derived. The common approaches for fault isolation and localization by employing the PCA model were discussed as well. Finally, an algorithm for fault diagnosis of a multivariate dynamical system was presented comprised of PCA modeling, calculation of statistical indices for fault detection and reconstruction-based contribution analysis for fault isolation. This powerful technique is combined with wavelet analysis which creates a strong fault diagnosis tool, this is the subject of the next chapter and would be discussed thoroughly there.

Chapter 4

Multiscale Fault Diagnosis

The wavelet transform and principal components analysis were discussed in the previous chapters. The wavelet transform is a powerful time-frequency analysis tool that decomposes a signal into several components with different frequency contents. PCA is a robust tool for multivariate analysis. The combination of the wavelet transform and PCA creates a strong multivariate multi-scale tool, abbreviated as MSPCA, which can be employed for fault diagnosis of complex dynamic systems. The derivation of this approach and new developments used to extract more information from measured data and improve outcomes are the main subjects of this chapter. The following section provides an explanation of the multi-scale PCA. It is continued by looking at the modified version of the multi-scale PCA and at the end the new improvements.

4.1 MSPCA Algorithms

The multivariate analysis with the aid of PCA which was discussed in the previous chapter is basically applied on data at a single scale. This is due to the fact that the in-control model is built on data represented only at the scale of the sampling interval. In terms of time-frequency representation, data are represented on basis functions with the same time-frequency localization at all locations. This property of the regular PCA is undesirable when events happening in the data set have various time and frequency localization characteristics. This is the case in many dynamical systems; an example of this is stochastic processes whose energy or power spectrum changes with time and/or frequency. Another shortcoming of the regular PCA appears when dealing with small magnitude abnormalities that are embedded in the

signal and are hardly separable. In these cases, variables are usually pre-processed by the aid of filters then fed to PCA. Macgregor and Kourtl state that filtering variables usually destroys the multivariate nature of the process data which is an essential feature for multivariate statistical process monitoring, [48]. The multi-scale PCA (MSPCA thereafter) approach has been developed as an integrated answer to both of these shortcomings. It was firstly developed by Bakshi [9] . MSPCA combines the ability of the wavelet transform to extract features in measurements and approximately decorrelate the autocorrelation with the ability of PCA to extract the relationship between the variables and decorrelate the cross-correlation. The MSPCA

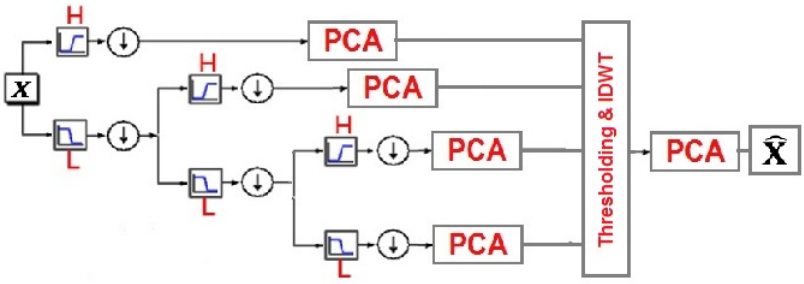

Figure 4.1: Schematic diagram of a three scale MSPCA algorithm

methodology proposed by [9] consists of the following steps:

- decompose each variable (for both baseline and testing data) on a selected family of wavelets;
- construct the PCA model at each scale using the wavelet coefficients of the baseline data;
- perform the multivariate statistical analysis by calculating statistical indices using the PCA model determined at each scale using testing data;
- keep the significant scales which are those that these indices violate the detection limits;

- reconstruct data (testing data only) by applying inverse wavelet transform on the thresholded scores at the significant scales; and

- perform the PCA and statistical analysis on the reconstructed variables.

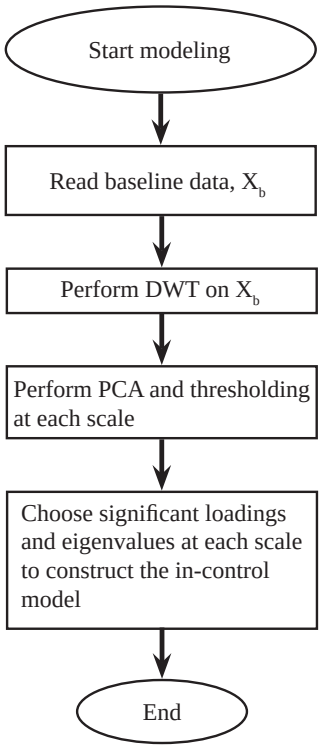

Figure 4.2: Procedure of deriving the in-control model in the Mod-MSPCA algorithm

This procedure is shown in the figure 4.1, recreated from the original chart in [9] . Respecting the characteristic of the DWT which down-samples the signal dyadically, this may lead to fewer number of samples at the coarsest scales and introduce numerical errors in statistical calculations. Furthermore, statistical indices are computed based on the wavelet coefficients which are not corresponding to the real time instances, therefore contribution analysis at each scale might not be meaningful unless the wavelet coefficients are up-sampled dyadically. The other alternative form of the

MSPCA is proposed by [49] . In this form of the MSPCA, the multi-resolution analysis is performed by the aid of DWT and the PCA is applied to the reconstructed signal components at each scale rather than the wavelet coefficients. This extension of prior MSPCA method enables one to use additional scale information for fault diagnosis. Considering the matrix form of DWT explained in chapter 2, the data matrix $\mathbf{X}$ can be decomposed into its components at J different scales as followings:

$$\mathbf{W_A X} = \mathbf{G}^{(1)}\mathbf{X} + \mathbf{G}^{(2)}\mathbf{X} + \mathbf{G}^{(3)}\mathbf{X} + \ldots + \mathbf{G}^{(J)}\mathbf{X} + \mathbf{H}^{(J)}\mathbf{X} \quad (4.1)$$

where $\mathbf{W_A}$ is the wavelet transform matrix. Reconstructing the signal can be accomplished by multiplying the inverse wavelet transform matrix which is called the wavelet synthesis matrix, $\mathbf{W_S}$, that is:

$$\begin{aligned} \mathbf{W_S W_A X} &= \mathbf{G}^{(1)T}\mathbf{G}^{(1)}\mathbf{X} + \mathbf{G}^{(2)T}\mathbf{G}^{(2)}\mathbf{X} + \mathbf{G}^{(3)T}\mathbf{G}^{(3)}\mathbf{X} + \ldots \\ &+ \mathbf{G}^{(J)T}\mathbf{G}^{(J)T}\mathbf{X} + \mathbf{H}^{(J)T}\mathbf{H}^{(J)}\mathbf{X} \\ &= \mathbf{X}_1 + \mathbf{X}_2 + \mathbf{X}_3 + \ldots + \mathbf{X}_J + \mathbf{X}_{J+1} \end{aligned} \quad (4.2)$$

The T is the transpose of the matrix. Considering that $\mathbf{W_S W_A} = \mathbf{I}$, then $\mathbf{W_S W_A X} = \mathbf{X}$. Consequently, the data matrix $\mathbf{X}$ is described as summation of its $(J+1)$ components obtained by direct and inverse wavelet transformation of the matrix $\mathbf{X}$ into J scales. The interesting achievement would be to construct a multi-scale in-control model for the system by applying the PCA on data matrix $\mathbf{X}_i$ at each scale, for $i = 1, 2, \ldots, J+1$. The modified MSPCA (Mod-MSPCA hereafter) algorithm for building a MSPCA model of the system is explained as follows:

- decompose the baseline data matrix $\mathbf{X}$ to its underlying components $\mathbf{X}_i$ with the aid of the DWT;

- determine loadings and eigenvalues at each scale by performing PCA on each scale data matrix $\mathbf{X}_i$; and

- specify the number of PCs at each scale using a proper thresholding technique.

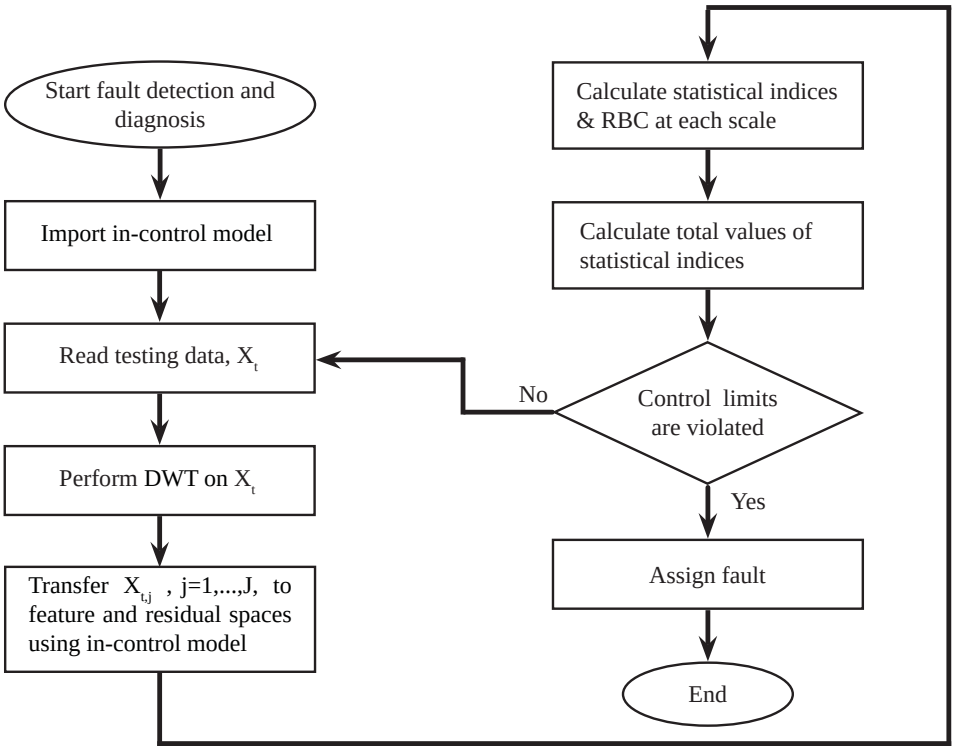

Figure 4.3: Procedure of performing fault detection and diagnosis in the Mod-MSPCA algorithm

Figure 4.2 illustrates these steps through a flowchart. Thus, when a MSPCA model is constructed, one can move forward to do the fault diagnosis by going through the following steps:

- decompose the testing data matrix $\mathbf{X}$ to its underlying components $\mathbf{X}_i$ with the aid of the DWT, the DWT depth and functions should be the same as the previous one

- use the PCA model at each scale and compute the statistical indices and contribution charts at each scale

- calculate the total value of the statistical indices by taking the statistical indices values of each scale into account

The plot of the total statistical indices can be initially employed for monitoring and detection purposes. When a fault is detected by exceeding the total confidence limits, one may look at the statistical indices plots at each scale for further diagnosis. Thus, Mod-MSPCA allows one to do the fault localization in scale domain (scales) in addition to time domain. This would be a valuable framework for the fault isolation end. The fault detection and diagnosis part of the Mod-MSPCA algorithm is illustrated in figure 4.3. The $\mathcal{T}^2$ statistic at each scale is determined using the following relationship:

$$\mathcal{T}_j^2 \;=\; \sum_{i=1}^{A} \frac{t_i^2}{\lambda_i} \qquad j \;=\; 1, 2, \ldots, J+1 \tag{4.3}$$

the $\mathcal{Q}$ statistic at each scale then would be obtained as follows:

$$\mathcal{Q}_j \;=\; \sum_{i=1}^{m} \tilde{x}_{i,j}^2 \qquad j \;=\; 1, 2, \ldots, J+1 \tag{4.4}$$

and φ statistic at each scale is calculated as follows:

$$\varphi_j \;=\; \frac{\mathcal{Q}_j}{\delta_j^2} \;+\; \frac{\mathcal{T}_j^2}{\tau_j^2} \qquad j \;=\; 1, 2, \ldots, J+1 \tag{4.5}$$

λ_i is the i^{th} eigenvalue at scale j, A is the number of principal components, m is the number of variables, $\tilde{x}_{i,j}$ is the i^{th} variable at scale j mapped to the residual space, and δ_j^2 and τ_j^2 are confidence limits estimated for the $\mathcal{Q}_j$ and $\mathcal{T}_j^2$ respectively. The way

the confidence limits at each scale is determined is slightly different from the overall confidence limit, this is discussed later in this section. The total statistical indices would be obtained through combining the statistical indices at each scale, that is:

$$\mathcal{T}^2 = \sum_{j=1}^{J+1} \mathcal{T}_j^2 \tag{4.6}$$

$$\mathcal{Q} = \sum_{j=1}^{J+1} \mathcal{Q}_j \tag{4.7}$$

$$\varphi = \frac{\mathcal{Q}}{\delta^2} + \frac{\mathcal{T}^2}{\tau^2} \tag{4.8}$$

The RBC charts for each of these statistical indices would be calculated by the aid of applying the relationships explained in chapter 2 at each scale. The contribution charts have been reported in literatures for fault isolation purpose. Nevertheless, the RBC analysis was chosen in this research as it is shown by [47] that it outperforms the conventional contribution analysis. The equations for the scale-wise RBC analysis are expressed in the following relationships:

$$RBC_{i,Q}^{j} = \frac{\left(\mathbf{x}_j \, \tilde{\mathbf{C}}_j \, \xi_i \right)^2}{\tilde{c}_{j,ii}} \qquad j = 1, 2, \ldots, J+1 \tag{4.9}$$

where $\tilde{c}_{j,ii} = \xi_i^T \, \tilde{\mathbf{C}}_j \, \xi_i$ which is the i^{th} diagonal element of the matrix $\tilde{\mathbf{C}}_j$. Matrix $\tilde{\mathbf{C}}_j$ is the projection matrix of data at scale j to the residual domain.

$$RBC_{i,T^2}^{j} = \frac{\left(\mathbf{x}_j \, \hat{\mathbf{D}}_j \, \xi_i \right)^2}{\hat{d}_{j,ii}} \qquad j = 1, 2, \ldots, J+1 \tag{4.10}$$

similarly $\hat{d}_{j,ii} = \xi_i^T \hat{\mathbf{D}}_j \xi_i$ which is the i^{th} diagonal element of the matrix $\hat{\mathbf{D}}_j$. Matrix $\hat{\mathbf{D}}_j$ is the projection matrix of data at scale j to the feature (score) domain.

$$RBC_{i,\varphi}^{j} = \frac{\left(\mathbf{x}_j \mathbf{\Phi}_j \xi_i \right)^2}{\phi_{j,ii}} \qquad j = 1, 2, \ldots, J+1 \tag{4.11}$$

where $\phi_{j,ii} = \xi_i^T \mathbf{\Phi}_j \xi_i$ is likewise the i^{th} diagonal element of the matrix $\mathbf{\Phi}_j$. Matrix $\mathbf{\Phi}_j$ is the combined statistic matrix at scale j.

The $\delta_{\mathcal{Q},\alpha}$, τ_α^2, ζ_α^2 are upper control limits with the confidence of $(1-\alpha)$ for $\mathcal{Q}$, $\mathcal{T}^2$ and φ statistics respectively. These control limits are calculated using relationships 3.16, 3.18 and 3.23. Macgregor et. al. and Yoon et. al. [48, 49] both suggested that for MSPCA monitoring, these limits should be adjusted by Bonferroni corrections in order to provide correct control limits at each scale which results in the overall confidence of $(1-\alpha)$. Yoon and Macgregor suggests that in the case of MSPCA with J levels of decomposition, the significance levels of the scale statistics, $\mathcal{Q}_j$ and $\mathcal{T}_j^2$ are adjusted as $\alpha_j = 1 - (1 - \alpha_{given})^{1/(J+1)}$, so that the total confidence limit remains to be $(1-\alpha)$, [49].

To summarize this section, two forms of the MSPCA approach for process monitoring and diagnosis were discussed. MSPCA approach benefits from the properties of PCA for multivariate analysis and extracting the correlation between variables as well as attractive properties of wavelet transform for multi-resolution analysis. These characteristics enable MSPCA to act better in modeling, monitoring and diagnosis of data containing contributions that change over time and frequency than either PCA or wavelet transform. When it comes to data compression applications, MSPCA works considerably better than PCA or wavelet alone as it just takes the scales and scores which have the most contribution to the data set. As far as the fault diagnosis application is concerned, MSPCA integrates the feature extraction and isolation with

process monitoring. This is achieved by decomposing variables to several scales (indirectly related to different frequency bands) and selecting the scales and performing the statistical process monitoring at each scale. Among the two MSPCA algorithms, the Mod-MSPCA was discussed in details. This algorithm was implemented and used for condition monitoring and fault diagnosis of two mechanical systems in this research. The Mod-MSPCA performs statistical monitoring at each scale on a data set which has the same length as the original data. This enables one to localize the fault and abnormalities in original domain at each scale. Therefore, a thorough fault diagnosis at each scale would be feasible besides multi-scale modeling of the process. The φ index and the reconstruction based contribution analysis based on φ index as well as the other statistical indices were discussed in relation to MSPCA and implemented for fault diagnosis. As already remarked in chapter 3, the reconstruction based contribution (RBC) analysis guarantees that the faulty variable has the greatest contributions and consequently provides more accurate diagnosis. Further to these developments, additional improvements were made in this research which technically turns MSPCA to a more powerful and useful fault diagnosis approach. This new developments and improvements are discussed in the next section.

4.2 New Contributions

Several contributions have been made through this research. The main contribution was to develop a new technique for fault detection and diagnosis of an internal combustion engine. This goal was achieved by combining the CAD analysis with the multi-scale multivariate analysis of vibration signals acquired from sensors attached to an engine. In addition to these, other conditions In addition to these, other contributions made through this research promote the application of multi-scale multivariate

analysis, and specifically the MSPCA algorithm, in fault detection and diagnosis of mechanical systems. These contributions are as follows:

- combining CAD analysis and the MSPCA algorithm to create the CAD-MSPCA technique for fault detection and diagnosis of engines;
- performing spectrum analysis of statistical indices and extracting the relationship between them and spectrum of faulty variables; and
- proposing two indices for localizing faults in the scale domain and isolating faulty variables.

In addition to these major contributions, the combined φ index and reconstruction-based contribution analysis (RBC) were introduced to the MSPCA algorithm. This facilitates fault detection and improves the fault isolation accuracy of the MSPCA algorithm. The above mentioned contributions are explained in details in the following.

CAD-MSPCA technique:

The combination of CAD (or in general angle domain) and MSPCA is quite helpful when one is dealing with the monitoring and diagnosis of rotary machines with many moving components where events and functions can be mapped over to the rotor angular position. The CAD analysis correlates measured signals (vibrations here) with mechanical events happening in the engine. The CAD transformation was explained in chapter 2. Considering the cyclic nature of the signal at the time domain, transformation to the CAD ends up with several cycles with the same number of samples at each transformed cycle. Therefore averaging over angles can suppress effect of noise and any random components and consequently improve the quality of the signal in the CAD. The number of cycles depend on the rotor speed and

sampling length. The number of samples in the CAD is defined by the resolution in the angle domain and depends on the rotor speed and the sampling rate. The number of samples is often limited to few thousands, much lesser than the time series length. Averaged signals in the CAD are put together to form the data matrix for multi-scale multivariate analysis. In the case of V-type engines, two data matrices are constructed for right bank and left bank respectively. This approach facilitates fault detection and isolation. Furthermore, in the case multiple faults happen at both sides of engine, separating these faults from each other would be easier. The data matrices would be scaled to zero mean and unit variance. The MSPCA method would then be employed for fault detection and diagnosis. The proposed procedure is described step by step as follows:

- transfer the time signal to CAD following the instructions described in chapter 2;
- take the average of the transferred signals over angles;
- repeat the CAD transformation for each measurement (sensor readings) and construct the data matrix by concatenating these transformed signals column-wise; and
- feed this data matrix to the Mod-MSPCA algorithm.

Taking into account that the data matrices in the CAD have much shorter length than the original measurements, a precaution in choosing proper wavelet depth must be taken in order not to end up with only a few samples in the last scale. On the other hand this fact can be beneficial as the MSPCA would be applied on a smaller data matrix, in terms of size, and consequently the processing would be quick. At the end, the fault would be localized in the CAD and the scale domain. The scale

domain specifies the frequency characteristics of the fault and the CAD domain reveals information about the nature of the fault and the corresponding event in the machine causing the fault. The CAD-MSPCA method therefore not only detects the fault in the measurement but also provide useful information about the characteristics of the fault and related phenomena in the machine. The latter can be used to accomplish the fault identification. Flowchart and details of implementing the CAD-MSPCA algorithm are explained in Appendix D

Spectrum analysis of statistical indices:

An interesting result can be inferred from both of the overall statistical indices ($\mathcal{Q}$ and $\mathcal{T}^2$ statistic) as well as scale-wise statistical indices ($\mathcal{Q}_j$ and $\mathcal{T}_j^2$ statistic). Taking the Fourier transform of the $\mathcal{Q}$ and Hotteling's $\mathcal{T}^2$ statistic reveals more information about the underlying anomalous content of the variables. Since we are dealing with the discrete signals, so the discrete Fourier transformation is used for this derivation. The discrete Fourier transformation matrix which is a special form of the Vandermonde matrix is as follows:

$$\mathbf{W} = \frac{1}{\sqrt{n}} \begin{pmatrix} 1 & 1 & 1 & 1 & \dots & 1 \\ 1 & \omega & \omega^2 & \omega^3 & \dots & \omega^{(n-1)} \\ 1 & \omega^2 & \omega^4 & \omega^6 & \dots & \omega^{2(n-1)} \\ 1 & \omega^3 & \omega^6 & \omega^9 & \dots & \omega^{3(n-1)} \\ \vdots & \vdots & \vdots & \vdots & \dots & \vdots \\ 1 & \omega^{(n-1)} & \omega^{2(n-1)} & \omega^{3(n-1)} & \dots & \omega^{(n-1)(n-1)} \end{pmatrix} \tag{4.12}$$

n is the number of samples and $\omega = e^{-\frac{2\pi i}{N}}$. Assuming that the total $\mathcal{Q}$ is denoted by vector $\mathbf{Q} = \sum_{i=1}^{m} \mathbf{q}_i$, then the DFT of the $\mathcal{Q}$ would be written as: $\mathbf{WQ} = \sum_{i=1}^{m} \mathbf{W}\mathbf{q}_i$. The vector $\mathbf{q}_i$ of the size $n \times 1$ is defined as $\mathbf{q}_i = \tilde{\mathbf{x}}_i^2$ and technically is the squared

of the i^{th} variable in the residual space. As a result, the DFT of the $\mathcal{Q}$ index is the summation of spectra of the squared value of each variable at the residual space. Thus, when a fault is detected by violating the $\mathcal{Q}$ detection limits, its characteristics and properties in the frequency domain would be achievable by accomplishing the spectrum analysis of the $\mathcal{Q}$ index. An important point is that if the fault frequency is ω_f, the frequency that peaks in the spectrum of the $\mathcal{Q}$ would be $2\omega_f$ [1]. In case that multiple faults occur in different scales, $\mathcal{Q}_j$ at the faulty scales would be only influenced by the presence of fault and therefore contribute to spectrum of the $\mathcal{Q}$ index. In this situation, one may identify peaks at frequencies equal to twice the actual frequencies of faults. The hardest case would turn out when multiple faults are located in a single scale or there exists more than one fault at a scale. The $\mathcal{Q}$ index spectrum in this situation would include more peaks than the number of faults. This is due to the fact that $\mathcal{Q}$ index is calculated using the *squared* value of the error ($\tilde{\mathbf{x}}_i^2$) which creates redundant overlapping frequencies [2].

Another fascinating phenomena captured by the aid of spectrum analysis of the $\mathcal{Q}$ index is to extract the envelop properties of the fault in case the fault has cyclic and modulating characteristics. This feature would be monitored with the aid of this new finding. This enhances the capabilities of the MSPCA algorithms and make them suitable for fault diagnosis applications of other mechanical systems. Envelope analysis calculates the envelope of the signal. In order to detect the envelope of a signal, the corresponding analytic format of that signal should be constructed using

[1] $\mathbf{WQ} = \sum_{i=1}^{m} \mathbf{W}\mathbf{q}_i = \sum_{i=1}^{m} \mathbf{W}\tilde{\mathbf{x}}_i^2$, respecting the above mentioned assumption and using the complex Fourier transform, the faulty variable in the residual space can be written as $\tilde{\mathbf{x}}_f = c\, e^{i\omega_f}$ and therefore $\tilde{\mathbf{x}}_f^2 = c\, e^{i2\omega_f}$. The DFT of $\tilde{\mathbf{x}}_f^2$ then is: $\mathbf{W}\tilde{\mathbf{x}}_f^2$ which peaks at the frequency of $2\omega_f$.

[2] in case of multiple faults in a single scale or a fault with multiple harmonics the $\tilde{\mathbf{x}}_f$ is then written in form of complex Fourier transform as follows: $\tilde{\mathbf{x}}_f = c_1\, e^{i\omega_{1f}} + c_2\, e^{i\omega_{2f}} + \ldots + c_p\, e^{i\omega_{pf}}$ where p is the number of components. Hence $\tilde{\mathbf{x}}_f^2 = (c_1\, e^{i\omega_{1f}} + c_2\, e^{i\omega_{2f}} + \ldots + c_p\, e^{i\omega_{pf}})^2$. The DFT of $\tilde{\mathbf{x}}_f^2$ then is: $\mathbf{W}\tilde{\mathbf{x}}_f^2$ which peaks at frequencies of $2\omega_{1f},\ 2\omega_{2f}, \ldots,\ 2\omega_{pf}$ and mutual combination frequencies, they are: $(\omega_{if} + \omega_{jf})$ for any different $i, j \in \{1, 2, \ldots, p\}$.

Hilbert transform. Analytic signal is a complex signal which its real component is the original signal and its imaginary component is the Hilbert transform of the original signal. The envelope is then equal to the magnitude of the analytic signal. Hilbert transform for a continuous time function is defined as follows:

$$\mathcal{H}(s(t)) \;=\; s(t) \star \frac{1}{\pi t}$$

where $\star$ refers to the convolution product. The envelope of a discrete signal $s(k)$, k is the sample number, is mathematically defined as:

$$e(k) \;=\; \sqrt{s(k)^2 \;+\; \mathcal{H}(s(k))^2} \tag{4.13}$$

where $\mathcal{H}(s(k))$ is the Hilbert transform of signal $s(k)$. Hilbert transform technically creates a version of the signal $s(k)$ that its phase has been shifted by $\pi/2$. Rewriting the above equation in vector format, the spectrum of the squared envelope would be obtained through: $\mathbf{We}^2 \;=\; \mathbf{Ws}^2 \;+\; \mathbf{WH}_s^2$ where $\mathbf{e}^2$ is the vector of squared envelope values, $\mathbf{s}^2$ is the vector of values of the squared signal ($\mathbf{s}^2 = \mathbf{s} \circ \mathbf{s}$), and $\mathbf{H}_s$ is the vector containing the Hilbert transform of the signal, ($\mathbf{H}_s^2 = \mathbf{H}_s \circ \mathbf{H}_s$). Taking this point into account that the Hilbert transformation of a discrete signal is the 90 degree phase shifted version of that signal, the Fourier transformation of a signal and its Hilbert transform would be akin in amplitude but would have different phase [3]. Therefore the DFT of the squared signal, i.e. $\mathbf{s}^2$ would capture the contents of the DFT of the squared envelope, but not the vice versa necessarily. Considering this statement and the derivation of the D FT of the $\mathcal{Q}$ remarked above, the following corollary can be

[3] considering the definition of the Hilbert transform, its Fourier transform would be equal to: $s_H(\omega) = s(\omega)(-jsgn(\omega))$ where s_H is the Hilbert transform of s and $sgn()$ is the sign function. Therefore magnitudes of $s_H(\omega)$ and $s(\omega)$ are equal but their phases are different.

made:

Corollary 4.2.1 *If anomaly or fault possesses harmonic characteristic and is detected by the $\mathcal{Q}$ index, the spectrum of the $\mathcal{Q}$ index captures the contents of the spectrum of the faulty variable squared. In case this type of fault is repeated periodically, then the spectrum of the $\mathcal{Q}$ index captures the contents of the spectrum of squared envelope of the faulty variable.*

Proof: Assuming that the fault is harmonic and it only happens in one variable, for example variable x_j where $j \in \{1, 2, \ldots, m\}$. Furthermore, lt is assumed that fault is detected by the $\mathcal{Q}$ index. Therefore $\tilde{\mathbf{x}}_j$ should have the most contribution to the total value of the $\mathcal{Q}$ index. Consequently, the investigation would be limited to the $\mathbf{q}_j = \tilde{\mathbf{x}}_j^2$. Considering equations 3.11 and 3.14, the following relationship can be derived:

$$\tilde{\mathbf{X}} = [\ \tilde{\mathbf{x}}_1, \ldots, \tilde{\mathbf{x}}_j, \ldots, \tilde{\mathbf{x}}_m\ ] = \mathbf{X}\ [\ \tilde{\mathbf{c}}_1, \ldots, \tilde{\mathbf{c}}_j, \ldots, \tilde{\mathbf{c}}_m\ ]$$

therefore $\tilde{\mathbf{x}}_j = \mathbf{X}\tilde{\mathbf{c}}_j$, where $\tilde{\mathbf{x}}_j$ and $\tilde{\mathbf{c}}_j$ are vectors of the size $n \times 1$ and $m \times 1$ respectively [4]. Therefore the vector $\mathbf{q}_j$ would be equal to $\mathbf{q}_j = \tilde{\mathbf{x}}_j \circ \tilde{\mathbf{x}}_j$. This equation can be expanded as follows:

$$\mathbf{q}_j = [\ (\mathbf{X}(1)\ \tilde{\mathbf{c}}_j)^2, \ldots,\ (\mathbf{X}(k)\ \tilde{\mathbf{c}}_j)^2, \ldots,\ (\mathbf{X}(n)\ \tilde{\mathbf{c}}_j)^2\ ]^T$$

where $\mathbf{X}(k)$ is the k^{th} row of matrix $\mathbf{X}$. Expanding the terms at each row of vector $\mathbf{q}_j$, this vector can be written as summation of $\frac{m(m+1)}{2}$ vectors. One of them is the following vector: $[\ x_j^2(1)\ \tilde{\mathbf{c}}_{j,j}^2, \ldots,\ x_j^2(k)\ \tilde{\mathbf{c}}_{j,j}^2, \ldots,\ x_j^2(n)\ \tilde{\mathbf{c}}_{j,j}^2\ ]^T$. Here, $x_j^2(k)$ is squared of the value of the variable x_j at the time instant k and $\tilde{\mathbf{c}}_{j,j}$ is the j^{th} element of the vector $\tilde{\mathbf{c}}_j$. Discrete Fourier transform of $\mathbf{q}_j$ is $\mathbf{W}\mathbf{q}_j$ which is actually the summation of $\frac{m(m+1)}{2}$

[4] To recap, n is number of samples and m is number of variables.

spectra of its underlying vectors. One of them is the vector derived above which is constituted by the faulty variable x_j, i.e.: $\mathbf{W}[\ x_j^2(1)\ \tilde{\mathbf{c}}_{j,j}^2, \ldots,\ x_j^2(k)\ \tilde{\mathbf{c}}_{j,j}^2, \ldots,\ x_j^2(n)\ \tilde{\mathbf{c}}_{j,j}^2\ ]^T$. Therefore, one can safely draw a conclusion that the spectrum of the $\mathcal{Q}$ index includes the spectral contents of the faulty variable squared. As it is derived in the envelope analysis, the spectrum of the squared signal includes the contents of the spectrum of the squared envelope. Comparing this with the conclusion made above, it is obvious that spectrum analysis of $\mathcal{Q}$ index actually contains the spectral content of the squared envelope of the faulty variable. This is observable in case of periodic harmonic faults.

This is an important and useful result which demonstrates that the principal components analysis can be used for diagnosis of complex faults. Another important conclusion is that the MSPCA besides performing denoising (by selecting only significant variables at score domain as well as significant scales at scale domain), data compression (likewise), monitoring, diagnosis (fault isolation with RBC analysis) can perform envelope analysis, sort of, as well. Practically, this makes MSPCA a viable tool for diagnosis of rolling bearing faults in systems with multiple bearings or components. In cases that this type of fault is strong enough to violate the $\mathcal{T}^2$ statistic upper control limit, the spectrum analysis of the $\mathcal{T}^2$ index reveals useful information as well. One can see the envelope frequency and its harmonics in the spectrum of $\mathcal{T}^2$ statistic too. Assuming that the $\mathcal{T}^2$ is denoted by the vector:

$$\mathcal{T}^2 = \sum_{i=1}^{A} \mathcal{T}_i^2$$

then the DFT of the $\mathcal{T}^2$ can be written as:

$$\mathbf{W}\mathcal{T} = \sum_{i=1}^{A} \mathbf{W}\mathcal{T}_i^2$$

where the vector $\mathcal{T}_i^2$ is of size $n \times 1$ and includes the squared of the scores of n samples mapped on the principal axis i which has the corresponding eigenvalue of λ_i. One should note that this spectrum is determined based on the transformation of all variables to the feature (scores) domain by only taking the first A major components. The scores matrix therefore can be rewritten based on its constituting vectors, that is:

$$[\ \mathbf{T}_1\ \ \mathbf{T}_2\ \ \ldots\ \ \mathbf{T}_m\ ] = \mathbf{X}\,[\ \mathbf{P}_1\ \ \mathbf{P}_2\ \ \ldots\ \ \mathbf{P}_m\ ]$$

therefore the $\mathcal{T}_i^2 = (\mathbf{T}_i \circ \mathbf{T}_i) \circ \mathbf{I}_{\lambda_i} = (\mathbf{X}\mathbf{P}_i \circ \mathbf{X}\mathbf{P}_i) \circ \mathbf{I}_{\lambda_i}$ where $\mathbf{I}_{\lambda_i} = \frac{1}{\lambda_i}[1\ 1\ 1\ \ldots\ 1]^T$ is a $n \times 1$ vector. Due to definition of the Hadamard product, one can observe that each element of the $\mathcal{T}_i^2$ is comprised of the summation of squared values of variables at the corresponding instant. Consequently the spectrum of $\mathcal{T}^2$ is technically the summation of weighted spectra of the squared and mutual product of variables mapped to the score space along different principal axes. The weightings are determined by the transformation matrix $\mathbf{P}$ and inverse of matrix $\mathbf{\Lambda}$ which are basically the eigenvectors and eigenvalues of the covariance matrix of the data. As is discussed above, this feature enables one to observe the frequency content of the envelope spectrum in the spectrum of the $\mathcal{T}^2$ index. It is shown so far that the spectra of $\mathcal{Q}$ and $\mathcal{T}^2$ indices contain the information that one may get by applying the envelope analysis on the faulty variable in case the fault has cyclic and modulating properties. In other situations, these spectra indicate the frequency characteristics of the fault. This is an extremely useful tool for fault identification as it is demonstrated in the bearing fault diagnosis example in the next chapter.

Covariance-based indices:

In order to investigate the fault detectability and identification with recon-

struction based contribution analysis, the measured variables matrix $\mathbf{X}$ are usually modeled as a linear combination of matrix $\mathbf{X}^*$ which represents the normal operating condition data and additional fault $\mathcal{F}$, that is [47]:

$$\mathbf{X} \;=\; \mathbf{X}^* \;+\; \mathcal{F} \tag{4.14}$$

$\mathbf{X}^*$ is unknown when a fault has occurred. In the case of baseline data [5], one may assume that the system is operating under normal condition and consequently the measurement matrix $\mathbf{X}$ and $\mathbf{X}^*$ coincides. Therefore the loading matrix $\mathbf{P}$ is essentially determined based on the $\mathbf{X}^*$. According to the equation 3.1, the PCA transformation for testing data $\mathbf{X}$ would be:

$$\mathbf{T} \;=\; \mathbf{XP} \tag{4.15}$$

In order to perform statistical process monitoring (SPM) using $\mathcal{Q}$ and $\mathcal{T}^2$ statistics, variables are assumed to be random and follow a multivariate normal distribution [42, 48, 50]. Considering this condition, performing statistical analysis of the scores may be a reasonable measure for further investigation in the score (feature) domain. Indeed, this has already been considered in the PCA by looking at the eigenvalues of scores which are technically the variance along each principal component axis. The covariance matrix in the score domain can then be calculated as follows:

$$COV(\mathbf{T}) \;=\; E(\mathbf{T}\mathbf{T}^T) \;-\; E(\mathbf{T})E(\mathbf{T})^T \tag{4.16}$$

$$\;=\; E(\mathbf{X}\mathbf{P}\mathbf{P}^T\mathbf{X}^T) \;-\; E(\mathbf{X}\mathbf{P})E(\mathbf{X}\mathbf{P})^T \tag{4.17}$$

[5] assuming that baseline data and testing data are collected under (almost) similar running condition

Modeling a fault in an additive form, one gets $\mathbf{X} = \mathbf{X}^* + \mathcal{F}$, substituting this equation into relationship 4.17 and rearranging, the covariance matrix is obtained as:

$$\begin{aligned} COV(\mathbf{T}) &= E(\mathbf{X}^*\mathbf{P}\mathbf{P}^T\mathbf{X}^{*T}) + E(\mathcal{F}\mathbf{P}\mathbf{P}^T\mathcal{F}^T) \\ &\quad + E(\mathbf{X}^*\mathbf{P}\mathbf{P}^T\mathcal{F}^T) + E(\mathcal{F}\mathbf{P}\mathbf{P}^T\mathbf{X}^{*T}) \end{aligned} \tag{4.18}$$

It should be noted that $\mathbf{X}^*$ and $\mathcal{F}$ are the only stochastic elements. In order to simplify this relationship, it is assumed that the system variables under normal operating condition are independent from the fault variables organized in the matrix $\mathcal{F}$. This is a valid assumption in some cases such as a sensor drift or other sensor faults in general. If this assumption does not hold, then additional terms would appear in the following equations as shown in Appendix C. Since the data matrix has already been normalized and centered, its expectation ($E(\mathbf{X})$) for each variable can be approximated to be zero, therefore $E(\mathbf{X}^*) = -E(\mathcal{F})$. Taking these two points into consideration, the above equations may be simplified to the following one:

$$\begin{aligned} COV(\mathbf{T}) &= E(\mathbf{X}^*\mathbf{P}\mathbf{P}^T\mathbf{X}^{*T}) - E(\mathbf{X}^*\mathbf{P})E(\mathbf{X}^*\mathbf{P})^T \\ &\quad + E(\mathcal{F}\mathbf{P}\mathbf{P}^T\mathcal{F}^T) - E(\mathcal{F}\mathbf{P})E(\mathcal{F}\mathbf{P})^T \\ &= COV(\mathbf{X}^*\mathbf{P}) + COV(\mathcal{F}\mathbf{P}) \\ &= \mathbf{\Lambda} + COV(\mathcal{F}\mathbf{P}) \end{aligned} \tag{4.19}$$

denoting $\mathbf{\Lambda}_T = COV(\mathbf{T})$ as the covariance matrix of the scores of the testing data, the above relationship can be simplified as:

$$\mathbf{\Lambda}_T = \mathbf{\Lambda} + COV(\mathcal{F}\mathbf{P}) \tag{4.20}$$

This is an important relationship. Regarding the PCA model, the model was derived for the system working under normal conditions, hence the $COV(\mathbf{X}^*\mathbf{P})$ would be equal to the covariance of the scores of the baseline data which is equal to $\mathbf{\Lambda}$. The whole idea behind doing PCA analysis is to analyze the multivariate data in a domain in which the variables are uncorrelated, thus the matrix $\mathbf{\Lambda}$ calculated using normal operation data would be diagonal. An immediate deduction would be that all off-diagonal elements of the $\mathbf{\Lambda}_T$ matrix are indeed due to the fault though its diagonal elements would be affected as well. Fault was presumed to be additive but it may actually be subtractive. So the sign of off-diagonal elements can be changed in the way the fault has been modeled. A subtle measure would be to define an index which correlates these changes in the covariance of the score matrix to the magnitude and severity of the fault. Considering the latter discussion, an index called scores covariance index and denoted by S_c is defined as:

$$S_c = \sum_{i=1}^{m} \frac{\sum_{i=1}^{m}(\mathbf{\Lambda}_T - \mathbf{\Lambda}) \circ (\mathbf{\Lambda}_T - \mathbf{\Lambda})}{\lambda_i} \tag{4.21}$$

where $\circ$ refers to Hadamard (or entry-wise) product. Since the covariance matrix is symmetric with respect to the main diagonal, thus it does not matter that the summation operators are applied column-wise or row-wise. The S_c index is a single number that indicates the presence and magnitude of a fault. When it comes to MSPCA, the S_c index can be used to identify which scale is more influenced by a fault and therefore can be used for fault localization in the scale domain. This works as a complementary simple approach besides investigating statistical indices plots at each scale. S_c is defined based on the quantities in the score domain (principal component or feature domain), therefore one cannot deduce any information about the faulty variable. Further elaboration is required to assess the contribution of each

variable to this index and therefore come up with a new fault isolation approach. Taking advantage of the covariance properties, one may further manipulate equation 4.20 to obtain an estimation of the fault covariance, as follows:

$$COV(\mathcal{F}) \;=\; \mathbf{P}(\mathbf{\Lambda}_T \;-\; \mathbf{\Lambda})\,\mathbf{P}^T \tag{4.22}$$

Having approximated the fault covariance (given earlier assumption) another index for measuring the contribution of each variable to the magnitude of fault can be defined using the above relationship. It is simply defined to be the summation of squared elements of the fault covariance matrix weighted by the inverse of the variance vector of the wavelet coefficients:

$$F_{c,j} \;=\; (\sum_{i=1}^{m} COV(\mathcal{F}) \circ COV(\mathcal{F})) \circ \Sigma_j \tag{4.23}$$

where Σ_j is the vector of inverse values of the variance of wavelet coefficients at scale j. Given that each scale includes contents of the signal at a particular frequency band, the variance of the wavelet coefficients at the corresponding scale is proportional to the energy of the stochastic signal at that scale, which is represented in the power spectrum of the filtered signal [6]. Since matrix $COV(\mathcal{F})$ is symmetric, the summation operation can be implemented either row-wise or column-wise.

In the MSPCA, one can use S_c for indicating the faulty scale and F_c for isolating the faulty variable. F_c can be normalized to have the maximum of unity to facilitate the comparison between contribution values. These new covariance based indices were used for fault localization and isolation as illustrated in chapter 5. The new S_c and F_c indices as well as spectrum analysis of the statistical indices can be appended

[6] for instance in the case of white noise, since the energy of signal is equally distributed over different frequency ranges, the variance of the wavelet coefficients is constant at all scales.

to the CAD-MSPCA technique as well.

Chapter 5

Results and Discussions

The techniques explained and developed in chapter 4 have been applied on several illustrative examples as well as real measurement and experimental data. The results confirm the capabilities of the multi-scale PCA techniques for fault diagnosis of complex systems like a V8 engine. The new developments made through this thesis were examined as well. Examples and systems investigated in this chapter demonstrate how these proposed tools can be used for fault detection and variable contribution estimation at each scale of the MSPCA algorithm. Furthermore, it is shown that one can extract more information on faults by investigating the spectrum of $\mathcal{Q}$ and $\mathcal{T}^2$ statistics. The overall confidence limits are set to 99% in all examples discussed in this chapter. This chapter is comprised of three sections, the multi-scale PCA is applied on several fault cases simulated in an illustrative uncorrelated variables example. It is then followed by employing this technique for fault diagnosis of two mechanical systems; namely a bearing fault in a DC motor and a collapsed lash adjuster fault in a valve train of a V8 engine.

5.1 Illustrative Examples

There are typical published examples used in simulation studies for verifying performance of multivariate fault diagnosis techniques. These examples taken from Bakshi are accounted to illustrate the performance of the multi-scale PCA with new developments for several types of faults, [9]. Faults may be observed in all variables or only some of them; they may be localized in a single frequency band or be more complex and appear in multiple frequency bands as well. In this study the case of

multiple-faults was considered and simulated too. The measured data matrix $\mathbf{X}$ includes four variables contaminated by uncorrelated measurement noise of zero mean and variance of 0.04. The first two variables are Gaussian noise with zero mean and unit variances. The other two variables are formed by adding and subtracting the first two ones. They are shown in the following equations:

$$\mathbf{X}(t) = [\ \mathbf{x_1}\ \ \mathbf{x_2}\ \ \mathbf{x_3}\ \ \mathbf{x_4}\ ]\ +\ 0.2\ \mathbf{N}(\mathbf{0}, \mathbf{I}) \tag{5.1}$$

where

$$\mathbf{x_1}(t) = \mathbf{N}(0, 1) \tag{5.2}$$

$$\mathbf{x_2}(t) = \mathbf{N}(0, 1) \tag{5.3}$$

$$\mathbf{x_3}(t) = \mathbf{x_1}(t)\ +\ \mathbf{x_2}(t) \tag{5.4}$$

$$\mathbf{x_4}(t) = \mathbf{x_1}(t)\ -\ \mathbf{x_2}(t) \tag{5.5}$$

The data matrix $\mathbf{X}$ has 4096 data points sampled at a frequency of 8192Hz. This data is the baseline used for deriving the in-control model and the correlation structure between variables. The following fault scenarios are then simulated by manipulating this matrix. The cases are considered as follows:

- Case 1: unit bias in all variables.
- Case 2: unit bias in one variable.
- Case 3: fault with a localized frequency content.
- Case 4: repeated fault with a localized frequency content.
- Case 5: multiple fault situation with localized frequency contents.

These cases are discussed separately in the following sections.

Case 1: Unit bias in all variables

The abnormality is a mean shift of unity in all variables between the sample numbers 524 to 824. The modified MSPCA technique was applied for detection. The total $\mathcal{Q}$ and $\mathcal{T}^2$ statistics were determined initially to identify whether there is an abnormality in the signals. Violation of detection limits indicates the presence of a new fault that did not previously exist in the healthy data set. One can further analyze the problem by examining the plots of these statistical indices as well as the φ statistics at different scales. The scale that has the most contribution to the final values is the one that captures the most energy of the fault (new changes in the time series), therefore it provides us with an extremely useful tool to localize the fault in the scale domain (wavelet domain). Subsequently one may use the relationship between each scale and frequency range of the applied band-pass filter to localize the content of this additional signal component in the frequency domain as well. Reconstruction based contribution bar charts indicate the contribution of each variable to the relevant statistical index at the scale influenced by the fault. Putting these tools together, one can detect a fault, extract its features in the frequency domain and identify the faulty variable. Charts obtained by estimating the covariance matrices of scores, (S_c and F_c indices), are additional tools for fault localization in the scale domain and contribution analysis. Figure 5.1 shows the results obtained by applying the modified MSPCA technique on the case 1 data. The total statistical indices detect the presence of a fault between samples 520 and 811. Either by checking out the statistical indices charts at each scale one by one or looking at the S_c index , depicted in figure 5.3 charts, one may readily localize the fault to the approximation scale (scale 6) in the scale domain. Figure 5.2 demonstrates the φ index in approximation scale. One can clearly see that this index exceeds the upper control limit in the sample interval ranging from 520 to 810. Furthermore, RBC chart calculated based on the φ

statistic at approximation scale, depicted in figure 5.4, shows that almost all variables contribute to the fault in the time span that it occurs. The same observation can be made by assessing the F_c index shown in figure 5.5. Therefore, one may safely deduce that all of the variables have been affected by the abnormal disturbance.

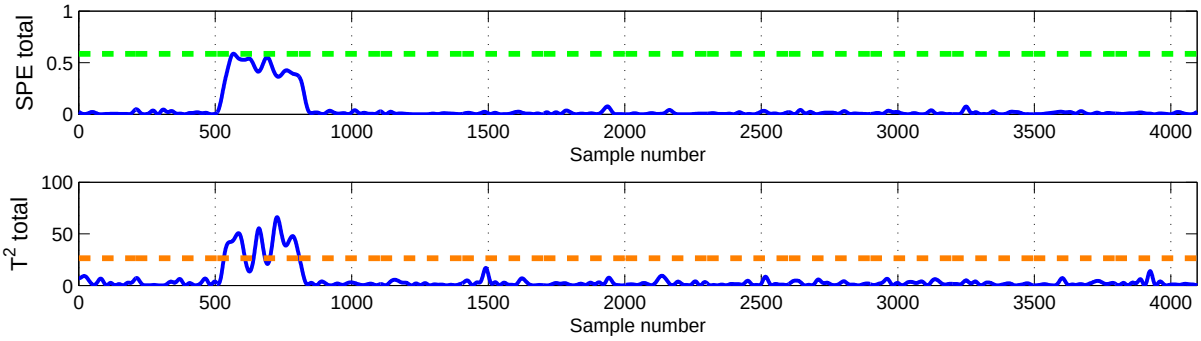

Figure 5.1: The total $\mathcal{Q}$ and $\mathcal{T}^2$ statistics

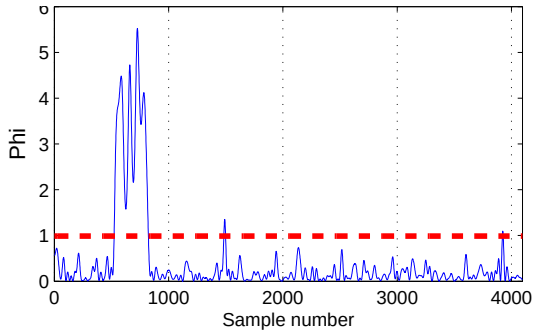

Figure 5.2: φ statistic computed at the coarsest scale (approximation), case 1 fault condition

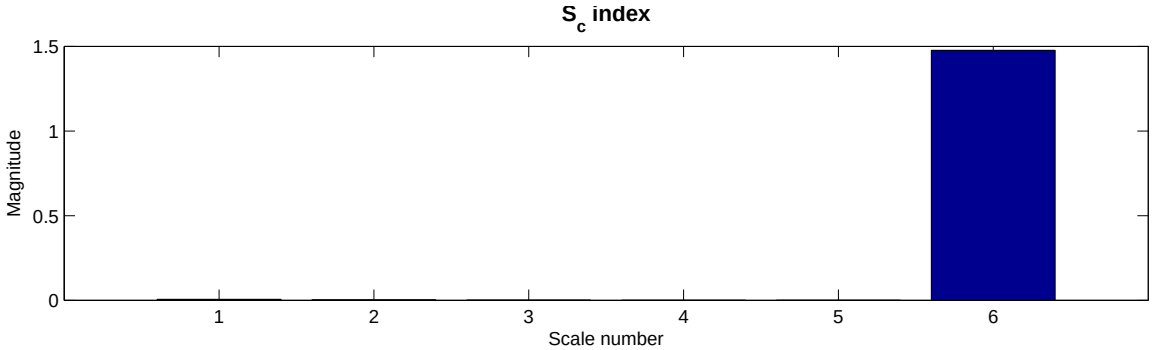

Figure 5.3: S_c index at different scales, case 1 fault

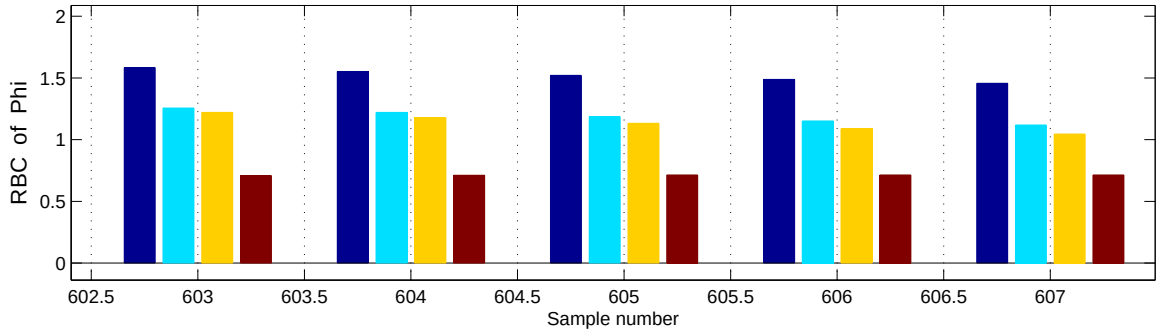

Figure 5.4: RBC plot determined based on the φ statistic, magnified around instances in the faulty interval, case 1 fault condition. Four colors represents all four variables (blue:variable 1, cyan:variable 2, yellow: variable 3, red: variable 4) and they all present with comparable amplitudes.

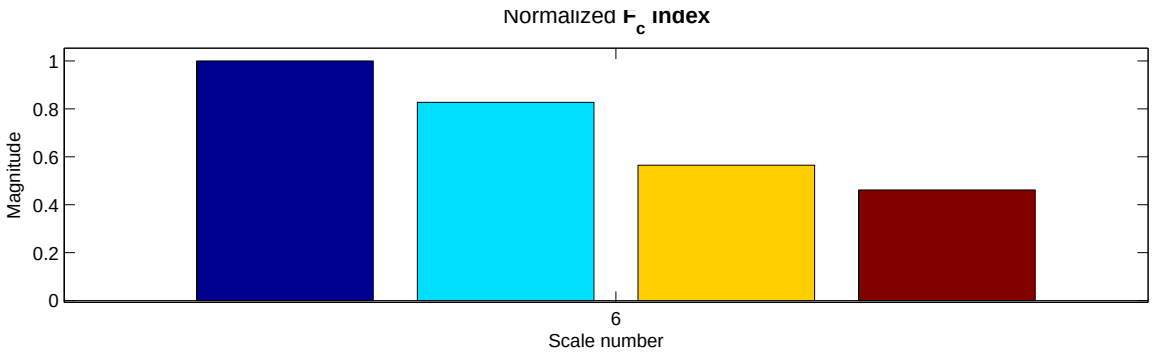

Figure 5.5: F_c index at approximation scale (scale 6), case 1 fault

Further to chapters 2 and 4, the coiflet wavelet of order five with a decomposition depth of five was selected for the Mod-MSPCA algorithm.

Case 2: Unit bias in one variable

The abnormality is a mean shift of unity that happens in one variable only, it's assumed that variable number three is the one that undergoes unit bias between sample number 524 to 824. The results obtained by applying the modified MSPCA technique were plotted in figures 5.6 to 5.10. The total $\mathcal{Q}$ and $\mathcal{T}^2$ statistics shown in 5.6 identified the presence of a fault. The S_c index reveals that the fault is dominant

in the approximation scale, see figure 5.9. This result is confirmed by inspecting the statistical charts at each scale one by one. Reconstruction based contribution analysis for any of these indices points to the third variable as being source of deviation, see figure 5.8. The F_c contribution bar chart as shown in figure 5.10 identifies the third variable containing the fault signature likewise the RBC technique.

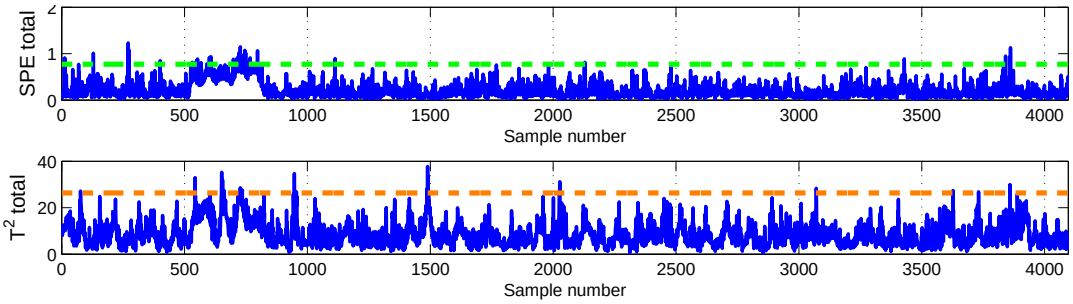

Figure 5.6: The total $\mathcal{Q}$ and $\mathcal{T}^2$ statistics, case 2 fault condition

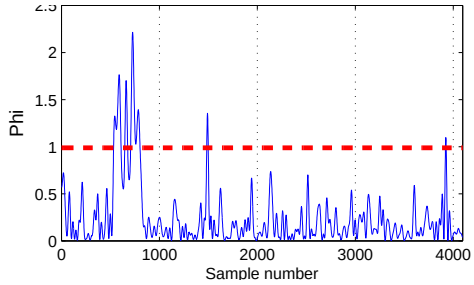

Figure 5.7: φ statistic computed at the coarsest scale (approximation), case 2 fault condition

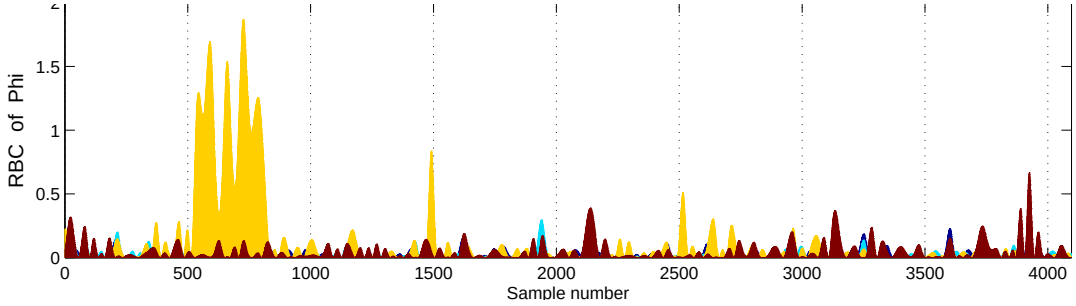

Figure 5.8: RBC plot determined based on the φ statistic, case 2 fault condition. The yellow bar refers to the variable number three

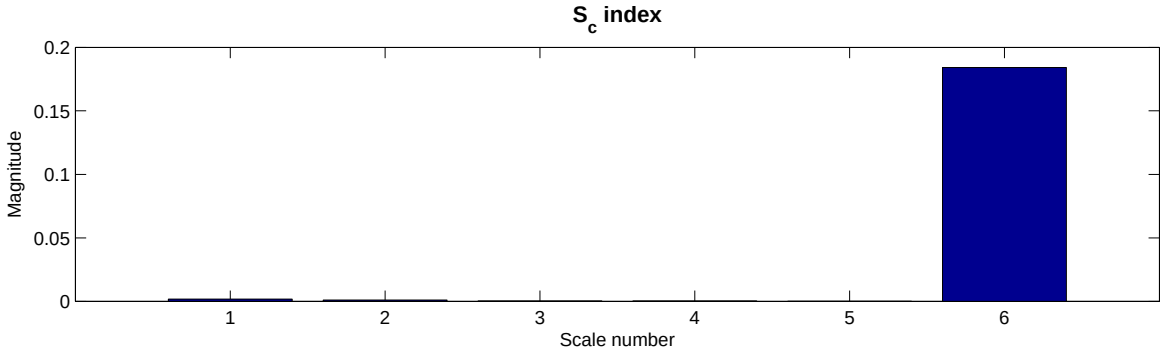

Figure 5.9: S_c index at different scales, case 2 fault.

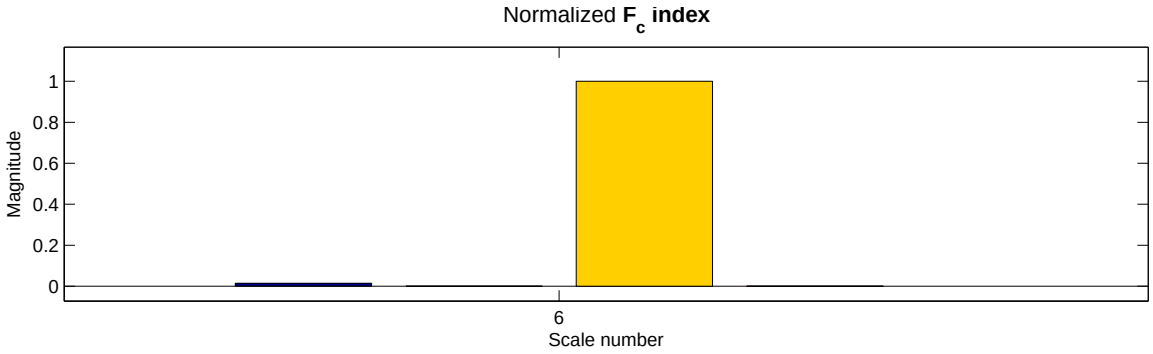

Figure 5.10: F_c index at approximation scale, case 2 fault. The yellow bar represents variable number three.

Case 3: Fault with a localized frequency content

This example is the simulation of an impulsive fault condition, that commonly occurs when there is an impact. The impulsive fault was simulated by the following equation and applied to one variable, namely the second variable, in the sample range of 500 to 1000:

$$\mathbf{s} \;=\; 3\ sin(\ 2\ \pi\ 330\ t)\ e^{(-20\ t)} \tag{5.6}$$

Like the previous cases, the total $\mathcal{Q}$ and $\mathcal{T}^2$ statistics specify whether there is a fault or not and can localize it in the time domain. Figure 5.12 shows that the fault is detected. The S_c index plotted in figure 5.14 indicates that fault is dominant in the

fourth scale. Taking in to consideration that the sampling frequency was 8192Hz, the fourth scale represents the contents of the signal in the frequency range of 256Hz to 512Hz. According to equation 5.6, this scale is the one that includes the fault frequency ,i.e. 330Hz. The statistical indices calculated at scale four confirm that a fault occurs at the sample number 500, strongly exceeding the detection limits. Reconstruction based contribution analysis for all statistical indices points to the second variable as the one that contributes most to the fault, as shown in figure 5.13. A similar fault isolation result was obtained by the aid of the F_c index bar chart as shown in figure 5.15.

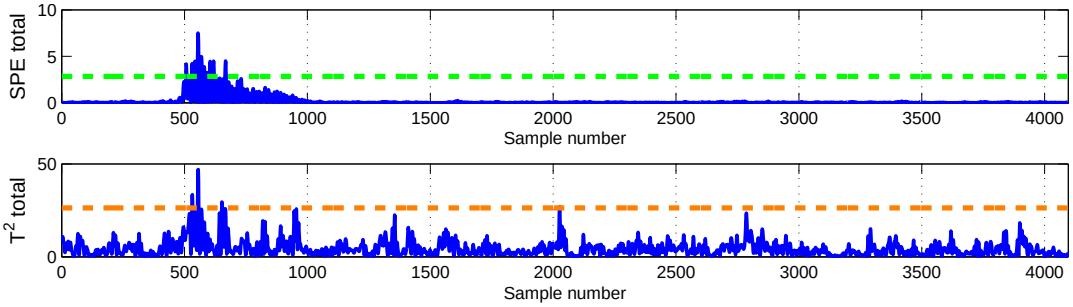

Figure 5.11: The total $\mathcal{Q}$ and $\mathcal{T}^2$ statistics, case 3 fault condition

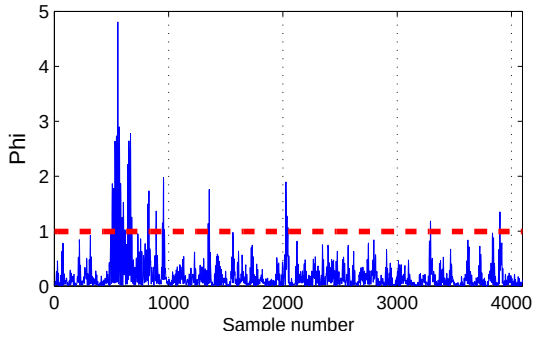

Figure 5.12: φ statistic computed at the scale 4, case 3 fault condition

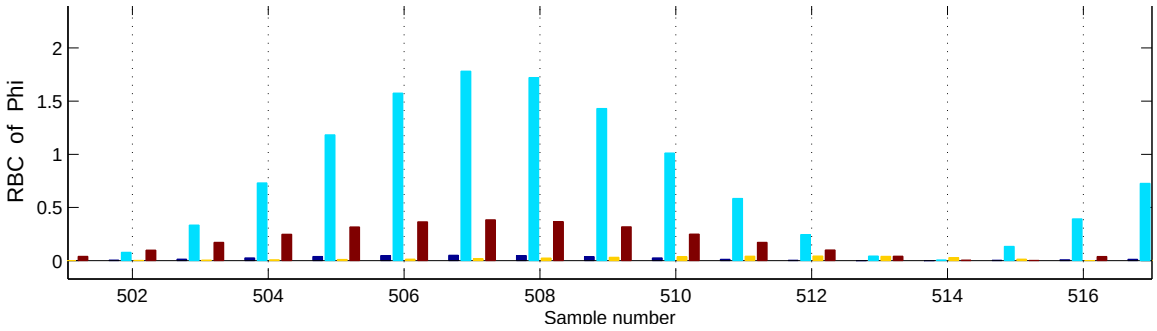

Figure 5.13: RBC plot determined based on the φ statistic at scale 4. Magnified around the sample number 500 where fault happens, case 3 fault condition.The bar in cyan blue color refers to the variable number two.

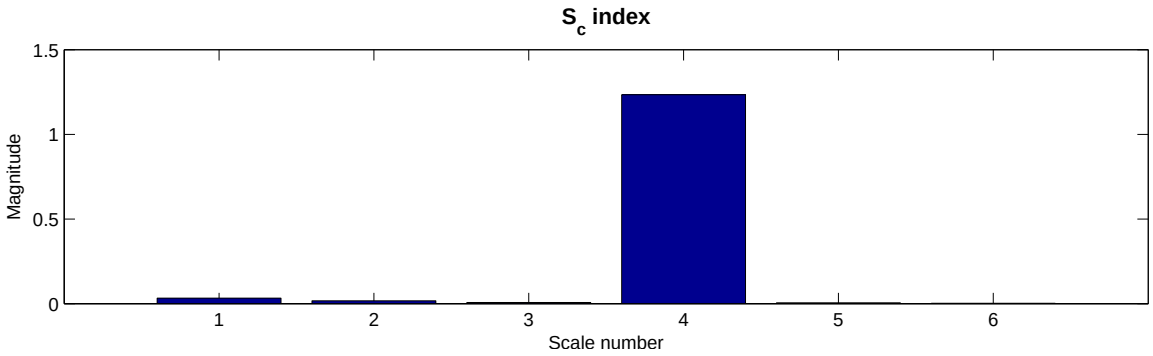

Figure 5.14: S_c index at all scales, case 3 fault condition.

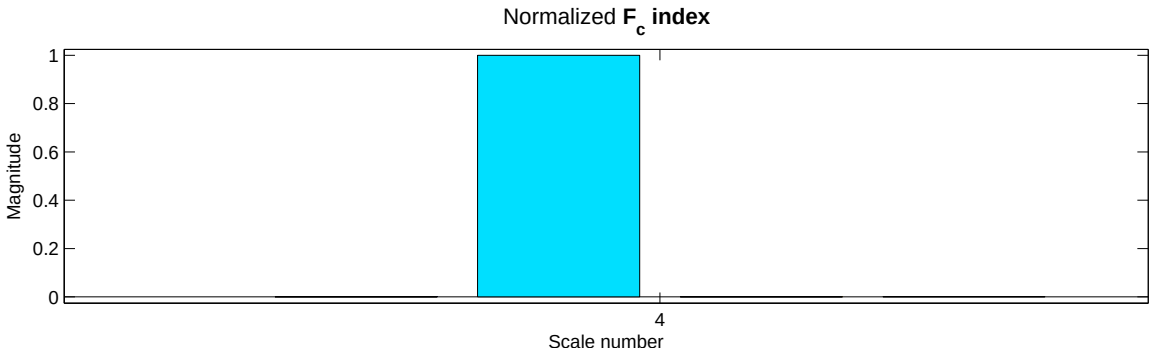

Figure 5.15: F_c index at scale 4, case 3 fault condition. The bar in cyan blue color refers to the variable number two

For the sensor bias faults simulated in cases 1 and 2, the bias is a constant added for a finite time period. It influences the deterministic part of the signal which

is extracted by the coarsest scale (scaling function) as it was observed in the covariance scores chart. In case 3 however, the fault signal has harmonic content and can be detected at any scale according to its spectrum. The new development explained in the chapter 4 can be used to further analyze the signals and extract more information about the fault. Figure 5.16 shows the spectrum of the squared signal of variable two. The ensuing figure, figure 5.17 depicts the spectra of the total $\mathcal{Q}$ and $\mathcal{T}^2$ statistics. The peak at 660Hz is evident in both the spectrum of the squared signal and the total $\mathcal{Q}$ statistic. The spectrum of the total $\mathcal{T}^2$ statistic shows some fluctuations and ripples around 660Hz but no clear peak exists. The 660Hz frequency is the double of the carrier frequency which was set as 330Hz. All in all, it's demonstrated that the spectra of the statistical indices contain harmonics equivalent to the spectrum of the squared signal as it was mathematically proven in chapter 4.

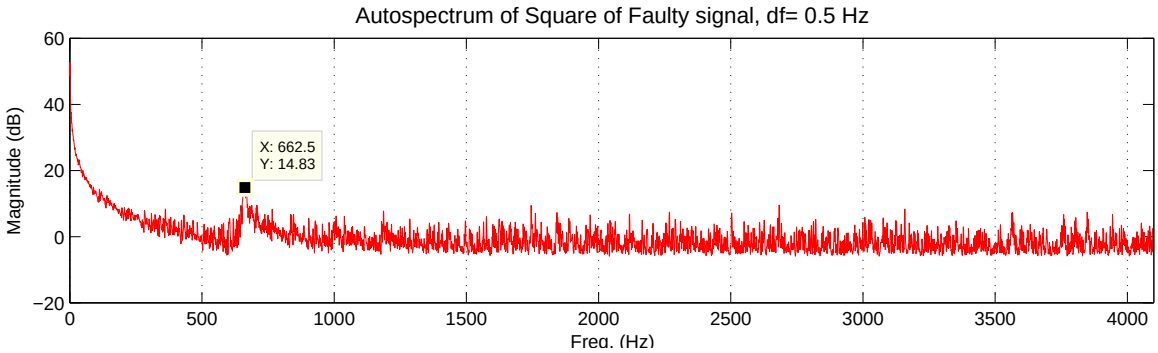

Figure 5.16: Spectrum of squared of signal of variable number 2, case 3 fault condition

Case 4: repeated fault with a localized frequency content

This example is an extension of the previous case and tries to investigate the performance of the developed technique for the periodic harmonic fault condition. Contrary to case 3 where the fault only occurred in the sample range of 500 to 1000, in this case the fault repeatedly happens. The fault frequency was increased to 1500Hz and the period of the fault is about 0.0244 seconds corresponding to 41Hz. This is an

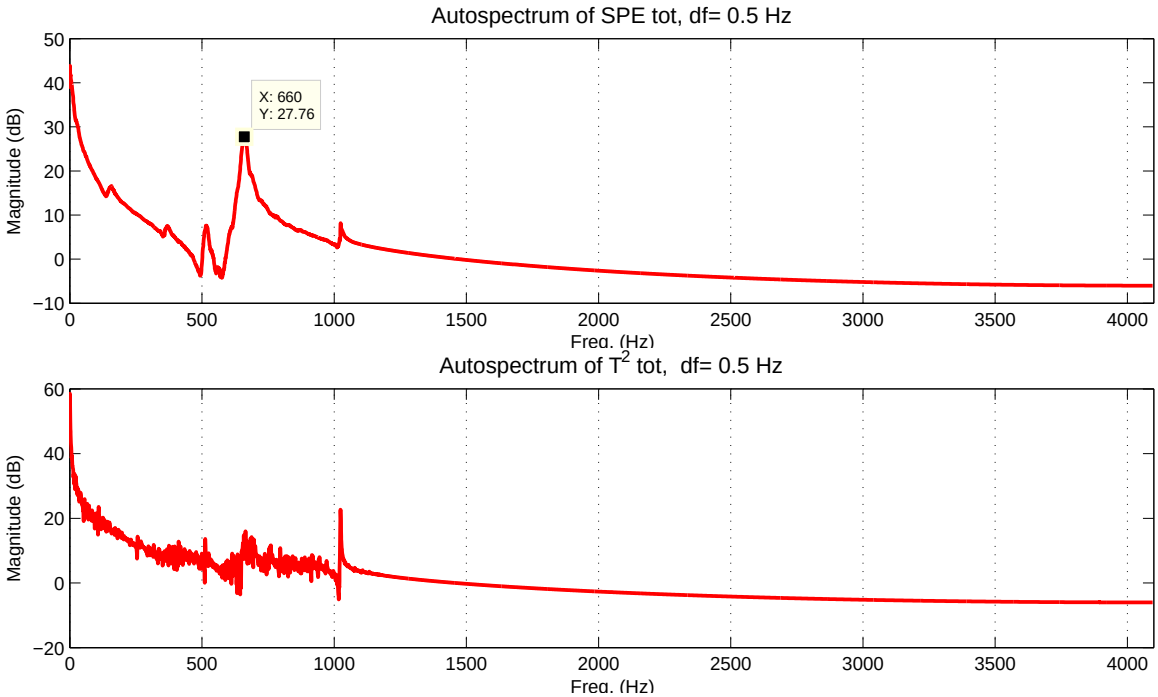

Figure 5.17: Spectrum of the total statistical indices, case 3 fault condition.

interesting example. This fault situation happens in many rotating machineries which have cyclic operations. Like the previous case, the fault happened in variable number two. The time series of the faulty signal along with the signal envelope are plotted in figure 5.18. The signal envelope was determined by calculating the absolute value of the Hilbert transform of the signal. This figure clearly shows that the period between envelope peaks is about 0.0244 second which is equal to the period that the fault was repeated in the time series. Applying the Mod-MSPCA technique, one can see that the total $\mathcal{Q}$ and $\mathcal{T}^2$ statistics charts detect the presence of the fault as well as the instants that it happened. The scores covariance index, see figure 5.20, estimates that the fault is localized in the first three scales mainly affecting the scale two content. This is in complete agreement with our expectation as the fault frequency was set to 1500Hz which locates at scale 2. Additionally, F_c contribution index, shown in figure 5.21, correctly indicates the variable number two as the faulty one. This result

is verified by the RBC chart zoomed in on one of the first instances that the fault was observed, see figure 5.22. In addition to these results, an utterly fascinating observation can be made by looking at the spectrum of the total $\mathcal{Q}$ and $\mathcal{T}^2$ statistics. These spectra as depicted in figure 5.24 consist of multiple peaks that are all integer orders of the 41HZ which is equivalent to the envelope frequency. The spectrum of the signal's envelop was shown in figure 5.23. The envelope frequency is technically the frequency that the fault is repeated. Tracking the orders to the higher frequency region, passing the 1000Hz frequency, one observes that these peaks deviate from integer factors of the 41Hz, some side lobes with comparable amplitudes show up as well. This variation was observed in a similar fault case but with a different carrier frequency. For instance the fault signal was re-produced but the tone frequency set to 300Hz. The spectra of the total $\mathcal{Q}$ and $\mathcal{T}^2$ statistics show that for harmonics in the vicinity and above 300Hz the side lobes appear and slowly change the peak frequencies from orders of the 41Hz to some other frequencies.

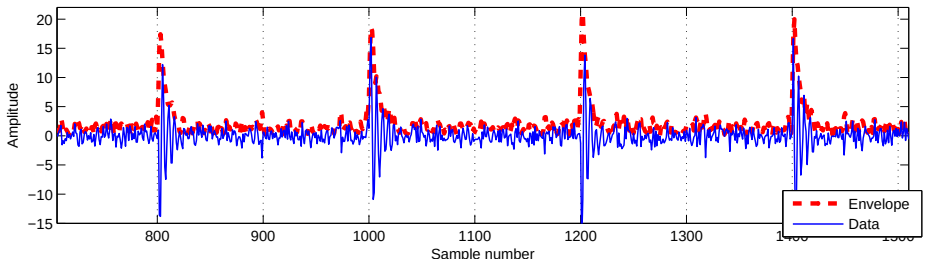

Figure 5.18: Time domain data and its associated envelope, case 4 fault condition.

Case 5: multiple fault situation with localized frequency contents

This example investigates the complex situation that multiple faults with different frequency contents occur. It is presumed that the faults fall in different wavelet scales. They may happen at the same time or different time instances. The simulation results showed that the technique is able to detect and diagnose the fault in both cases. The fault signals were generated using the same equations employed to

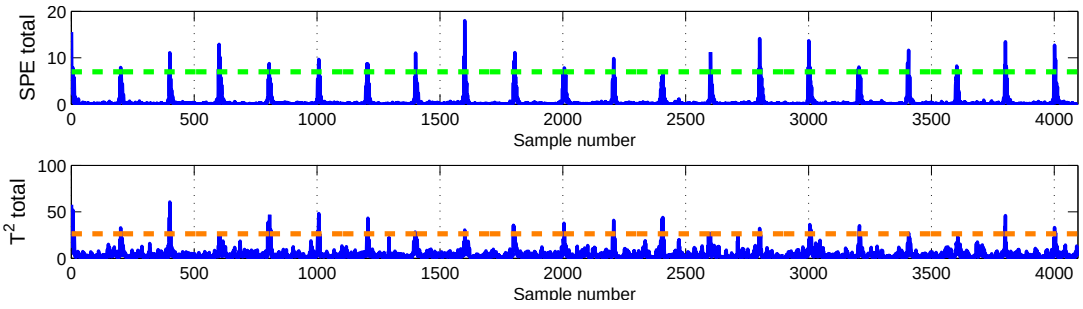

Figure 5.19: The total $\mathcal{Q}$ and $\mathcal{T}^2$ statistics, case 4 fault condition

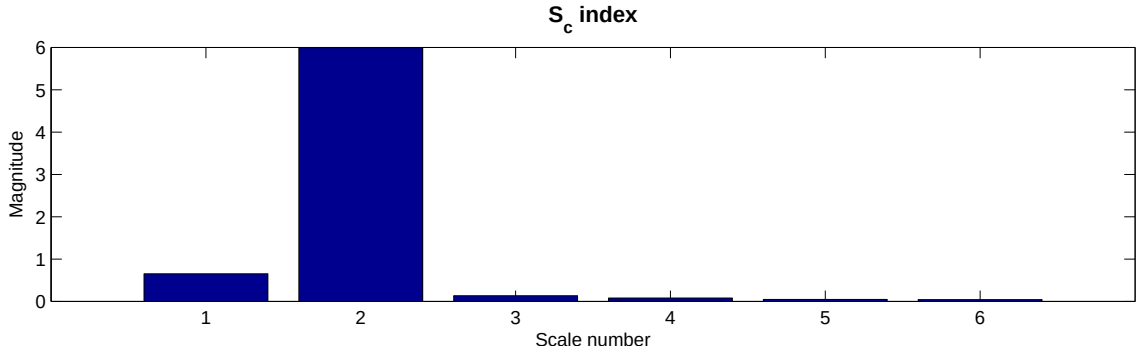

Figure 5.20: S_c index at all scales, case 4 fault condition.

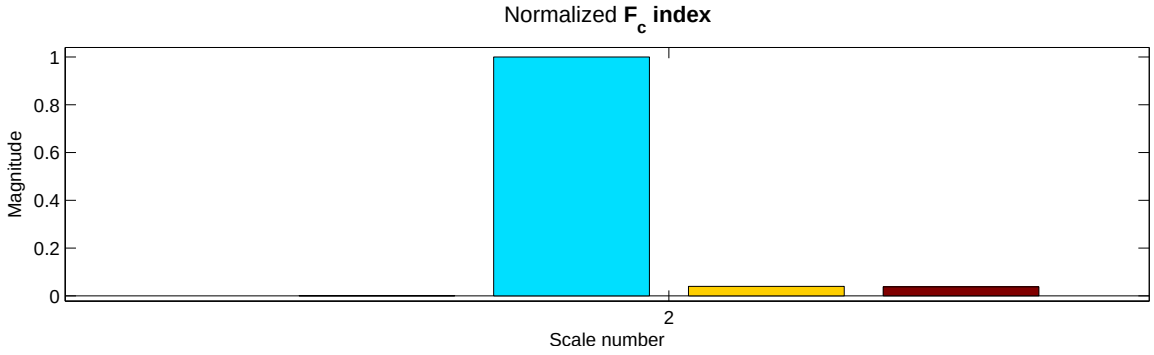

Figure 5.21: F_c index at scale two, case 4 fault condition. The cyan blue bar refers to the variable number two

simulate the fault in case 4. The high frequency fault occurs in the sample interval from 500 to 1000 in the second variable. It has the frequency content of 330Hz. The second fault is a decaying tone with a carrier frequency of 100Hz and its amplitude sets to be two thirds of the first fault. This fault is superimposed on the healthy signal through samples 700 to 1200 in variable number four. This situation simulates

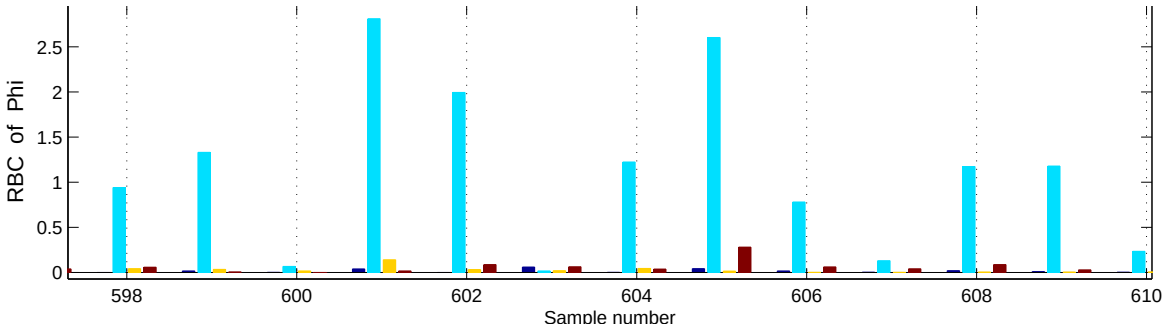

Figure 5.22: RBC chart computed based on the φ statistic at scale 2. It is magnified around one of the fault occurrence around sample number 600. Case 4 fault condition. The cyan blue bar refers to the variable number two

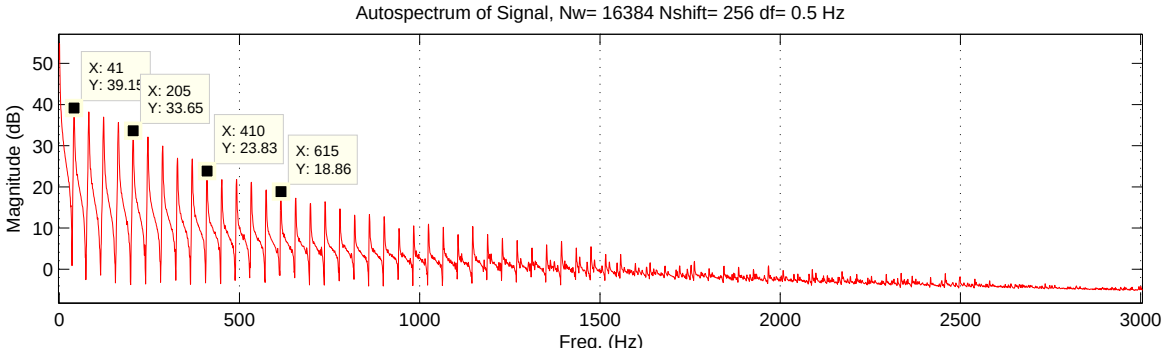

Figure 5.23: Spectrum of envelope of the variable number 2 signal, the fundamental frequency and its fifth and tenth harmonics are flagged, case 4 fault condition.

a simultaneous fault condition. The fault is only created and applied for one period. Like previous cases, the total $\mathcal{Q}$ and $\mathcal{T}^2$ statistics charts detect the presence of faults, see figure 5.25. The total $\mathcal{Q}$ index accurately peaks at the sample number 500 but it quickly decays and goes below the detection limit after the sample number 750. The total $\mathcal{T}^2$ statistic oscillates between sample numbers 500 and 1000 and exceeds the detection limit several times. The reason that they cannot detect the exact instant that the fault vanishes is that the SNR is small, about -2.5dB, for the tail of the impulsive fault. Checking the scales that statistical indices go beyond their limit reveals that scale number four and the approximation scale are the ones that are influenced by the faults. The S_c index chart shows the same result, see figure 5.26, there are

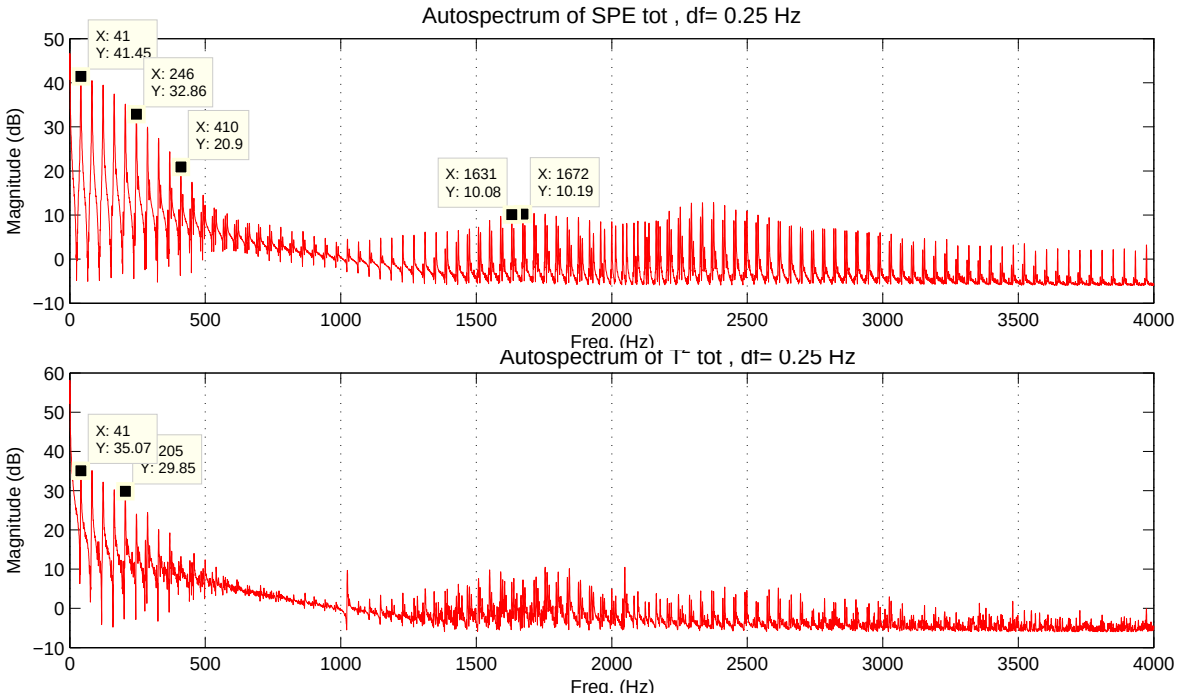

Figure 5.24: Spectrum of the total statistical indices, the fundamental frequency and its harmonics are flagged, case 4 fault condition.

peaks at the scales four and six (scale six corresponds to the approximation scale). An interesting observation is that the F_c contribution charts depicted in figures 5.27 and 5.28 indicate that variable number two in scale four and variable number four in scale six are those which have the maximum contributions associated with the fault at their scales respectively. Inspecting the RBC charts, these results are verified. The RBC of the φ statistic at scales four and six are depicted in figures 5.29 and 5.30. These plots are magnified around the samples 500 and 700 respectively. Spectra of the total $\mathcal{Q}$ and $\mathcal{T}^2$ statistics are depicted in figure 5.31. The spectrum of the total $\mathcal{Q}$ index evidently shows two peaks at the frequencies 200Hz and 660Hz whereas the spectrum of the total $\mathcal{T}^2$ statistic hardly indicates any peaks except some faint fluctuations about 200Hz and 660Hz. With respect to the spectrum of the total $\mathcal{T}^2$ statistic, the reason that the fault frequencies are not sharply present there can be due

to the nature of the fault that does not considerably affect the correlation structure between the variables and is mainly detectable in the residual space. Increasing the fault magnitude would enhance the influence of the fault in the total $\mathcal{T}^2$ statistic and make those peaks at 200Hz and 660Hz appear in the spectrum.

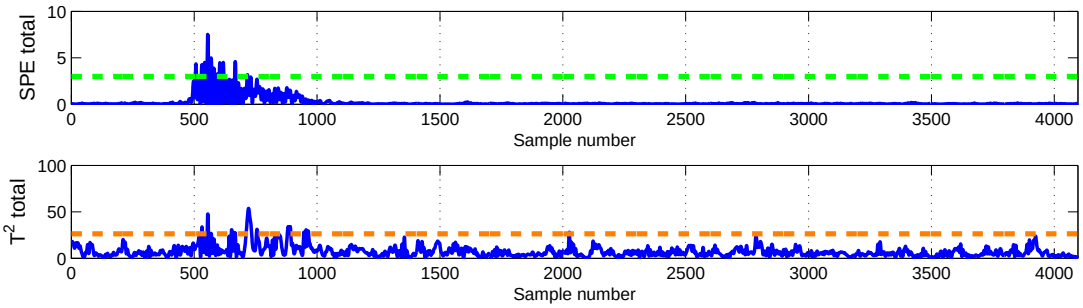

Figure 5.25: The total $\mathcal{Q}$ and $\mathcal{T}^2$ statistics, case 5 fault condition

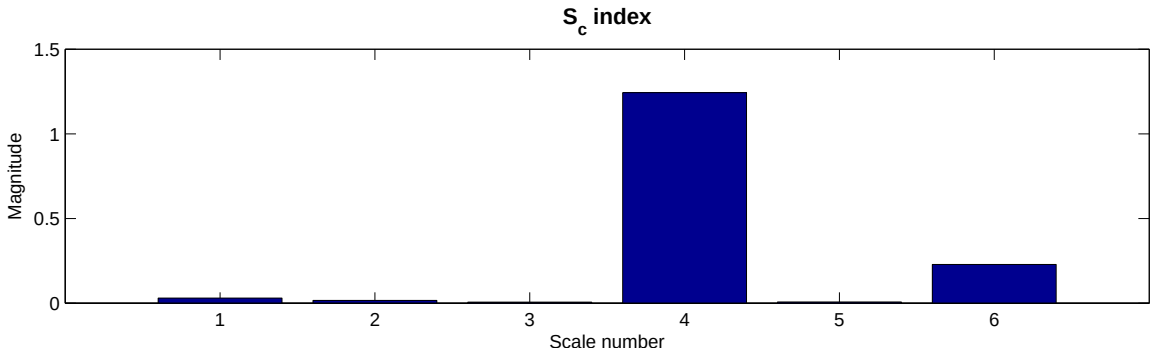

Figure 5.26: S_c index, case 5 fault condition.

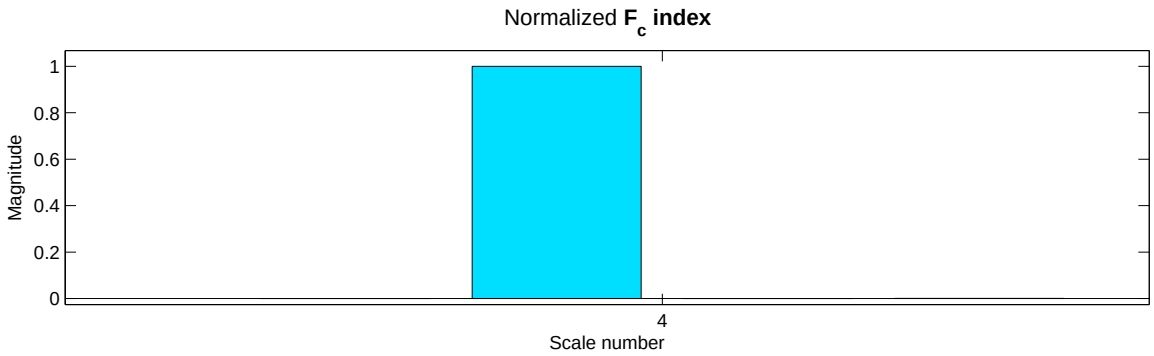

Figure 5.27: F_c indices at scales 4, case 5 fault condition. The cyan blue bar refers to the variable number two.

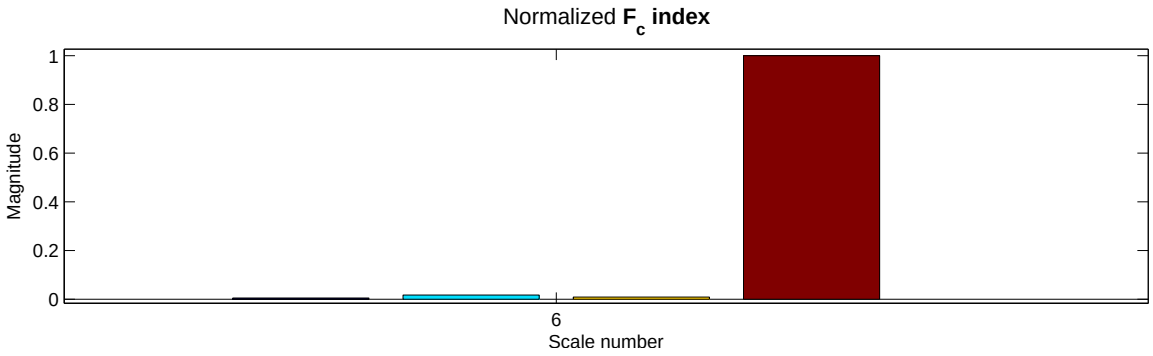

Figure 5.28: F_c indices at scales 6, case 5 fault condition. The dark red refers to the variable number four.

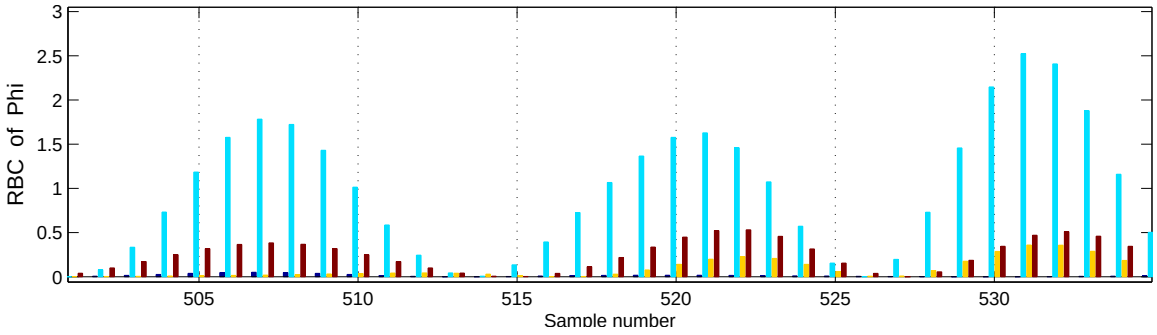

Figure 5.29: RBC chart computed based on the φ statistic at scale 4. It is magnified around the first fault commencement at sample number 500. Case 4 fault condition. The cyan blue bar refers to the variable number two and the dark red refers to the variable number 4

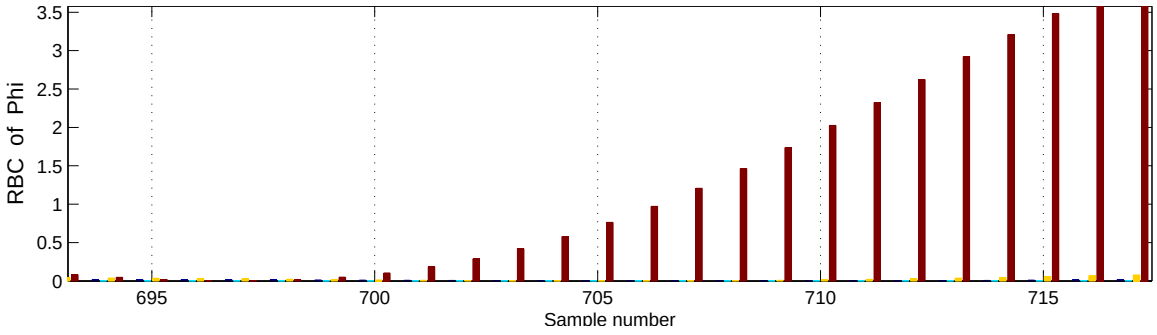

Figure 5.30: RBC chart computed based on the φ statistic at approximation scale. It is magnified around the second fault commencement at sample number 700. Case 4 fault condition. The dark red refers to the variable number 4

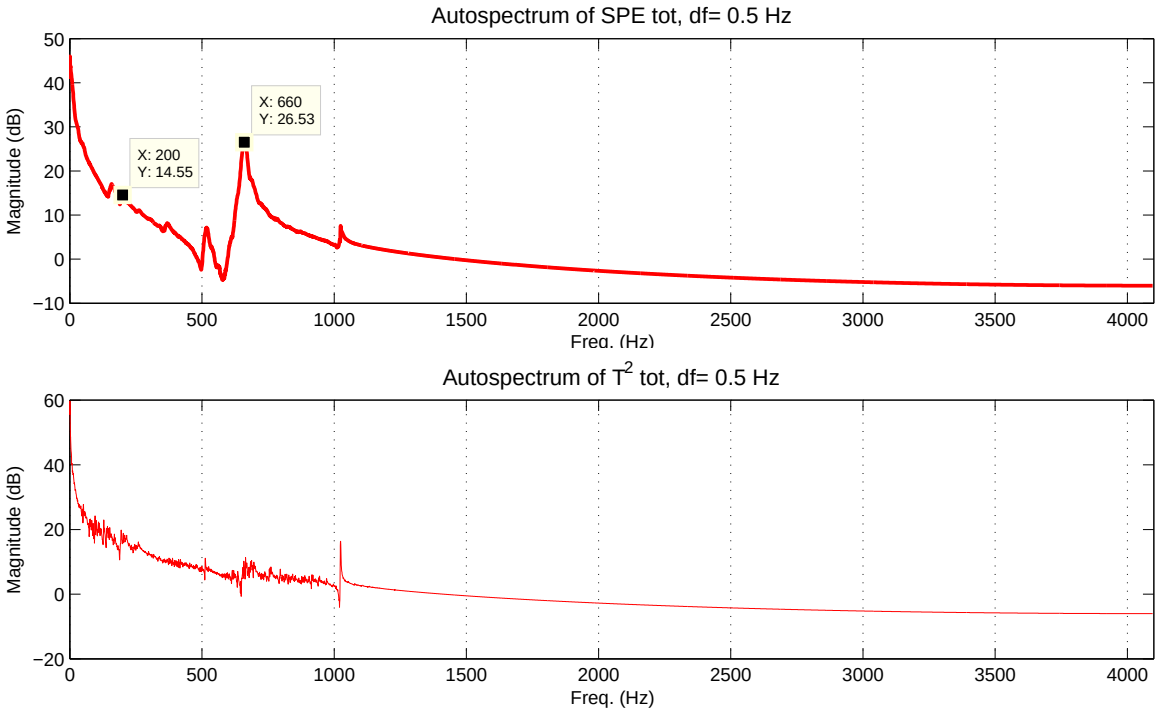

Figure 5.31: Spectrum of the total statistical indices, the fundamental frequency and its harmonics are flagged, case 5 fault condition.

5.2 Bearing Fault

The main objective of this section is to utilize the modified MSPCA along with new developments to monitor the condition of bearings of a DC motor. The test setup is explained in the Appendix B. The measured variables are acceleration signals recorded by two accelerometers attached to the casing of motor. These accelerometers were installed at the location of the bearings, one at the back side of the motor and the other one at the front side. The system was run under a normal fault-free condition initially and acceleration signals were recorded. Then the front bearing was replaced by another which a small indentation fault in its outer race. This defect causes a shock impulse that propagates through the bearing components and the structure, and generates excessive vibrations. For a severe defect, the vibration

amplitude becomes significant and radiates to the surrounding medium in the form of audible noise. Testing data were recorded under a constant loading and speed (1500rpm). More details about the fault conditions are provided in the Appendix B. The first data set was used to derive the *in-control* model of the motor. This model is then used for condition monitoring and fault diagnosis. Several wavelet functions were examined for signal decomposition. All of them were *real* despite the fact that complex wavelet functions are usually suggested in publications for bearing fault diagnosis [51, 52, 53]. The following results are based on using the *Coiflet* of order five and decomposing signals to seven levels (seven details scales and one approximation scale). This is a significant achievement as it simplifies the fault detection and diagnosis procedure and speeds up the processing. The data matrix includes two columns and 30,000 observations which are sampled in time domain at frequency of 10,000Hz. The columns of the data matrix represent readings of the front and rear accelerometers respectively.

The first step would be to calculate the total $\mathcal{Q}$ and $\mathcal{T}^2$ statistics. They are plotted in the figure 5.32. These statistical indices show that the system is malfunctioning due to a strong fault in the system. Confidence limits of both of the $\mathcal{T}^2$ and $\mathcal{Q}$ statistics were severely violated. These sharp peaks do appear and vanish periodically. Considering that these peaks are very sharp and do not remain for a long time, they have the impact fault characteristic simulated in cases three and four of the previous section. In order to extract more information about the fault and localize it in the system, further analysis is needed. The scores covariance index shown in figure 5.35 points to the scale three as the main faulty scale. Scale two has a small contribution too. Inspecting statistical indices plots at each scale confirms this result. The statistical indices determined at these two scales are shown in figures 5.33 and 5.34. The F_c contribution chart shown in figure 5.36 indicates variable number one,

the front bearing acceleration, as the one which is mainly affected by the fault. This is verified by the same results obtained from RBC calculations depicted in figure 5.37. To sum up, the fault has been detected, localized in the frequency domain as well as being isolated in the system so far. These are important information pertaining to the underlying fault. Further tools are still needed for extracting more information about the fault. Spectrum analysis of the total $\mathcal{Q}$ and $\mathcal{T}^2$ statistics are depicted in the figure 5.38. The spectrum of the total $\mathcal{Q}$ index shows the fundamental frequency of 90.33Hz and its harmonics. Harmonics exist only up to about 1KHZ, after which the frequency peaks are shifted to other frequencies. Analogous observations can be made from the spectrum of the total $\mathcal{T}^2$ statistic. Performing the envelope analysis of the front acceleration signal, a peak can be detected at 90Hz. When it comes to bearing fault diagnosis, there are *characteristic defect frequencies* which are determined based upon the geometry and rotational speed of the bearing and can be calculated from simple mathematical expressions. These characteristic frequencies can be used for fault diagnosis. Depending on the location of the defect; whether it is on the outer race, inner race or on the rolling elements one of these characteristic frequencies would be detected in the spectrum of the faulty bearing vibration.These frequencies are:

- **BPFO**: ball pass frequency outer race, BPFO=$S(\frac{N}{2})(1 - \frac{B}{P}cos(\theta))$;
- **BPFI**: ball pass frequency inner race, BPFI=$S(\frac{N}{2})(1 + \frac{B}{P}cos(\theta))$;
- **BSF**: ball spin frequency, BSF=$S(\frac{P}{2B})(1 - \frac{B^2}{P^2}cos^2(\theta))$; and
- **FTF**: fundamental train frequency, FTF=$S(\frac{1}{2})(1 - \frac{B}{P}cos(\theta))$, [54].

Where S is the rotor speed in Hertz, B is the ball diameter, P is the pitch diameter (two times the distance from center of bearing to the center of a ball in

the cage) and θ is the contact angle (between a ball and a race). The running speed of the motor was about 1500rpm in average. Taking the bearing specification into account, the characteristic defect frequencies for this rolling bearing would be [1]: $BPFO = 3.57\ f_o, BPFI = 5.43\ f_o, BSF = 4.61\ f_o$ where the f_o is the order frequency determined from the rotor speed, i.e. $f_o = RPM/60$. Taking the motor speed into account, one would get $f_o = 1500/60 = 25Hz$ and subsequently: $BPFO = 89.25Hz, BPFI = 135.75Hz, BSF = 115.25Hz$. The envelope analysis yields the frequency of 90Hz which is almost equal to BPFO. The spectra of the total statistical indices specified the same frequency, i.e 90.33Hz. Surprisingly, it is observed that the fault characteristic frequency could be identified through spectrum analysis of the total $\mathcal{Q}$ and $\mathcal{T}^2$ statistics. This experiment not only establishes another verification for the two corollaries stated in the chapter 4 but also demonstrates the application of these new contributions for bearing fault diagnosis.

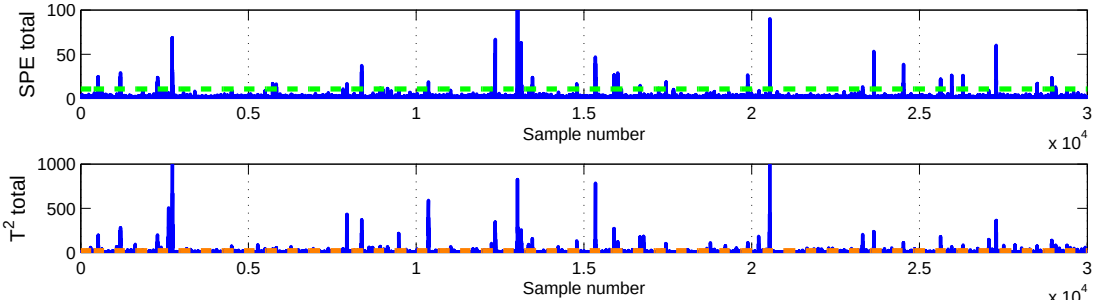

Figure 5.32: The total $\mathcal{Q}$ and $\mathcal{T}^2$ statistics, bearing fault condition

In summary, fault diagnosis of a DC motor with a faulty bearing was performed successfully. The bearing fault, that was physically simulated, was detected, localized in the time, scale and frequency domains. In addition to isolating the faulty component, the fault was diagnosed. The spectrum analysis of statistical indices indicated that this fault is most probably associated with a defect in the outer race of the faulty

[1] calculated with the aid of SKF website

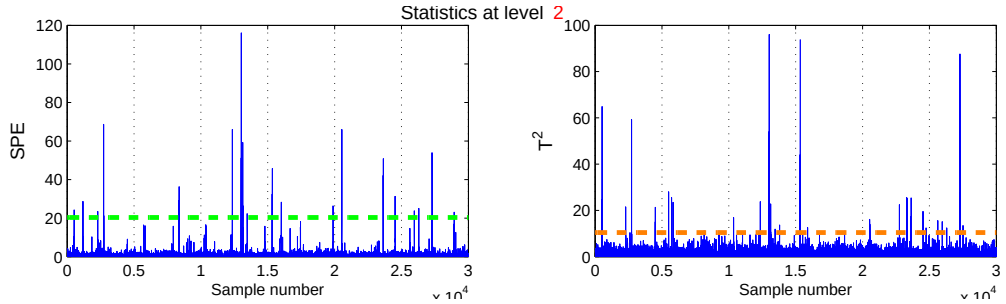

Figure 5.33: The $\mathcal{Q}$ and $\mathcal{T}^2$ statistics at scale 2, bearing fault condition.

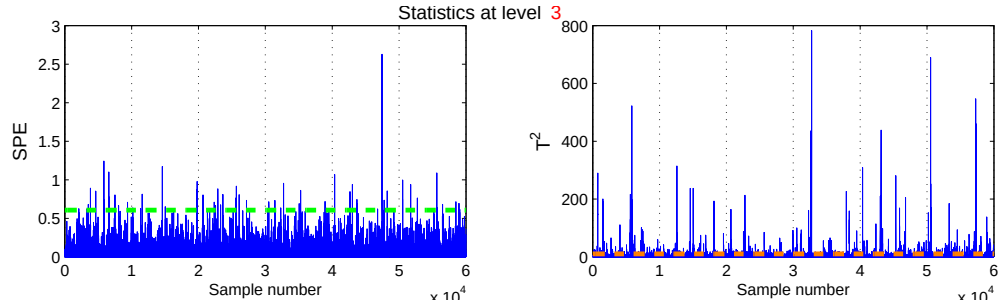

Figure 5.34: The $\mathcal{Q}$ and $\mathcal{T}^2$ statistics at scale 3, bearing fault condition.

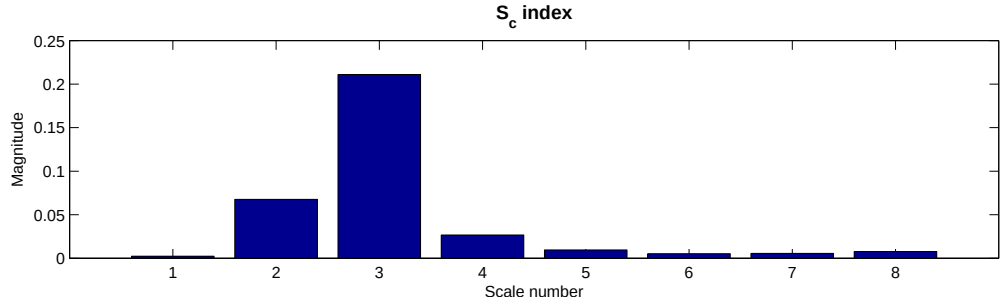

Figure 5.35: S_c index at different scales,bearing fault condition.

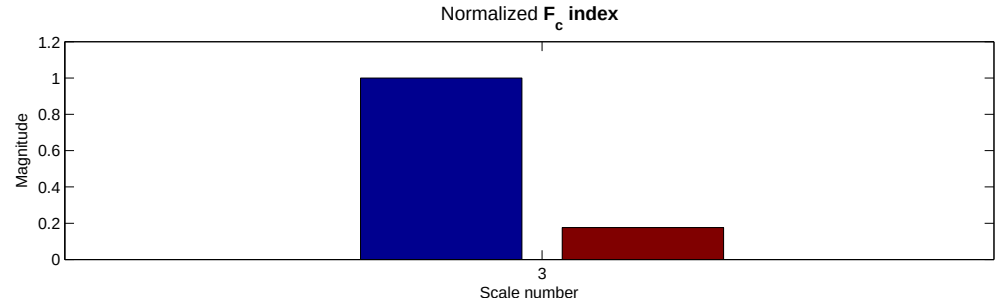

Figure 5.36: F_c index at scale three,bearing fault condition. The blue bar refers to the variable number one

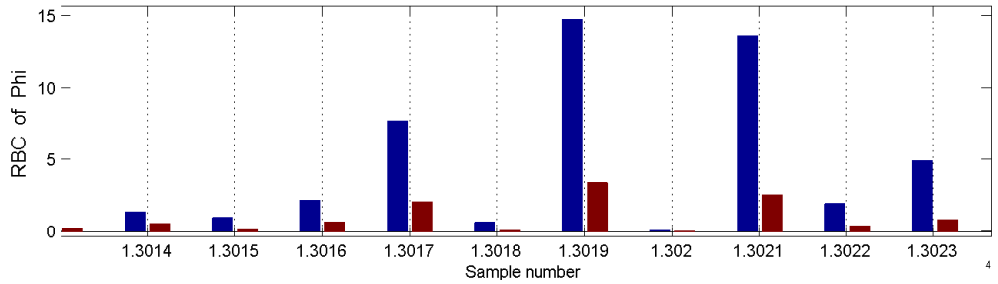

Figure 5.37: RBC chart computed based on the φ statistic at scale 2. It is magnified around one of the fault instances (peaks). Bearing fault condition. The blue and dark red bars refer to variable number one and two respectively.

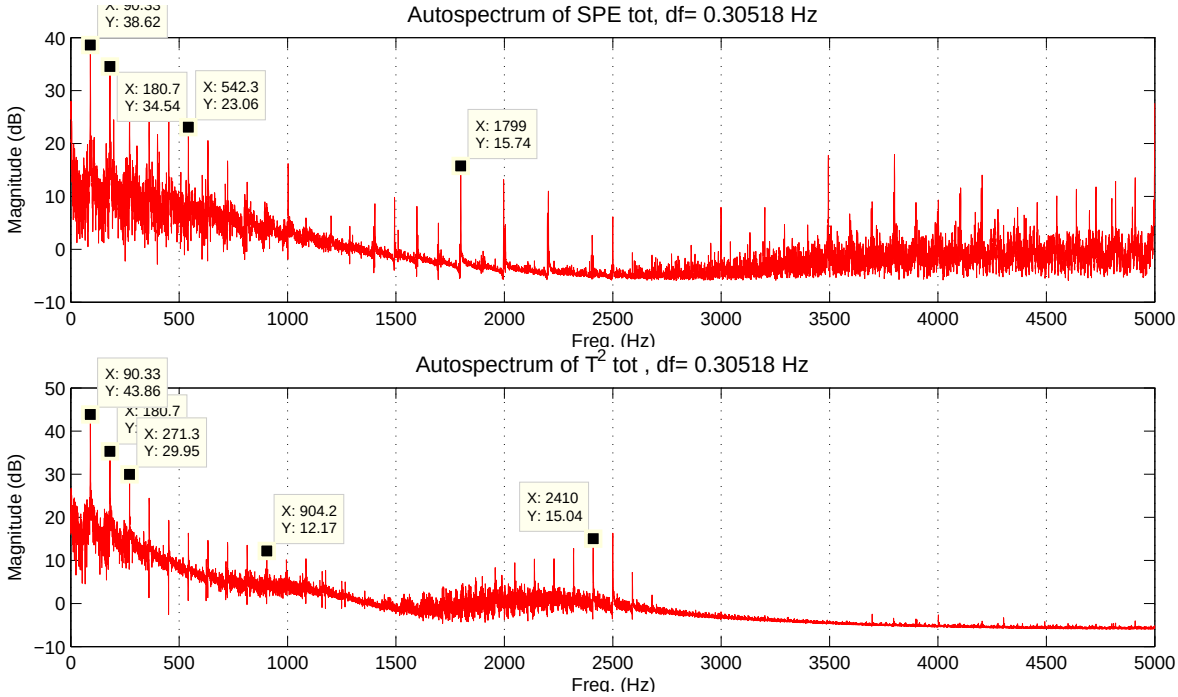

Figure 5.38: Spectrum of the total statistical indices, the fundamental frequency and its harmonics are flagged,bearing fault condition.

bearing. This example validates the contribution made in chapter 4 in regards to the relationship between spectral analysis of statistical indices and spectral analysis of the envelop of signals. Moreover, this example demonstrated a novel technique for fault detection and diagnosis of roller bearings in rotating machineries.

5.3 Lash Adjuster Fault in Engine

An internal combustion engine is a complicated mechanical system with many rotational and reciprocal components. It is expected that an abnormality in a moving component inside the engine (e.g. a valve, a piston, a cam shaft, and the crank shaft, etc.) would cause deviations in normal vibration signatures and should be identifiable by proper processing of vibration signals. This example is concerned with the application of the developed CAD-MSPCA technique for fault diagnosis of a V8 engine utilizing vibration data from eight accelerometers.The engine test setup is described in the Appendix B. Since this measurement setup and instrumentation has been used for NVH test of engines by the industrial partner of this research and they have already established a rich database of healthy and faulty engine measurements, the same configuration was used in this research as well. The baseline and testing data sets were captured and recorded in the time domain. The fault in the engine was a defective valve lash adjuster located at the valve train of the cylinder eight. The NVH test log sheets and manual inspection after tearing the engine down indicated that the collapsed lash adjuster at the cylinder eight is the root cause of excessive vibration and noise of the engine. Due to the advantages of analyzing the engine signals in the crank angle domain (CAD), as described in chapter 2, the fault diagnosis scenario applied the modified MSPCA on vibration data in the crank angle domain rather than the time domain. The instrumentation comprised of eight accelerometers mounted at eight points on the engine lug and the cylinder head surface and, a CID sensor. Since the engine is a V8, four accelerometers are installed on the right bank and four on the left bank. Transducer locations for one bank of the engine are shown in figure 5.39, the engine photo is taken from [55]. Sensors are mounted symmetrically in the other side of engine. Further information regarding test setup and experimentation is

provided in Appendix B. The readings of four accelerometers at each bank of engine form the data matrix at each side. Thus two data matrices were created and used in the diagnosis technique. The data matrix is configured in the following fashion:

$$\mathbf{X} = [\ \mathbf{x}_{\mathbf{Lug,Front}} \quad \mathbf{x}_{\mathbf{Lug,Rear}} \quad \mathbf{x}_{\mathbf{Head,Front}} \quad \mathbf{x}_{\mathbf{Head,Rear}}\ ]$$

In order to perform CAD-MSPCA analysis, the data matrices were initially trans-

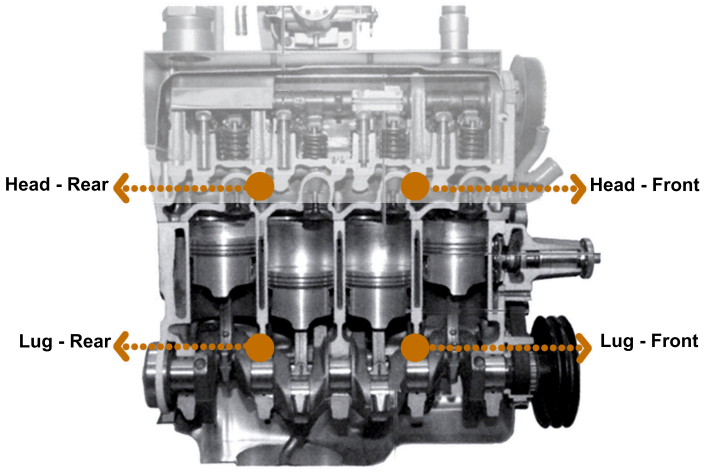

Figure 5.39: Positions of the accelerometers, two mounted on the head of engine and two attached to the engine lug. The locations are almost symmetrical at both banks of engine.

formed to the crank angle domain with the aid of the CID signal then used for multivariate analysis. The CAD transformation has already been discussed in chapter 2. The same procedure was employed for this transformation. The time series then would be segmented into several cycles and re-sampled at each cycle with respect to the angular position of the crank shaft. The resolution of CAD is 0.2 degree. In this case, the data matrix at each bank was divided into 34 cycles with each cycle having 3600 data points spaning from 0 to 720 degree. The average of these 34 cycles over

crank angles was then used for fault diagnosis. This averaging operation in CAD mitigates the effect of noise and random components while improving the deterministic elements. This procedure was performed for both the baseline and the testing data at each bank. The total $\mathcal{Q}$ and $\mathcal{T}^2$ statistics computed for each bank are plotted in figures 5.40 and 5.41.

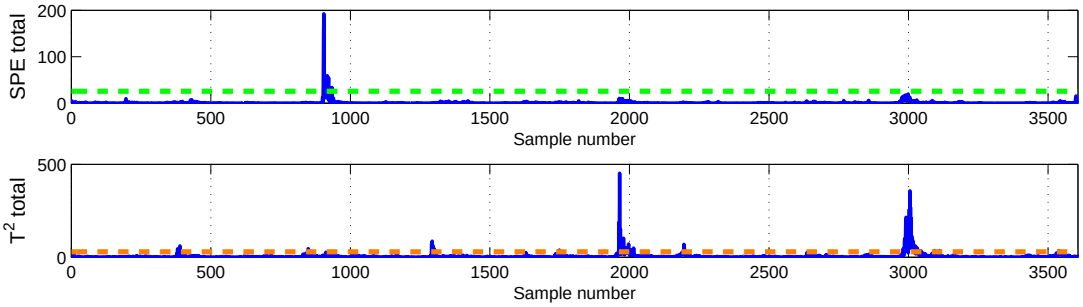

Figure 5.40: The total $\mathcal{Q}$ and $\mathcal{T}^2$ statistics, RHS bank of engine

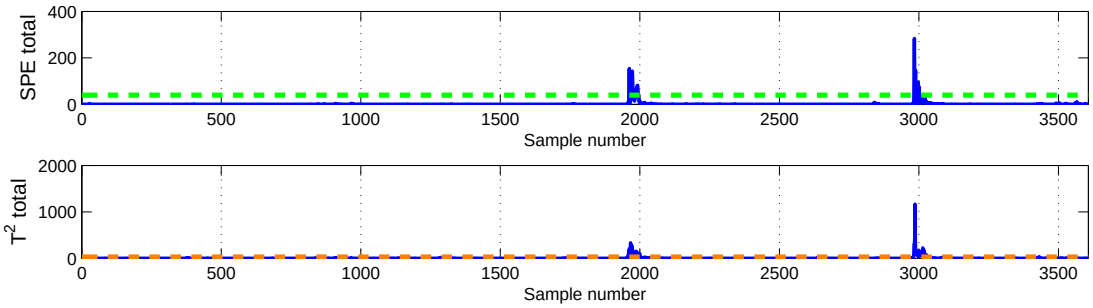

Figure 5.41: The total $\mathcal{Q}$ and $\mathcal{T}^2$ statistics, LHS bank of engine

One can see that there are strong peaks around samples 1960 and 3000 (corresponding to the crank angle degrees of almost 392° and 600°) in both total $\mathcal{Q}$ and $\mathcal{T}^2$ statistics of the Left bank and the $\mathcal{T}^2$ statistic of the Right bank. The total $\mathcal{Q}$ index plot of the right bank data matrix shows only one peak at the sample number 900 (corresponding to the crank angle degree of 180°). Consequently, it seems that there are two different faults that happen at two different points in the angle domain; one is occurring at the 392° and 600° and the other appears only at the angle 180°. In

order to further analyze this complex situation, some important properties of the $\mathcal{Q}$ and $\mathcal{T}^2$ statistics already mentioned in chapter 3 need to be considered. They are:

- if a fault violates both $\mathcal{T}^2$ and $\mathcal{Q}$ limits, its magnitude must be very large in order to exceed the τ_α^2 limit which is usually large; and
- there might be situations that a fault or normal change in process output takes place that conserves the correlation structure. In this case the $\mathcal{T}^2$ statistic limit is usually violated but not the $\mathcal{Q}-$statistic

Bearing these points in mind while inspecting the peaks at sample numbers 1960 and 3000, a conclusion would be that this fault originally happened in the left bank of the engine but has affected the entire system and thus sensed by sensors on the other side. This fault, however, has not changed the correlation structure of the measured variables of the right bank since it did not appear in the $\mathcal{Q}$ plot but it was detected in the $\mathcal{T}^2$ statistic chart. On the contrary, this fault was clearly detected and observed in both statistical charts of the left bank. This confirms the conclusion made earlier. Regarding the total $\mathcal{Q}$ index plot of the right hand side of the engine, one can clearly notice a peak at the sample number 900 which is not observed in the other total statistics plots. This points to a fault that has only happened in the right bank and is weaker than the other fault. Evaluating the statistical indices plots as well as the RBC plots at each scale for the each bank of the engine reveals important information. The plots for the right bank are shown in figures 5.42 to 5.44, 5.46 and 5.47. The observations are as follows:

1. Scale 1
    - $\mathcal{Q}$ *index plot:* only one strong peak at the sample number 900. The RBC of $\mathcal{Q}$ index points to variable number three (head-front accelerometer) as

having the highest contribution to the fault.

- $\mathcal{T}^2$ *statistic plot:* three peaks at sample numbers 900, 1960, 3000 are evident. The one at sample 3000 is the dominant one. The RBC bar chart shows that at the sample number 900, variable three is the main contributer. At the other two instances, the variables two and four are those which have the highest share.

2. Scale 2

- $\mathcal{Q}$ *index plot:* the peak at sample number 900 vanishes but two quite weak peaks at the other two locations show up.
- $\mathcal{T}^2$ *statistic plot:*multiple peaks appear but the strongest ones are those at sample numbers 1960 and 3000.

3. Scale 3

- $\mathcal{Q}$ *index plot:*the only peak is the one at the sample number 3000 with an amplitude comparable to the scale 2.
- $\mathcal{T}^2$ *statistic plot:*there is only one peak that exceeds the detection limit. It is the one at the sample number 3000. Its amplitude is a little higher than scale one but is smaller than scale 2.

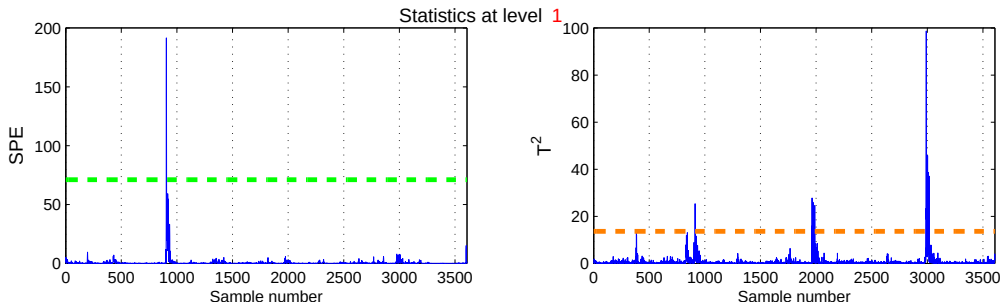

Figure 5.42: The $\mathcal{Q}$ and $\mathcal{T}^2$ statistics at scale 1, right bank of engine

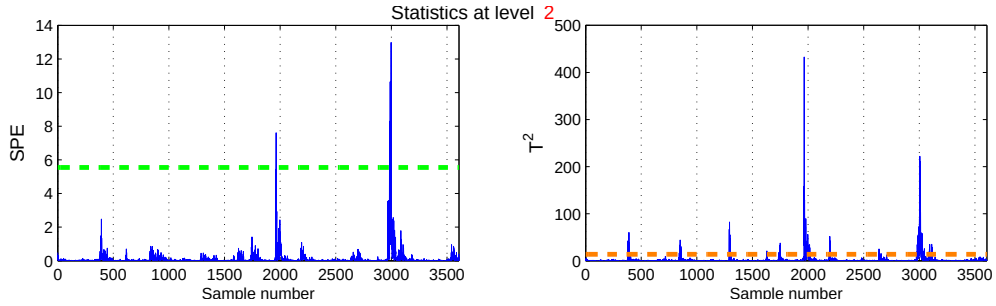

Figure 5.43: The $\mathcal{Q}$ and $\mathcal{T}^2$ statistics at scale 2, right bank of engine

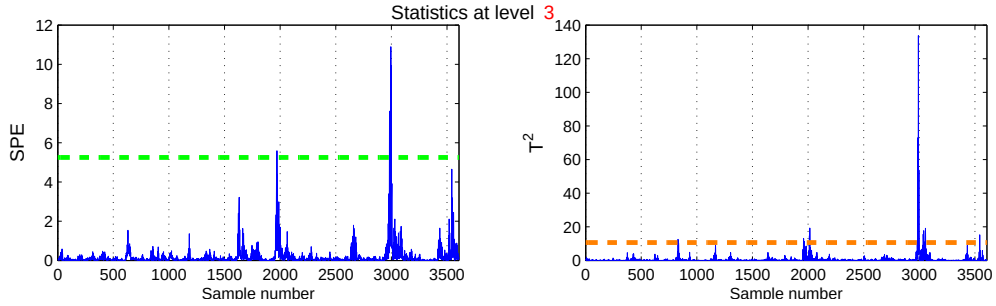

Figure 5.44: The $\mathcal{Q}$ and $\mathcal{T}^2$ statistics at scale 3, right bank of engine

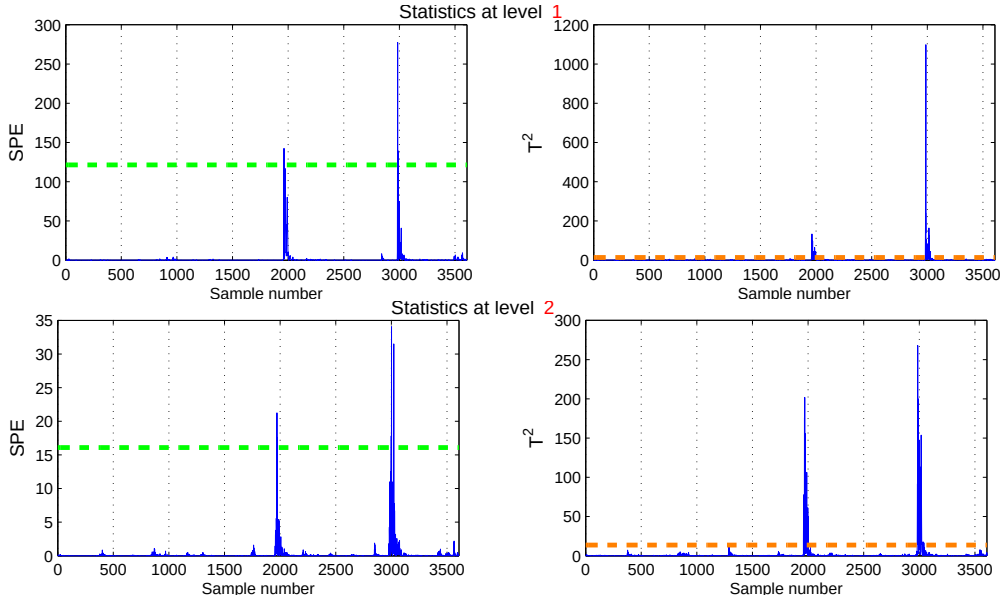

Figure 5.45: The $\mathcal{Q}$ and $\mathcal{T}^2$ statistics at scales 1 and 2, left bank of engine

The fault signature is mainly detected in these three scales. For the left side of engine, the detection limit is only exceeded at samples 1960 and 3000 and there is

no footprint of the other fault at sample 900. Therefore, the fault at sample 900 is only due to a phenomena that occurs in the right side of engine. The S_c bar chart for the right hand side, shown in figure 5.49, estimates these scales as the faulty ones too, though there are two high level bars at scales 8 and 9. The S_c index calculated for the left bank data matrix shown in figure 5.50 estimates that the underlying fault would be located in the first three scales although those high magnitude bars at scales 8 and 9 exist for this side too. Checking the statistical indices at each scale confirms this finding that the fault is contained in the first three scales . These erroneous high values of the S_c index at scales 8 and 9 may be due to the violation of the assumption made through deriving the S_c index which postulated that the fault and normal state of the system are independent from each other. Nevertheless, the F_c index determined at the scale 1, depicted in figures 5.51 and 5.52, clearly isolates the variable number three and four as the faulty variables in the right and left bank of engine respectively. The RBC chart calculated based on the $\mathcal{Q}$ index of the left side of engine, shown in figure 5.46, illustrates that the main contributing variables to the main fault detected in the left bank are variable number four and then variable number two in the second place. This result confirms the result obtained from F_c index. Considering that variable number two represents the accelerometer installed in the lug-rear point and the variable number four represents the accelerometer at the cylinder head-rear location, the location of the fault can be isolated to the left bank of engine at the rear side.

All in all, the analysis demonstrates that there are two faults happening, the stronger one is the fault probably due to a defective component located in the left bank of the engine at the rear and most probably at the head part rather than lug due to higher share of the variable number four in RBC plots. The weaker fault is identified in the right bank of the engine and is spotted to be in the front-head

location. Both of these possible faults possess high frequency contents since they are pinpointed in the first scale at the right side and first three scales at the left side. These are quite valuable information regarding the condition of the engine and possible faults in it. Consulting with the vibration analysis report composed by the industrial partner, it was observed that the exhaust valves of the cylinder 8 opens at angle 380° and closes at angle 630°. The cam-rocker and lash adjuster system should function earlier to have the exhaust valves completely closed at 630°. Taking these points into considerations, the root cause of the fault detected and isolated by the CAD-MSPCA technique would be due to the exhaust valve train fault at cylinder 8. The tear down report of this engine issued by the industrial collaborator confirms that the root cause of the fault was collapsed lash adjusters at cylinder 8. As far as the peak at angle 180° on the right bank of engine is concerned, the diagnosis reports of this engine do not point to any fault on the right bank. Since further information about the characteristics of the engine is not accessible, the root cause of this fault cannot be identified. Nevertheless, the CAD-MSPCA technique could detect and isolate it.

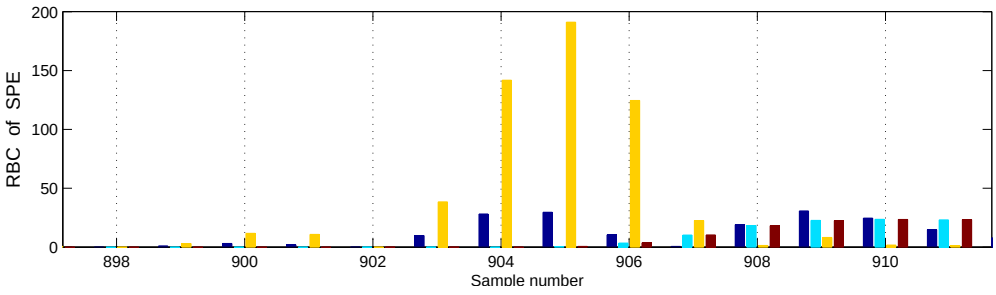

Figure 5.46: The RBC chart determined based on the $\mathcal{Q}$ index at scale 1, magnified around the sample number 900, right bank of engine

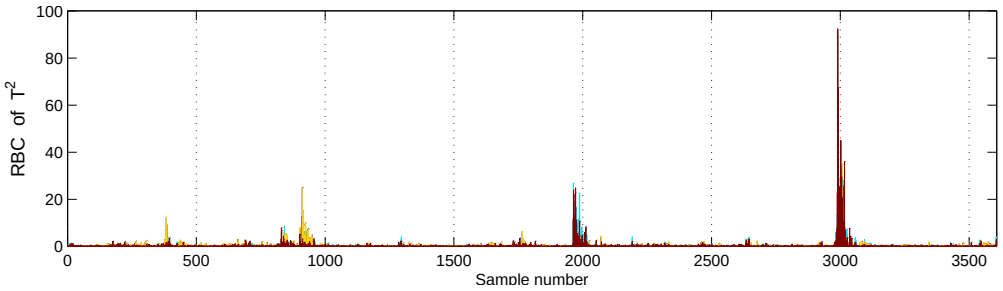

Figure 5.47: The RBC chart determined based on the $\mathcal{T}^2$ statistic at scale 1, variable number 3 is the main contributer at sample number 900 whereas variables 2 and 4 have the main contribution at sample number 1960 and 3000, right bank of engine,

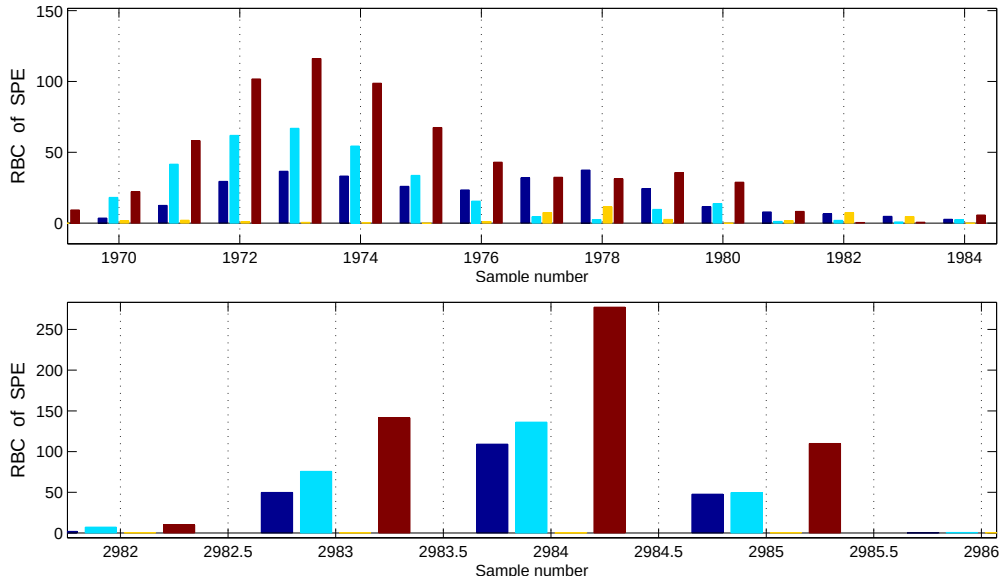

Figure 5.48: The RBC chart determined based on the $\mathcal{Q}$ index at scale 1, magnified around the sample number 1960 and 3000, left bank of engine

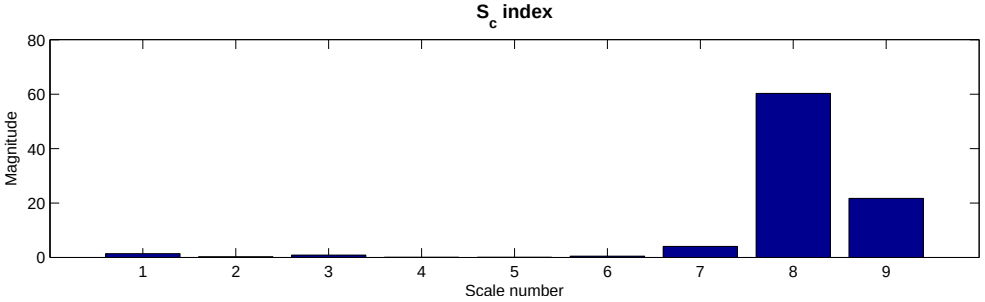

Figure 5.49: S_c index at all scales, right bank of engine

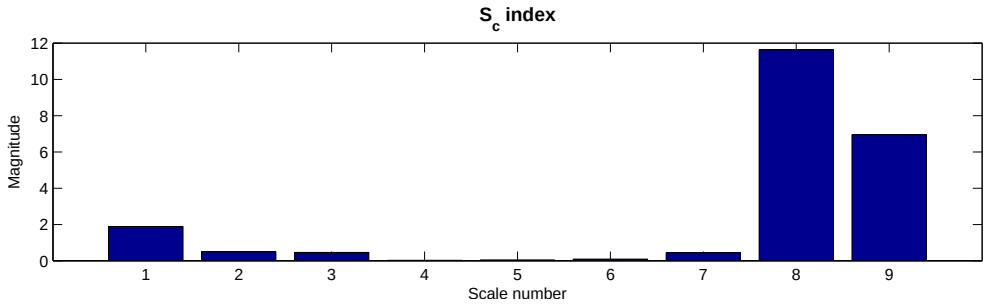

Figure 5.50: S_c index at all scales, left bank of engine

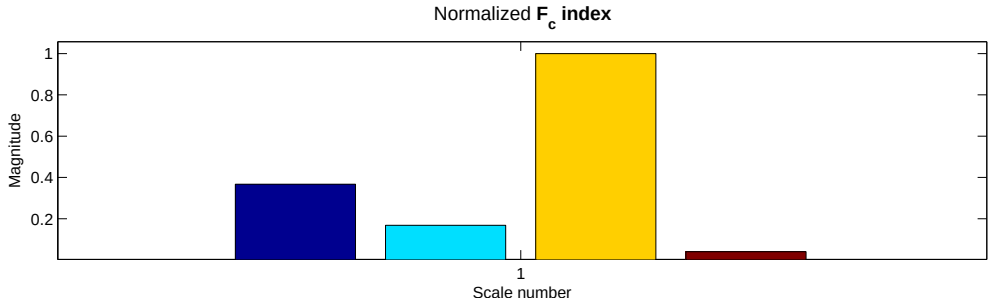

Figure 5.51: F_c index at scale one, right bank of engine. The yellow bar represents variable number three (head-front)

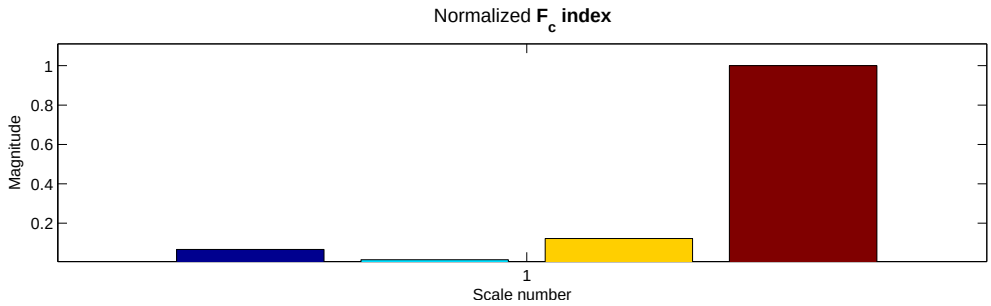

Figure 5.52: F_c index at scale one, left bank of engine. The dark red bar represents variable number four (head-rear)

To sum up this section, this experiment demonstrated the capability of the combination of CAD transformation and the Mod-MSPCA technique, CAD-MSPCA for fault diagnosis of a complicated system like a V-type engine, even for the situation that two different faults at two different locations of engine have happened. Analyzing signals in CAD helps in tracing back the root cause of the fault and defective

component.Additionally, MSPCA analysis not only detects the occurrence of faults, but also characterizes them in the scale and frequency domains and also helps to differentiate the minor abnormalities from the major system fault. Another important feature of the CAD-MSPCA is that it processes readings of all sensors at once then isolates the sensor(s) which has picked up the fault, this is practically significant as it saves post-processing time and efforts. The CAD-MSPCA approach developed in this research is suitable for off-line processing but it can be adapted for real time condition monitoring after some modifications.

Chapter 6

Conclusions and Outlook

Condition monitoring and fault diagnosis of mechanical systems are two important issues that have received considerable attention from both academia and industry. Several techniques have been developed to date to address these issues. One category of these techniques which has been successfully applied in many industrial plants is based on the multivariate analysis algorithms and more specifically the principal component analysis. The strong capabilities of the PCA has been enhanced by combining it with multi-resolution techniques, namely the discrete wavelet analysis. The multi-resolution PCA has in turn lead to the development of the MSPCA technique. PCA and MSPCA techniques can identify the occurrence of abnormalities in the system by monitoring statistical indices, namely the $\mathcal{Q}$ statistics or the SPE and $\mathcal{T}^2$ statistics. Variable contribution analysis is the conventional approach for isolation of abnormalities in the system. The φ statistic and reconstruction based contribution (RBC) analysis developed by Qin [45] were introduced to MSPCA in this research. The RBC guarantees that the faulty variable has the largest contribution and consequently leads to more accurate results than the traditional contribution analysis. The φ statistic also benefits from properties of both SPE and $\mathcal{T}^2$ statistics simultaneously since it is defined as a combined index and consequently facilitates the detection task. Another new contribution in this research was the estimation of both the scores covariance matrix and the fault covariance matrix. Two new indices, they are S_c and F_c, were defined using these matrices and employed for both detection and isolation purposes. Further, the S_c index can be an additional tool for fault localization in the scale domain while using the MSPCA algorithm for fault detection and diagnosis.

Some researchers have used SPE and $\mathcal{T}^2$ statistic for fault identification or classification purposes by importing them to algorithms like neural networks or support vector machines.A large number of publications propose these indices only for fault detection. An absolutely fascinating discovery made through this research project was the use of these statistical indices for fault identification. It is mathematically demonstrated that if there is a fault in the system which is detected by either of these indices, one can obtain the frequency characteristics of the fault by performing the spectrum analysis of these indices. Moreover, it is mathematically demonstrated that in case of periodic modulating faults, spectra of these indices contain information that one can get by doing the envelope analysis of the faulty variable. This result is practically very desirable as one can identify the nature of the fault by inspecting these spectra. As already remarked, these statistical indices are an inevitable part of the multivariate analysis for monitoring and fault isolation applications. Therefore extracting more information from them using fast and well-developed mathematical operation like the discrete Fourier transform would be greatly desirable. These new developments were validated through simulation examples as well as real fault conditions pertaining to bearings in a DC motor, a lash adjuster fault in an internal combustion engine..

The last development of this research has been the adoption of the MSPCA technique for fault detection and diagnosis of a complex dynamical system like the internal combustion engine. In order to fulfill this goal, the crank angle domain analysis was combined with MSPCA. This variation of the MSPCA was named CAD-MSPCA which performs monitoring and diagnosis in the CAD. The performance of the CAD-MSPCA for fault diagnosis of a V8-DOHC engine was verified by applying this algorithm on a real experimental vibration data. The technique correctly identified two distinctive faults in the engine. Additionally, the CAD-MSPCA processed

the readings of multiple transducers (eight accelerometer in this case) simultaneously and showed the analysis results in a few graphs and charts. This accelerates the monitoring and diagnosis procedure quite considerably.

The new contributions made through this research work proves that the MSPCA and CAD-MSPCA are viable approaches for fault detection and diagnosis of complex mechanical systems. A potential improvement may be obtained in the performance of the MSPCA in multiple fault scenarios by using the wavelet packet analysis as a multi-resolution analysis technique instead of DWT. The filters defined in DWT dyadically split up the frequency range to several bandwidths which end up in wide high frequency bandwidths (in fine scales) and narrow low frequency ones (in coarse scales). As a result, if multiple high frequency faults happen such that they coincide in a single scale, it will not be feasible to separate them in the scale domain and they would be considered as one fault. Furthermore, one always has the capability of dividing up the low frequency bandwidths by adjusting the wavelet depth but this is not possible for high frequency bandwidths (fine scales). The wavelet packet would be a reasonable alternative for DWT in order to deal with this situation. The CAD-MSPCA should be tested on various faults. The spectrum analysis of statistical indices can be employed to correlate different faults in engines with their characteristic frequencies. This will be an invaluable resource for fault identification in engine.

Appendices

Appendix A

Appendix A

Calculating Fourier transform of the $\bar{\psi}_s(t)$

The Fourier transform of the $\bar{\psi}_s(t)$ is calculated in this section, that is: assuming that

$$\hat{\psi}^*(\omega) = \int_{-\infty}^{\infty} \psi^*(-t)\, e^{-j\omega t}\, dt \tag{1}$$

then

$$\hat{\bar{\psi}}_s(\omega) = \int_{-\infty}^{\infty} \frac{1}{\sqrt{s}}\, \psi^*(\frac{-t}{s})\, e^{-j\omega t}\, dt \tag{2}$$

$$= \frac{s}{\sqrt{s}} \int_{-\infty}^{\infty} \psi^*(a)\, e^{-j\Omega a}\, da \tag{3}$$

$$a = \frac{t}{s}\ and\ \Omega = s\omega$$

considering equation 1, one can conclude the following equation:

$$\hat{\bar{\psi}}_s(\omega) = \sqrt{s}\ \hat{\psi}^*(\Omega) \tag{4}$$

$$= \sqrt{s}\ \hat{\psi}^*(s\omega) \tag{5}$$

The simple and important conclusion comes after this is:

$$\hat{\psi}(0) = \int_{-\infty}^{\infty} \psi(t)\, dt = 0 \tag{6}$$

Appendix B

Appendix B

Experimental Test Setup

The experimental test setup and fault description for both DC Motor and engine experimentations are described in this appendix. The first part is dedicated to the DC motor test setup, followed by the engine instrumentation and test description.

DC Motor Setup and Bearing Fault: This setup was developed by Mr. Wanlin Zhang, a master's student at the mechatronics lab. The permanent magnet brushless DC Motor used in this research, shown in the figure 1, has the specifications listed in the table 1. The motor was controlled by a Siemenss SimoDrive 611 system. A built-in absolute encoder was used for rotor position and speed measurement, with a resolution of 2048 lines per revolution.

Table 1: The specification of motor

Parameter	**Value**
Rated Speed	3000 rpm
Number of poles	8
Moment of Inertia	$4.8 \times 10^{-3} kg/m^2$
Torque Constant	1.52 Nm/A
Voltage Constant	0.77 V/(rad/s)
Winding Resistance	0.5 Ohm
Field Inductance	$4.8 \times 10^{-3} H$

The motor has two roller bearings, one is mounted at the rear of motor and the other one is located in the front side. Bearing fault was simulated by replacing

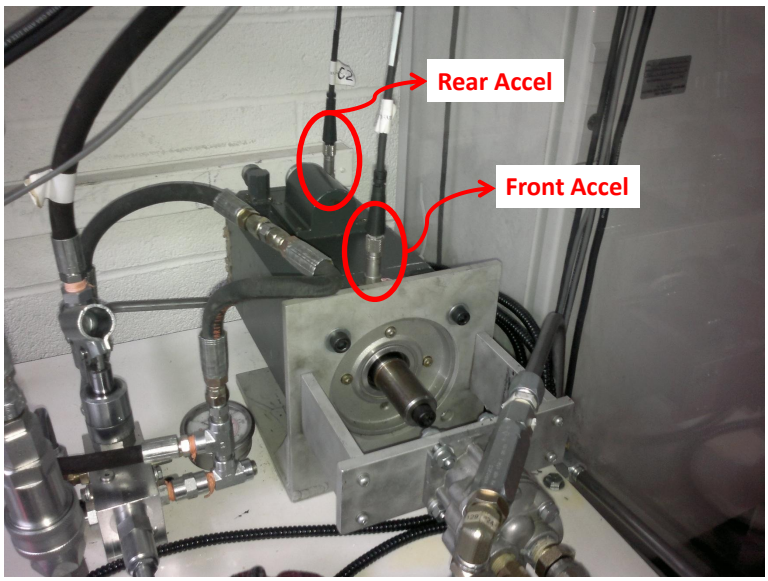

Figure 1: DC Motor and attached accelerometers, test setup is at the mechatronics lab

the healthy front bearing of the motor with the faulty one of the same type. The ball bearing was of the type NACHI-6207NSE manufactured by SKF. The bearing fault was simulated by creating small dents on the outer race of the bearing with electrical-chemical etching method. Two accelerometers (AC240-1D) were screwed on the casing of the motor for vibration measurement. A National Instrument DAQ board (NI PCI-6229, 16-Bit, 833 kS/s, 32 analog inputs) was used along with a built-in anti-aliasing filter for data collection. Setting a proper sampling rate for measurement is quite important as it defines the upper frequency band can be measured. Since the desired frequency range is 0-4KHz, the sampling rate was set to 10KHz. The sampling period mainly depends on the motor speed. In this experimentation, the test was repeated at different motor speed between 800rpm to 2000rpm. Therefore the sampling period was chosen to be 10sec in order to capture enough cycles for

post-processing. Eventually, prior to run the test, a 10 minutes warm-up was performed with the motor running at a constant speed of 3000 RPM, no load condition.

Engine Test Setup and Lash Adjuster Fault: This research project was carried out in close collaboration with the Ford Powertrain Engineering Research and Development Center (PERDC) located at the Ford Motors' Essex Engine Plant in Windsor, Canada. The engine test facilities were therefore provided by the PERDC. The engine test and vibration measurements were performed in the dynamometer laboratory under controlled situation to simulate the real working condition of an engine in a vehicle. The engine used for diagnosis was an eight cylinder, 5.0L, double overhead cam (DOHC) with four valves engine. The engine test setup located in a semi-anechoic test cell included the following elements: engine mounted on two elephant stands using regular mounts; front end accessories including belts, tensioners and pump;and clutch and transmission assembly connected to a dynamometer. Several parameters influence the engine vibration characteristics, namely the engine speed, load and temperature of coolant and oil [56]. The operating condition of engine was set to 600 rpm at idle condition [56]. Since running engine under high temperature may affect clearances and cause local distortions and consequently lead to excessive vibrations, the oil and cooling water temperature were controlled to be between 180-190degF. The experimental test setup of engine inside the test cell is depicted in the figure 2 [56].

The engine is instrumented by attaching eight accelerometers to the engine body. This is done according to the standard followed in the PERDC for fault diagnosis of engine using vibration analysis. The accelerometers used are PCB and B&K charge type accelerometers where their readings were sampled by the rate of 32768 samples per second per channel. The data acquisition system used was a PROSIG

Figure 2: The engine test setup in the semi-anechoic test cell at PERDC

5600 unit. The anti-aliasing filter was set to 13KHz since the interested frequency band is up to 10KHz. Setting the sampling frequency to 32768 sample per second satisfies the Nyquist frequency criteria. The data acquisition time was set to eight seconds in order to collect enough engine cycles. For this operating condition data vectors cover 34 complete engine cycles.

Considering the engine is a V type engine with four cylinders at each bank, four transducers were placed at each bank, two on the cylinder head and two on the engine lug. Locations of transducers are shown in the figure 3. The accelerometers mounted on the engine lug are able to capture vibrations generated and propagated from the lower part of the engine such as piston, connecting rod related phenomena and bearings [56]. On the other hand, transducers installed on the cylinder head capture vibrations originating from the cylinder head components like valve train, lash adjuster, and phaser related phenomena. All of the accelerometers were screwed into brass bases and glued to the engine surface using Loctite super glue. Besides these eight accelerometers, the cam identification sensor's (CID) signal was also measured by the same data acquisition system. The CID signal is used for converting the time

domain signal to the crank angle domain one. The engine photo in figure 3 is from

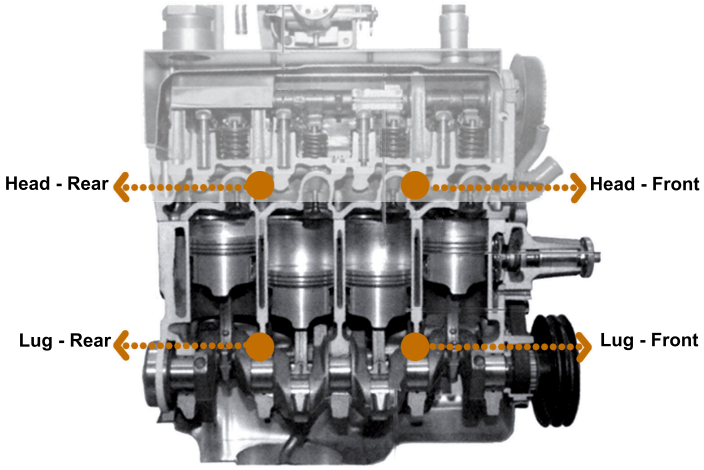

Figure 3: Positions of the accelerometers, two mounted on the cylinder head and two attached to the engine lug. The locations are almost symmetrical at both banks of engine.

[55]. Engine vibration data are measured at almost similar positions for both healthy and faulty engines. Both engines are the same type and have similar properties except the faulty one had an unknown fault which generated excessive noise. The faulty engine is a returned engine. The engine was run under similar condition as the healthy one, i.e. drive idle condition stated above. This engine was torn down and investigated thoroughly by expert technicians. The root cause of fault was detected to be a collapsed lash adjuster located at the cylinder head of the cylinder eight. The lash adjuster also known as a hydraulic tappet is a device designed to adjust the clearance between valve and its cam follower. This device is consisted of a small expanding piston inside a chamber filled with the engine oil through an oil gallery. The operation principle is as follows: when the valve is opening the oil feed to lash adjuster is blocked and lash adjuster works as a piece of solid component maintaining

Table 2: The location of attached accelerometers

Location	Notation	Comments
Right Lug Front	RLF	Mounted between cylinder 1 and 2 on the engine lug, right bank
Right Lug Rear	RLR	Mounted between cylinder 3 and 4 on the engine lug, right bank
Right Head Front	RHF	Installed between cylinder 1 and 2 on the cylinder head, right bank
Right Head Rear	RHR	Installed between cylinder 3 and 4 on the cylinder head, right bank
Left Lug Front	LLF	Mounted between cylinder 5 and 6 on the engine lug, left bank
Left Lug Rear	LLR	Mounted between cylinder 7 and 8 on the engine lug, left bank
Left Head Front	LHF	Installed between cylinder 5 and 6 on the cylinder head, left bank
Left Head Rear	LHR	Installed between cylinder 7 and 8 on the cylinder head, left bank

pressure against the rocker arm, where as when the valve is closed the oil feed is open and release the applied pressure to by some degree. In the case of collapsed lash adjuster, this hydraulic component fails to maintain the required clearance. This leads to noise and excessive vibrations. The lash adjuster along with an overhead cam-follower mechanism is shown in the figure 4. Figure 4 is from [57].

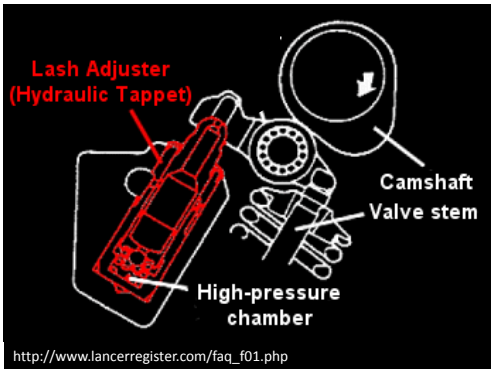

Figure 4: The hydraulic lash adjuster cross-section along with the valve train elements.

Appendix C

Appendix C

Calculating the covariance of scores, general case

The equation 4.18 is brought in the following:

$$COV(\mathbf{T}) = E(\mathbf{X}^*\mathbf{P}\mathbf{P}^T\mathbf{X}^{*T}) + E(\mathcal{F}\mathbf{P}\mathbf{P}^T\mathcal{F}^T) \quad (7)$$

$$+ E(\mathbf{X}^*\mathbf{P}\mathbf{P}^T\mathcal{F}^T) + E(\mathcal{F}\mathbf{P}\mathbf{P}^T\mathbf{X}^{*T}) \quad (8)$$

considering the fact that $E(\mathbf{X}^*) = -E(\mathcal{F})$, by adding and subtracting the expected values of transformed $\mathbf{X}^*$ and $\mathcal{F}$ into the above equations, one may end up to:

$$\begin{aligned}
COV(\mathbf{T}) &= E(\mathbf{X}^*\mathbf{P}\mathbf{P}^T\mathbf{X}^{*T}) - E(\mathbf{X}^*\mathbf{P})E(\mathbf{X}^*\mathbf{P})^T \\
&+ E(\mathcal{F}\mathbf{P}\mathbf{P}^T\mathcal{F}^T) - E(\mathcal{F}\mathbf{P})E(\mathcal{F}\mathbf{P})^T \\
&+ E(\mathbf{X}^*\mathbf{P})E(\mathbf{X}^*\mathbf{P})^T + E(\mathcal{F}\mathbf{P})E(\mathcal{F}\mathbf{P})^T \\
&+ E(\mathcal{F}\mathbf{P}\mathbf{P}^T\mathbf{X}^{*T}) + E(\mathbf{X}^*\mathbf{P}\mathbf{P}^T\mathcal{F}^T) \\
&= COV(\mathbf{X}^*\mathbf{P}) + COV(\mathcal{F}\mathbf{P}) + E(\mathcal{F}\mathbf{P}\mathbf{P}^T\mathbf{X}^{*T}) + E(\mathbf{X}^*\mathbf{P}\mathbf{P}^T\mathcal{F}^T) \\
&+ 2\,E(\mathbf{X}^*\mathbf{P})E(\mathbf{X}^*\mathbf{P})^T
\end{aligned}$$

Appendix D

Appendix D

Implementation Algorithm

Data: Baseline, CID signal and vibration data in time domain;

Begin

load the CID signal;

find zeros of the CID signal with any zero-finding algorithm;

while processing the entire CID signal **do**

find the location of missed tooth of toothed wheel;

find the first zero on the falling side of the CID signal after the missing tooth location;

set this zero as the degree zero in the crank angle domain;

find the first next similar zero and set it to degree 720 of this cycle and zero degree of the subsequent cycle;

save the samples corresponding to the location of these zeros in an array;

name the array the zero-loc;

end while

read baseline vibration signals;

while processing the entire vibration data **do**

divide the vibration data using the zero-loc array and save them in a matrix named vib-cycls;

re-sample the contents of vib-cycls using linear interpolation algorithm with

respect to zero-loc array;

save the CAD transfered vibration data in the vib-cad matrix;

average the vib-cad over angles;

save the results in vib-cad-avg matrix;

construct two data matrices using the vib-cad-avg matrix for right and left bank measurements;

save these matrices as X_L and X_R;

end while

set wavelet function and depth;

perform DWT on both of the X_L and X_R matrices;

for $j = 1 : depth$ **do**

calculate the components of data at scale j;

perform PCA on each component, save the loadings and eigenvalues at P_j and Λ_j matrices;

end for

Data: Testing, CID signal and vibration data in time domain;

load the CID signal;

find zeros of the CID signal with any zero-finding algorithm;

while processing the entire CID signal **do**

find the location of missed tooth of toothed wheel;

find the first zero on the falling side of the CID signal after the missing tooth location;

set this zero as the degree zero in the crank angle domain;

find the first next similar zero and set it to degree 720 of this cycle and zero degree of the subsequent cycle;

save the samples corresponding to the location of these zeros in an array;

name the array the zero-loc;

end while

read testing vibration signals;

while processing the entire vibration data **do**

divide the vibration data using the zero-loc array and save them in a matrix named vib-cycls;

re-sample the contents of vib-cycls using linear interpolation algorithm with respect to zero-loc array;

save the CAD transfered vibration data in the vib-cad matrix;

average the vib-cad over angles;

save the results in vib-cad-avg matrix;

construct two data matrices using the vib-cad-avg matrix for right and left bank measurements;

save these matrices as $X_{L,testing}$ and $X_{R,testing}$;

end while

perform DWT on both of the $X_{L,testing}$ and $X_{R,testing}$ matrices;

for $j = 1 : depth$ **do**

calculate the components of data at scale j;

use the loadings and eigenvalues P_j and Λ_j at scale j to map data to principal components domain;

determine statistical indices at scale j;

calculate F_c at scale j

calculate RBCs at scale j

end for

calculate the total statistical indices and control limits;

plot the total statistical indices;

if control limits are violated **then**

calculate and plot the S_c index;

select scale(s) with highest S_c value(s);

check statistical indices at this(ese) scale(s) to double check the occurrence of the fault;

plot F_c and RBC charts to isolate the fault;

spectral analysis of the total statistical indices (or statistical indices at faulty scale) can be performed for further analysis;

end if

End

References

[1] V. Venkatasubramanian, R. Rengaswamy, K. Yin, and S. Kavuri, "A review of process fault detection and diagnosis part i: Quantitative model-based methods," *Computers and Chemical Engineering*, vol. 27, no. 3, pp. 293–311, 2003.

[2] V. Venkatasubramanian, R. Rengaswamy, K. Yin, and S. Kavuri, "A review of process fault detection and diagnosis part iii: Process history based methods," *Computers and Chemical Engineering*, vol. 27, no. 3, pp. 327–346, 2003.

[3] S. Zanoli, G. Astolfi, and L. Barboni, "Fdi of process faults based on pca and cluster analysis," *2010 Conference on Control and Fault-Tolerant Systems (SysTol)*, pp. 197–202, 2010.

[4] S. Borguet and O. Leonard, "Coupling principal component analysis and kalman filtering algorithms for on-line aircraft engine diagnostics," *Control Engineering Practice*, vol. 17, no. 4, pp. 494 – 502, 2009.

[5] Y. Chang, Y. Wang, l. Liu, and Z. Wang, "Fault diagnosis of a mine hoist using pca and svm techniques," *Journal of China University of Mining and Technology*, vol. 18, no. 3, pp. 327 – 331, 2008.

[6] N. Baydar, Q. Chen, A. Ball, and U. Kruger, "Detection of incipient tooth defect in helical gears using multivariate statistics," *Mechanical Systems and Signal Processing*, vol. 15, no. 2, pp. 303 – 321, 2001.

[7] I. Trendafilova, "An automated procedure for detection and identification of ball

bearing damage using multivariate statistics and pattern recognition," *Mechanical Systems and Signal Processing*, vol. 24, no. 6, pp. 1858 – 1869, 2010.

[8] G. Halligan and S. Jagannathan, "Pca-based fault isolation and prognosis with application to pump," *The International Journal of Advanced Manufacturing Technology*, vol. 55, no. 5-8, pp. 699–707, 2010.

[9] B. Bakshi, "Multiscale pca with application to multivariate statistical process monitoring," *AIChE Journal*, vol. 44, no. 7, 1998.

[10] C. Wenying, "Application of multi-scale principal component analysis and svm to the motor fault diagnosis," *2009 International Forum on Information Technology and Applications*, pp. 131–134, 2009.

[11] A. Lachouri, K. Baiche, R. Djeghader, N. Doghmane, and S. Ouhtati, "Analyze and fault diagnosis by multi-scale pca," *2008 3rd International Conference on Information and Communication Technologies: From Theory to Applications*, pp. 1–6, 2008.

[12] P. Jayaswal, A. Wadhwani, and K. Mulchandani, "Machine fault signature analysis," *International Journal of Rotating Machinery*, vol. 2008, pp. 1–10, 2008.

[13] M. Lebold, K. Mcclintic, R. Campbell, C. Byington, and K. Maynard, "Review of vibration analysis methods for gearbox diagnostics and prognostics," in *Proceedings of the 54th meeting of the society for machinery failure prevention technology*, pp. 623–634, 2000.

[14] N. Jones and H. Li, "A review of condition monitoring and fault diagnosis for diesel engines," *Tribotest*, vol. 6, no. 3, pp. 267–291, 2000.

[15] N. Tandon and A. Choudhury, "A review of vibration and acoustic measurement methods for the detection of defects in rolling element bearings," *Tribology International*, vol. 32, no. 8, pp. 469 – 480, 1999.

[16] J. Mohammadpour, M. Franchek, and K. Grigoriadis, "A survey on diagnostic methods for automotive engines," *International Journal of Engine Research*, vol. 13, no. 1, pp. 41–64, 2011.

[17] X. Wang, U. Kruger, G. Irwin, G. McCullough, and N. McDowell, "Nonlinear pca with the local approach for diesel engine fault detection and diagnosis," *Control Systems Technology, IEEE Transactions on*, vol. 16, pp. 122 –129, jan. 2008.

[18] C. Hu, A. Li, and X. Zhao, "Multivariate statistical analysis strategy for multiple misfire detection in internal combustion engines," *Mechanical Systems and Signal Processing*, vol. 25, no. 2, pp. 694 – 703, 2011.

[19] P. King and K. Burnham, "Application of a pca model approach for misfire monitoring," in *UKACC Control Conference*, 2008.

[20] H. Sohn and C. Farrar, "Damage diagnosis using time series analysis of vibration signals," *Smart Materials and Structures*, vol. 10, no. 3, pp. 446–451, 2001.

[21] N. Pontoppidan, *Condition monitoring and management from acoustic emissions*. Phd thesis, Technical University of Denmark, 2005.

[22] J. Tjong and Z. Relf, "Development and applications of engine dynamic signal monitoring and diagnostic system," in *IMAC XIII - 13th International Modal Analysis Conference*, no. 1, pp. 1081–1085, Society for experimental mechanics (SEM), 1995.

[23] Y. Chin and F. Coats, "Engine dynamics time-based versus crank angle based," in *SAE International*, 1986.

[24] S. Yurkovicht and M. Simpsonf, "Crank-angle domain modeling and control for idle speed," in *SAE International*, 1997.

[25] I. Arasaratnam, S. Habibi, C. Kelly, T. Fountaine, and J. Tjong, "Engine fault detection using vibration signal reconstruction in the crank angle domain," in *SAE International*, SAE International, 2011.

[26] L. Cohen, "Time-frequency distributions-a review," *Proceedings of the IEEE*, vol. 77, no. 7, pp. 941 – 981, 1989.

[27] N. Baydar and A. Ball, "Comparative study of acoustic and vibration signals in detection of gear failures using wignerville distribution," *Mechanical Systems and Signal Processing*, vol. 15, no. 6, pp. 1091–1107, 2001.

[28] Q. Meng and L. Qu, "Rotating machinery fault diagnosis using wigner distribution," *Mechanical Systems and Signal Processing*, vol. 5, no. 3, pp. 155 – 166, 1991.

[29] N. vanderMerwe and A. Hoffman, "A modified cepstrum analysis applied to vibrational signals," in *14th International Conference on Digital Signal Processing*, vol. 2, pp. 873 – 876, 2002.

[30] C. Harris and A. Piersol, *Harris' Shock and Vibration Handbook (5th Edition)*. McGraw-Hill, 2002.

[31] J. Stack, R. Harley, and T. Habetler, "An amplitude modulation detector for fault diagnosis in rolling element bearings," in *28th Annual Conference of the Industrial Electronics Society*, pp. 3377 – 3382, 2002.

[32] R. Almeida, S. daSilva, and L. Padovese, "New technique for evaluation of global vibration levels in rolling bearings," *Shock and Vibration*, vol. 9, no. 4, pp. 225–234, 2002.

[33] A. Lakis, "Rotating machinery fault diagnosis using time-frequency methods," in *7th WSEAS International Conference on Electric Power Systems, High Voltages, Electric Machines*, pp. 139–144, 2007.

[34] P. Bonato, R. Ceravolo, A. DeStefano, and M. Knaflitz, "Bilinear time-frequency transformations in the analysis of damaged structures," *Mechanical Systems and Signal Processing*, vol. 11, no. 4, pp. 509 – 527, 1997.

[35] I. Daubechies, "Where do wavelets come from?," *Proceedings of the IEEE*, vol. 84, no. 4, pp. 510–513, 1996.

[36] Y. Meyer and D. Ryan, *Wavelets algorithms and applications*. Society for Industrial and Applied Mathematics, 1993.

[37] S. Mallat, *A Wavelet tour of signal processing, 3rd edition*. Academic Press, 2008.

[38] R. Yan and X. Gao, "Base wavelet selection for bearing vibration signal analysis," *International Journal of Wavelets, Multiresolution and Information Processing*, vol. 07, no. 04, pp. 411–426, 2009.

[39] K. Ranjeet and A. Farida, "Retained signal energy based optimal wavelet selection for denoising of ecg signal using modified thresholding," in *International Conference on Multimedia, Signal Processing and Communication Technologies*, no. 1, pp. 196–199, Ieee, 2011.

[40] N. Singh and K. Tiwari, "Optimal selection of wavelet basis function applied to ecg signal denoising," *Digital Signal Processing*, vol. 16, no. 3, pp. 275–287, 2006.

[41] J. Jackson, *A User's guide to principal components*. John Wiley and Sons Inc., 1991.

[42] J. Qin, "Statistical process monitoring basics and beyond," *Journal of Chemometrics*, vol. 17, no. 8-9, pp. 480–502, 2003.

[43] P. Nomikos and J. Macgregor, "Multivariate spc charts for monitoring batch processes," *Technometrics*, vol. 37, no. 1, pp. 41–59, 1995.

[44] N. Tracy, J. Young, and R. Mason, "Multivariate control charts for individual observations," *Journal of Quality Technology*, vol. 24, p. 8895, 1992.

[45] H. Yue and J. Qin, "Reconstruction-based fault identification using a combined index," *Industrial and Engineering Chemistry Research*, vol. 40, no. 20, pp. 4403–4414, 2001.

[46] C. Alcala and J. Qin, "Reconstruction-based contribution for process monitoring," in *Proceedings of the 17th World Congress The International Federation of Automatic Control*, no. 5, pp. 7889–7894, IFAC, 2008.

[47] R. Dunia and J. Qin, "A unified geometric approach to process and sensor fault identification and reconstruction : the unidimensional fault case," *Computers and Chemical Engineering*, vol. 22, no. 7, pp. 927–943, 1998.

[48] J. Macgregor and T. Kourtl, "Statistical process control of multivariate processes," *Control Engineering Practice*, vol. 3, no. 3, pp. 403–414, 1995.

[49] S. Yoon and J. MacGregor, "Principal-component analysis of multiscale data for process monitoring and fault diagnosis," *AIChE Journal*, vol. 50, no. 11, pp. 2891–2903, 2004.

[50] J. Jackson and G. Mudholkar, "Control procedures for residuals associated with principal component analysis," *Technometrics*, vol. 21, no. 3, pp. pp. 341–349, 1979.

[51] Y. Wang, Z. He, and Y. Zi, "Enhancement of signal denoising and multiple fault signatures detecting in rotating machinery using dual-tree complex wavelet transform," *Mechanical Systems and Signal Processing*, vol. 24, no. 1, pp. 119 – 137, 2010.

[52] H. Li, "Complex morlet wavelet amplitude and phase map based bearing fault diagnosis," in *Intelligent Control and Automation (WCICA), 2010 8th World Congress on*, pp. 6923 –6926, july 2010.

[53] N. Nikolaou and I. Antoniadis, "Demodulation of vibration signals generated by defects in rolling element bearings using complex shifted morlet wavelets," *Mechanical Systems and Signal Processing*, vol. 16, no. 4, pp. 677 – 694, 2002.

[54] S. McInerny and Y. Dai, "Basic vibration signal processing for bearing fault detection," *IEEE Transactions on Education*, vol. 46, no. 1, pp. 149–156, 2003.

[55] `http://biology-forums.com/index.php?action=gallery%3Bsa=view%3Bid=5339`.

[56] B. Ray, "Engine defect detection using wavelet analysis," Master's thesis, University of Windsor, 2007.

[57] `http://www.lancerregister.com/faq_f01.php`.

MULTIRESOLUTION-MULTIVARIATE ANALYSIS OF VIBRATION SIGNALS; APPLICATION IN FAULT DIAGNOSIS OF INTERNAL COMBUSTION ENGINES

Multiresolution-multivariate analysis of vibration signals; application in fault diagnosis of internal combustion engines

By

SEYYED REZA HAQSHENAS, B.Sc., M.Sc.

A Thesis
Submitted to the School of Graduate Studies
in Partial Fulfillment of the Requirements
for the Degree
Master's of Applied Science

McMaster University

MASTER'S OF APPLIED SCIENCE (2012) MCMASTER UNIVERSITY
(Mechanical Engineering) Hamilton, Ontario

TITLE: Multiresolution-multivariate analysis of vibration signals; application in fault diagnosis of internal combustion engines

AUTHOR: SEYYED REZA HAQSHENAS
B.Sc., M.Sc.

SUPERVISOR: Professor Saeid Habibi, Professor Samir Ziada